Mathematical Modeling and Finite Element Computation of Cosserat Elastic Plates

by

Roman Kvasov

A dissertation submitted in partial fulfillment of the requirements for the degree of

DOCTOR OF PHILOSOPHY

in

COMPUTING AND INFORMATION SCIENCES AND ENGINEERING

UNIVERSITY OF PUERTO RICO
MAYAGÜEZ CAMPUS

April, 2013

Approved by:

Robert Acar, Ph.D Member, Graduate Committee	Date
Paul Castillo, Ph.D Member, Graduate Committee	Date
Frederick Just, Ph.D Member, Graduate Committee	Date
Lev Steinberg, Ph.D President, Graduate Committee	Date
Mauricio Cabrera-Ríos, Ph.D Representative of Graduate Studies	Date
Wilson Rivera, Ph.D CISE PhD Program Coordinator	Date

Abstract of Dissertation Presented to the Graduate School
of the University of Puerto Rico in Partial Fulfillment of the
Requirements for the Degree of Doctor of Philosophy

Mathematical Modeling and Finite Element Computation of Cosserat Elastic Plates

by

Roman Kvasov

April 2013

Chair: Lev Steinberg
COMPUTING AND INFORMATION SCIENCES AND ENGINEERING

In this dissertation the mathematical modeling of Cosserat elastic plates and their Finite Element computation are presented. The mathematical model for bending of Cosserat elastic plates, which assumes physically and mathematically motivated approximations over the plate thickness for stress, couple stress, displacement, and microrotation is developed. The approximations are consistent with the three-dimensional Cosserat elasticity equilibrium equations, boundary conditions and the constitutive relationships. The Generalized Hellinger-Prange-Reissner Principle allows to obtain the equilibrium equations, constitutive relations and optimal value for the minimization of the elastic energy with respect to the splitting parameter.

On of the main contributions of this dissertation is the comparison of the maximum vertical deflection for simply supported square plate with the analytical solution of the three-dimensional Cosserat elasticity. It confirms the high order of approximation of the three-dimensional (exact) solution. The computations produce a relative error of the order 1% in comparison with the exact three-dimensional solution that is stable with respect to the standard range of the plate thickness. The results are compatible with the precision of the well-known Reissner model used for bending of simple elastic plates.

For the Finite Element formulation, the Cosserat plate field equations are presented as an elliptic system of nine differential equations in terms of the kinematic variables. The system includes an optimal value of the splitting parameter, which is the minimizer of the Cosserat plate stress energy. The Finite Element Method for Cosserat elastic plates based on the efficient numerical algorithm for the calculation of the optimal value of the splitting parameter and the computation of the corresponding unique solution of the weak problem is proposed. The numerical validation of the Finite Element Method shows its convergence to the analytical solution with optimal linear rate of convergence in $\mathbf{H}^1$-norm.

The Finite Element computation of bending of clamped Cosserat elastic plates of arbitrary shapes under different loads is provided. The numerical results are obtained for the elastic plates made of dense polyurethane foam used in structural insulated panels.

Resumen de Disertación Presentado a Escuela Graduada
de la Universidad de Puerto Rico como requisito parcial de los
Requerimientos para el grado de Doctor en Filosofia

Modelado Matemático y Computación por medio del Elemento Finito de Placas Elásticas de Cosserat

por

Roman Kvasov

Abril 2013

Consejero: Lev Steinberg
COMPUTACIÓN Y CIENCIA DE INFORMACIÓN E INGENIERIA

En esta disertación se presenta el modelo matemático para las placas elásticas de Cosserat y su computación utilizando el método del elemento finito. En la misma se desarrolla un modelo matemático para la flexión de las placas elásticas de Cosserat, que asume aproximaciones de tensión, momento tensional, desplazamiento y microrotación, las cuales están física y matemáticamente motivadas. Estas aproximaciones son consistentes con las ecuaciones de equilibrio de la elasticidad tridimensional de Cosserat, condiciones de frontera y las ecuaciones constitutivas. El Principio Generalizado de Hellinger Prange-Reissner permite obtener las ecuaciones de equilibrio, ecuaciones constitutivas y el valor óptimo del parámetro de separación para la minimización de la energía elástica.

Una de las contribuciones de esta disertación es la comparación de la deflexión vertical máxima de las placas simplemente apoyadas con la solución analítica de la elasticidad de Cosserat, la cual confirma el alto orden de la aproximación de la solución tridimensional exacta. Los cómputos producen el error relativo de orden de

1% en comparación con la solución exacta. Este error es estable en el rango estándar del espesor de la placa. Los resultados son compatibles con la precisión del modelo de Reissner utilizado para las placas elásticas clásicas.

Para la formulación del método del elemento finito, se presentan las ecuaciones de campo como un sistema elíptico de nueve ecuaciones diferenciales parciales en términos de las variables cinemáticas. El sistema incluye el valor óptimo del parámetro de separación. Se propone el método del elemento finito para las placas elásticas de Cosserat basado en un algoritmo eficiente para calcular el valor óptimo del parámetro de separación y computar la solución correspondiente de la formulación débil. Se muestra que el método del elemento finito propuesto, converge a la solución analítica con la razón de convergencia óptima (lineal).

Se provee el método modelado por el método del elemento finito de las placas elásticas de Cosserat de forma arbitraria bajo la acción de diferentes cargas. Se obtuvieron resultados numéricos para las placas hechas de la espuma densa de poliuretano, las cuales se utilizan en los paneles de sándwich de poliuretano inyectado.

To my mother Lyudmila Kvasova

Acknowledgments

I would like to express my deepest gratitude to my advisor Dr. Lev Steinberg. He patiently guided me throughout my graduate studies and always encouraged my scientific research with endless effort and care. I feel very privileged to have him as my academic role model and being to able learn from him. During all these years Dr. Steinberg has been providing an environment of aspiration and confidence. Without his guidance, assistance and support this dissertation would not have been possible.

I am indebted to my committee members Dr. Paul Castillo, Dr. Robert Acar and Dr. Frederick Just for helpful discussions, assistance in the work on the dissertation and their irrefutable contribution to my education. Dr. Paul Castillo has taught me the essentials of the Finite Element method and has been my mentor for the implementation of the numerical algorithms developed in the dissertation. Dr. Robert Acar has instructed me in the area of Numerical Analysis and Dr. Frederick Just has given me the insight into the fundamentals of Continuum Mechanics.

I would like to thank Dr. Domingo Rodríguez, who offered his server for large mesh numerical experiments and his student Juan Valera, who assisted in running the code. I also want to thank Miguel Angel Goenaga, who allowed to run the early experiments in the computer laboratory.

I am grateful to my mathematics teacher Michael Yakir, who dedicated his time to teach me the basics of mathematics and encouraged me to pursue graduate studies.

I am thankful to my family and friends for being supportive and providing warm atmosphere during all these years.

Preface

This work is divided into five chapters.

The first chapter discusses the importance of the Cosserat materials in modern engineering, the historical survey of the mathematical descriptions of elastic plates and the development of Finite Element Method and its importance for the numerical modeling of physical systems in a variety of engineering disciplines.

The second chapter is dedicated to the development of the mathematical model for Cosserat elastic plates. We obtain the complete theory of Cosserat elastic plates. Based on the Generalized Hellinger-Prange-Reissner Principle we obtain the equilibrium equations, constitutive relations and the optimal value for the minimization of the elastic energy with respect to the splitting parameter in the approximation of the σ_{33} stress component. We also obtain the Cosserat plate field equation and represent them as a system of nine partial differential equations in terms of the kinematic variables. We prove the ellipticity of the obtained system and derive an explicit expression for the optimal value of the splitting parameter minimizing the elastic energy.

The third chapter contains the validation of the proposed mathematical model for Cosserat elastic plates. We obtain the analytical solution for the square Cosserat plate and compare it with the analytical (exact) solution for the three-dimensional Cosserat Elasticity.

The fourth chapter contains the Finite Element computation of the bending of Cosserat elastic plates of arbitrary shape. We develop the Finite Element Method for Cosserat elastic plates based on the efficient numerical algorithm for the calculation of the optimal value of the splitting parameter and the computation of the corresponding unique solution of the weak problem. We discuss the validation of the proposed FEM and its convergence. We also provide the Finite Element modeling of the bending of clamped Cosserat elastic plates of arbitrary shapes under different loads.

The fifth chapter consists of the conclusion and the discussion of the future work.

Table of Content

List of Tables

List of Figures

List of Abbreviations

2D	Two-dimensional
3D	Three-dimensional
HPR	Hellinger-Prange-Reissner Principle
FEM	Finite Element Method
BVP	Boundary Value Problem(s)
DE	Differential Equation(s)
ODE	Ordinary Differential Equation(s)
PDE	Partial Differential Equation(s)
BC	Boundary condition(s)
MPa	Megapascal
mm	millimeter

List of Symbols

ε_{ijk}	Levi-Civita symbol
δ_{ij}	Kronecker delta
$\hat{a} \cdot \hat{b}$	Dot product of two vectors $\hat{a}$ and $\hat{b}$
$\hat{a} \times \hat{b}$	Cross product of two vectors $\hat{a}$ and $\hat{b}$
$\hat{\mathbf{e}}_i$	Unit vectors of the Cartesian grid
x_i	Cartesian coordinates
$\mathbb{R}^3$	Three-dimensional real vector space
$\mathbb{R}^2$	Two-dimensional real vector space
$\hat{\mathbf{n}}$	Normal vector
$\hat{\mathbf{s}}$	Tangent vector
V	Volume
h	Thickness of the plate
a	Length of the side plate
$\mathbf{div}$	Divergence operator
$\boldsymbol{\nabla}$	Del operator
$\boldsymbol{\sigma}$	Stress tensor
$\boldsymbol{\mu}$	Couple stress tensor
$\boldsymbol{\gamma}$	Strain tensor
$\boldsymbol{\chi}$	Torsion tensor
$\hat{\mathbf{u}}$	Displacement vector
$\hat{\boldsymbol{\varphi}}$	Rotation vector
$\mathbf{f}^{(\hat{\mathbf{n}})}$	Stress vector associated with the direction $\hat{\mathbf{n}}$
$\mathbf{m}^{(\hat{\mathbf{n}})}$	Moment vector associated with the direction $\hat{\mathbf{n}}$
B	Elastic body
∂B	Boundary of the elastic body B
U_C	Strain energy
U_K	Stress energy
η	Splitting parameter
p	Initial pressure distribution
$\mathscr{S}$	Cosserat stress set
$\mathscr{E}$	Cosserat strain set
$\mathscr{U}$	Solution set
λ	Lame's first parameter
μ	Shear modulus
L	Linear differential operator
Ψ_α	Rotations in the middle plane around x_α-axis

∂_i	Differential operator $\frac{\partial}{\partial x_i}$
E	Young's modulus
ν	Poisson's ratio
l_b	Characteristic length for bending
l_t	Characteristic length for torsion
N	Coupling number
$a(\cdot,\cdot)$	Bilinear form
$b(\cdot)$	Linear form
$\mathbf{L}^2(B_0)$	Hilbert space of square-integrable on B_0 functions
$\mathbf{H}^1(B_0)$	Sobolev space of functions that are square-integrable on B_0 together with their first partial derivatives
$\mathbf{H}_0^1(B_0)$	Sobolev space of functions that vanish on the boundary ∂B_0 and that are square-integrable on B_0 together with their first partial derivatives

Chapter 1

Introduction

1.1 Scope of the Chapter

In this chapter we make a brief survey of the topics that will be discussed in the dissertation: Cosserat materials, elastic plates and Finite Element Method. We discuss the constitution of modern materials with microstructure (Cosserat materials) and their importance in the modern engineering. We provide a brief historical survey of the mathematical descriptions of plates and give several examples of the applications of plates in different areas of technology. We finish this chapter with the discussion of the development of an effective numerical technique for solving partial differential equations – Finite Element Method.

1.2 Cosserat Materials in Modern Engineering

The Classical Theory of Elasticity is based on the idealized model of elastic continuum, where the body forces acting on the surface element are described by the force vector. This assumption leads to symmetric stress and strain tensors. The theory gives accurate description of the behavior of such construction materials as steel, aluminum and concrete when the strains lie in the elastic limits. However some significant difference between the theory and the experiment can be observed when the gradient of the strain is large enough, as in cases of the concentration of strain around holes. The microstructure of the material has a large impact on the experimental results when dealing with small wavelengths and high frequency oscillations. Finally the Classical Theory of Elasticity does not give a fair description of the processes in granular media and when acoustic waves travel through crystals, polymers and polycrystal structures.

Many modern materials possess certain microstructure (cellular solids, pores, macromolecules, fibers, grains, voids, etc.) and exhibit experimental behavior that cannot be adequately described by the Classical Elasticity. Cosserat Elasticity describes the influence of the microstructure on the deformation of the material and is a very useful framework for modeling solid composites (fiber, platelet, or particulate), porous media (including solids with fissures or microcracks) and suspensions (containing isometric or anisometric particles) [5], [6].

Cosserat Theory of Elasticity assumes that the transmission of forces through an area element is carried out by means of force and moment vectors. This leads to the asymmetry of the stress tensor and the introduction of the couple stress tensor. The introduction of three additional degrees of freedom for microrotations results in the asymmetric micropolar strain. The symmetric part of the micropolar strain corresponds to the classic strain [40], [7].

The examples of Cosserat solids include rocks, concrete, polymers and different composites [6], [8]. The experimental observation of coupled rotational-translational modes in a noncohesive granular phononic crystal is reported in [9]. These elastic wave modes are predicted by the Cosserat theory and are not described by the Classical Elasticity [9].

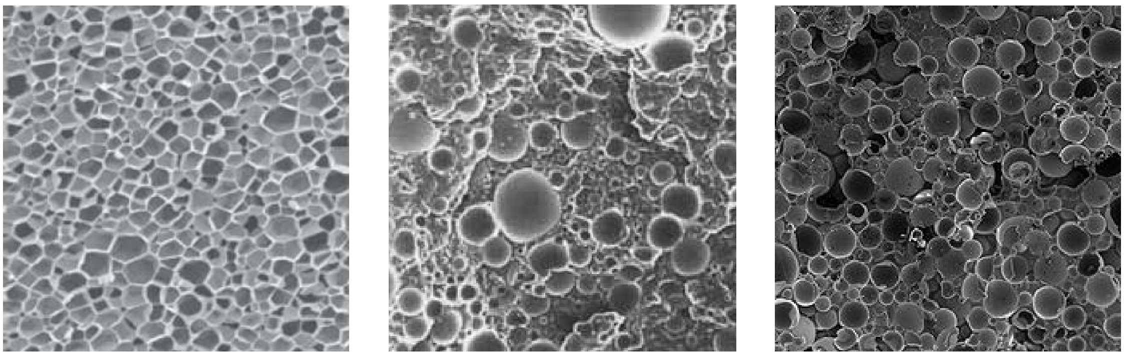

Figure 1–1: Closed-cell polymer foam, polypropylene-based particulate composite, syntactic foam [1], [2]

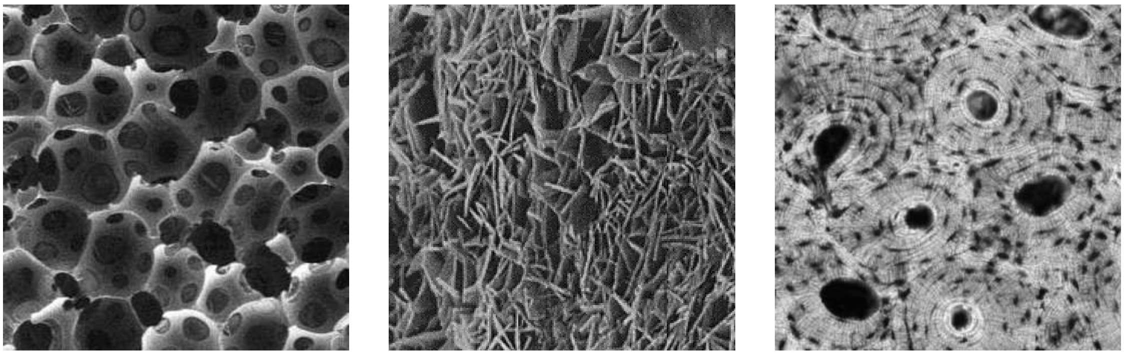

Figure 1–2: Polyurethane foam, sand-aerated concrete, human bone [1], [3], [4]

Aluminum-epoxy composites being used in aircraft and aerospace industries [10], [11], were found to be micropolar materials. The values of the relevant parameters based on specimen of an aluminum-epoxy composite were investigated in [12], [13]. Grained composites and closed-cell polymenthacrylimide foams were investigated and shown to be micropolar materials [13]. The micropolar moments and rotations, in addition to forces and displacements, were included in the model of the behavior of reinforced concrete in [14]. The engineering properties of lightweight aggregate were investigated in [15]. The human bones were reported to be micropolar materials [16]. The micropolar elasticity model was used for the stress analysis of human bones [17].

In this dissertation we will make numerical computations for the plates made of dense polyurethane foam reported to be Cosserat material [16]. Insulation materials made from polyurethane foam are used in the construction of large industrial buildings and therefore the prediction of the behavior of the polyurethane foam under bending stress is extremely important [18]. Polyurethane foam is also used in structural insulated panels widely used in walls, floor slabs and roofs [19].

1.3 Historical Overview of Plate Theories

Elastic plates are flat solids bounded by two parallel planes (faces) and an orthogonal surface called boundary. The distance between the faces of the plate is called thickness. The dimensions of the faces are assumed to be much larger than the thickness of the plate: the width to thickness ratio of a plate is considered to be greater than 10 [20], [21]. The mathematical descriptions of the deformation of the elastic plates are called plate theories. Plate theories reduce the problem of determining displacements and stresses of the plate under load from three dimensional problem to two-dimensional [22].

Nowadays plates play a crucial part in a variety of branches of modern technology. Such a widespread use of thin-walled structures arises from their fundamental properties: light weight, high load-carrying capacity and technological effectiveness [20]. For this reason plates are widely used in aeronautical and aerospace industry where light weight is essential (aluminum alloy plates) [23]. Marine engineering makes use of elastic plates for the design of the hull in shipbuilding: floor and sealing plates, frames, side girders, keel and margin plates (made of steel). Plates are being increasingly utilized in chemical engineering (plate type heat exchangers), steam systems (orifice plate steam traps), plant and process design, powerplants (waterwalls, boilers, superheaters, steam pipes, columns), civil, structural and mechanical engineering, construction and industrial machinery, transportation and mining equipment, heat exchangers, reaction vessels, evaporators, transfer piping systems (nickel plates) and many other practical applications [24], [25].

The interest in the theory of deformed surfaces and the first appearance of the mathematical description of plates can be traced back to late 18th century. In 1776 Euler performed a free vibration analysis of certain plate problems. In his "Discoveries in the Theory of Sound" in 1787, Chladni described the experiments on various modes of free vibrations of plates [26], [27]. J. Bernoulli developed theoretical justification of Chladni experiments in 1789 and used the direct approach for the derivation of the governing differential equation, considering the plate being a two-dimensional deformable continuum [27], [28], [20], [29].

The beginning of the 19th century was marked by the development of the general plate equation based on the direct approach. In 1813 Lagrange added a missing warping term to the equilibrium equation in the work of Germain and thus produced what is now known as Germain-Lagrange bending equation [20]. In 1821 Navier proposed the Newtonian conception that let him for the first time formulate the general theory of elasticity: elastic reaction arises from variation in intermolecular forces which result from shifts in the unchangeable structure of molecular configuration [30].

Not long after the three-dimensional elasticity equations were developed, Cauchy (1828) and Poisson (1829) used it to formulate the plate bending problem. The new technique, essentially different from the direct approach used in the previous works, was based on the splitting of the unknown stress components and thus reducing the three-dimensional equations to a two-dimensional problem. Even though the obtained governing differential equation coincided with the Germain-Lagrange bending equation, the Poisson approach and the introduced boundary conditions became a subject for much debate and were widely criticized [28], [20].

In 1850 the revolutionary contribution was made by Kirchhoff. In his thesis, he presented the basis of the classical bending theory of thin elastic plates and triggered the future widespread use of the theory in practice. The energy functional of the three-dimensional elasticity theory was successfully simplified thus reducing the three-dimensional theory to a two-dimensional plate bending problem [20].

In order to derive the bi-harmonic Germain-Lagrange differential equation, Kirchhoff came up with the following assumptions: straight lines normal to the mid-surface remain straight after deformation, straight lines normal to the mid-surface remain normal to the mid-surface after deformation and the thickness of the plate does not change during deformation [31]. In 1888 based on these assumptions, Love developed what is now called Kirchhoff - Love theory of plates – two-dimensional model describing the deformation of thin elastic plates [32], [33]. Saint-Venant proposed an extension to Kirchhoffs plate which takes into account both stretching and bending. In 1899, Levy obtained the first solution of the Kirchhoffs differential equation for the case of rectangular plate [31].

The development of the aircraft industry, nuclear physics and chemical industry invoked a lot of analytical research of plates. This lead to many extensive studies in the area of plate bending theory such as contributions to the theory of large deformations and the general theory of elastic stability of thin plates, theoretical and experimental investigations associated with the accuracy of Kirchhoffs plate theory, simplification of the general equations for the large deflections of very thin plates and the development of the final form of the differential equation of the large-deflection theory, investigation of the postbuckling behavior of plates, solution of plates subjected to nonsymmetrical distributed loads and edge moments, development of the bases of the general theory of anisotropic plates and nonlinear plate analysis [20].

Since Kirchhoff plate theory assumes the normal to the middle plane remaining normal during deformation, it automatically neglects transverse shear strain effects. A rigorous system of equations, which takes into account the transverse shear deformation, has been developed only in the middle of 20th century by Reissner [34], [35], [36].

One of the main advantages of Reissner model is that it is able to determine the reactions along the edges of a simply supported rectangular plate, where classical theory leads to a concentrated reaction at the corners of the plate [31]. The study of the relationships between the classical theory and Reissner model has proved that the solution of the clamped Reissner plate approaches the solution of the Kirchhoff plate as the thickness approaches zero and that the maximum bending can reach up to 20% for moderate plate thickness [37], [38]. In addition, the numerical calculations of bending behavior of the plate of moderate thickness, show high level of agreement between three-dimensional and Reissner models [39], [37].

The theory of Cosserat Elasticity takes into account the effect of microstructure on the deformation of the body and gives a more precise description than the Classical Elasticity. In 1967 Eringen was the first to propose a theory of plates in the framework of Cosserat Elasticity [40]. Eringen based his theory on the assumption of no variation of microrotations in the thickness direction and a technique that is very similar to the one used for Kirchhoff plate – integration of the three-dimensional equations [40], [37]. More remarks on the development of other theories of Cosserat plates and shells can be found in [41], [42], [43].

In 2010 Steinberg proposed to use Reissner plate theory in the framework of Cosserat Elasticity [36]. The developed mathematical model described the deformation of thin Cosserat elastic plates and took into account the transverse variation of microrotation. The analytical solution for simple rectangular plate was developed in [44]. The numerical simulation of bending of Cosserat elastic plates of different shapes according to Steinberg model is presented in [45].

In this dissertation we develop the mathematical model for Cosserat elastic plates, which is an enhanced version of the bending plate model presented in [36]. The new plate theory includes the assumptions of both Eringen [40] and Steinberg [36] models. One of the main contributions of this work is the comparison of the proposed mathematical model and the three-dimensional Cosserat Elasticty. The numerical computations for a plate bending produce a relative error of the order 1% in comparison with the exact three-dimensional solution, which is compatible with the precision of the Reissner model for classical plates [46].

1.4 Development of the Finite Element Method

Finite Element Method (FEM) is a numerical method for finding an approximate solution of both ordinary and partial differential equations. FEM is based on the weak formulation of the differential equation and the discretization of the domain into finite elements. Nowadays FEM is used in almost every area of engineering that employs models of nature given by partial differential equations (PDE). Some of the important features that make FEM very attractive technique include treatment of complex geometries, handling of a wide variety of engineering problems, robustness and stability (in contrast to finite difference methods) and solid mathematical foundation [47].

It is difficult to name one single work from which all the concepts behind FEM originated. The idea of approximating the solution of PDE in the weak form as a linear combination of the linearly independent functions was developed by Galerkin (1915), which he applied to the plates analysis problems [48], [49]. Since Bubnov (1913) independently developed a similar approach for the solution of the variational problems, the method is sometimes called Bubnov-Galerkin. The development of the modern FEM concepts can be traced to the work of Courant (1943), who was the first to propose the piecewise polynomial approximation of the Dirichlet problem over a set of triangles [50], [47]. Similar technique of the discretization of the domain into sub-domains were used earlier by Hrennikoff (1941) and McHenry (1943), when solving one-dimensional elasticity problems [51], [52]. Finite Element techniques of local approximations and the stiffness matrix assembly strategies were first employed in the work of Turner, Clough, Martin and Topp in 1956 [53]. The term "Finite Element Method" was introduced for the first time by Clough (1960) in the analysis of the linear plane elasticity using triangular and rectangular elements [54].

Since 1960s FEM started to receive general acceptance in civil and mechanical engineering: many papers and books were written on the subject and countless developments of finite element techniques were made. The range of applications of FEM was extended to many engineering disciplines such as heat transfer, fluid mechanics, aerospace engineering, electromagnetism, biomechanics and acoustics [55]. During 1970s some significant advances in the mathematical foundation and the establishment of the main results on stability, error estimation and convergence for different problems were made by Babuŝka, Aziz, Brezzi, Nitsche, Strang, Ciarlet, Oden, Reddy, Douglas, among many others [56], [57], [58]. For a detailed development of FEM we will refer to [47] where the history of FEM is given in much detail.

Nowadays, Finite Element Method is successfully used in almost every field of engineering analysis. It provides the solution to complex problems and helps reach a safe and cost-effective design. There is a variety of both opensource and commercial software packages, that implement the Finite Element algorithms for solving partial differential equations or aid in the pre-processing and post-processing of Finite Element models. Among the most powerful ones are ABAQUS, ANSYS, NASTRAN, PATRAN, LS DYNA, etc.

Chapter 2

Mathematical Model for Cosserat Elastic Plates

2.1 Scope of the Chapter

In this chapter we develop the mathematical model for Cosserat elastic plates. We obtain the corresponding equilibrium equations and constitutive relations for Cosserat elastic plates. We develop the algorithm for the minimization of the elastic energy with respect to the splitting parameter in the approximation of the σ_{33} stress component. The obtained solution is proved to be unique. We also obtain the Cosserat plate field equations and represent them as a system of nine partial differential equations in terms of the kinematic variables. We prove the ellipticity of the obtained system and derive an explicit expression for the optimal value of the splitting parameter.

2.2 Cosserat Linear Elasticity

2.2.1 Fundamental Equations

Let us consider a Cosserat elastic body B_0 and recall the main equations of the Cosserat elasticity satisfied for all points of the body B_0: equilibrium equations, strain-displacement relations and the constitutive equations.

Let u_i be the displacement vector, φ_i – rotation vector, σ_{ji} – stress tensor, μ_{ji}– couple stress tensor, γ_{ji} – strain tensor and χ_{ji} – torsion tensor.

Equilibrium equations without body forces and body moments represent the balance of linear and angular momentums and have the following form

$$\begin{aligned} \sigma_{ji,j} &= 0, && (2.1)\\ \varepsilon_{ijk}\sigma_{jk} + \mu_{ji,j} &= 0, && (2.2) \end{aligned}$$

where ε_{ijk} is the Levi-Civita symbol.

The strain-displacement and torsion-rotation relations are given as [40]

$$\begin{aligned} \gamma_{ji} &= u_{i,j} + \varepsilon_{ijk}\varphi_k && (2.3)\\ \chi_{ji} &= \varphi_{i,j}. && (2.4) \end{aligned}$$

The constitutive equations are given as [59]:

$$\begin{aligned} \sigma_{ji} &= (\mu+\alpha)\gamma_{ji} + (\mu-\alpha)\gamma_{ij} + \lambda\gamma_{kk}\delta_{ij}, && (2.5)\\ \mu_{ji} &= (\gamma+\epsilon)\chi_{ji} + (\gamma-\epsilon)\chi_{ij} + \beta\chi_{kk}\delta_{ij}, && (2.6) \end{aligned}$$

where λ and μ are the Lamé constants and α, β, γ and ϵ are asymmetric constants.

The constitutive equations (2.5) - (2.6) can be also written in the reverse form:

$$\begin{aligned} \gamma_{ji} &= (\mu'+\alpha')\sigma_{ji} + (\mu'-\alpha')\sigma_{ij} + \lambda'\sigma_{kk}\delta_{ij}, && (2.7)\\ \chi_{ji} &= (\gamma'+\epsilon')\mu_{ji} + (\gamma'-\epsilon')\mu_{ij} + \beta'\mu_{kk}\delta_{ij}, && (2.8) \end{aligned}$$

where

$$
\begin{aligned}
\mu' &= \frac{1}{4\mu}, \\
\alpha' &= \frac{1}{4\alpha}, \\
\gamma' &= \frac{1}{4\gamma}, \\
\epsilon' &= \frac{1}{4\epsilon}, \\
\lambda' &= \frac{-\lambda}{6\mu(\lambda + \frac{2\mu}{3})} \\
\beta' &= \frac{-\beta}{6\mu(\beta + \frac{2\gamma}{3})}.
\end{aligned}
$$

The equilibrium equations (2.1) - (2.2) with constitutive formulas (2.5) - (2.6) and kinematic formulas (2.3) - (2.4) are accompanied by the following mixed boundary conditions

$$\hat{\mathbf{u}} = \hat{\mathbf{u}}_{\mathbf{0}}, \ \hat{\boldsymbol{\varphi}} = \hat{\boldsymbol{\varphi}}_{\mathbf{0}} \qquad \text{on } \mathscr{G}_1 = \partial B_0 \backslash \partial B_\sigma, \tag{2.9}$$

$$\hat{\boldsymbol{\sigma}}_{\hat{\mathbf{n}}} = \boldsymbol{\sigma} \cdot \hat{\mathbf{u}} = \hat{\boldsymbol{\sigma}}_{\mathbf{0}} \qquad \text{on } \mathscr{G}_2 = \partial B_\sigma, \tag{2.10}$$

$$\hat{\boldsymbol{\mu}}_{\hat{\mathbf{n}}} = \boldsymbol{\mu} \cdot \hat{\mathbf{n}} = \hat{\boldsymbol{\mu}}_{\mathbf{0}} \qquad \text{on } \mathscr{G}_2 = \partial B_\sigma, \tag{2.11}$$

where $\hat{\mathbf{u}}_{\mathbf{0}}, \hat{\boldsymbol{\varphi}}_{\mathbf{0}}$ are prescribed on $\mathscr{G}_1$, $\hat{\boldsymbol{\sigma}}_{\mathbf{0}}$ and $\hat{\boldsymbol{\mu}}_{\mathbf{0}}$ on $\mathscr{G}_2$, and $\hat{\mathbf{n}}$ denotes the outward unit normal vector to ∂B_0 [37].

2.2.2 Cosserat Elastic Energy

The strain stored energy U_C of the body B_0 is defined by the integral [59]:

$$U_C = \int_{B_0} W\{\boldsymbol{\gamma}, \boldsymbol{\chi}\}\, dv, \tag{2.12}$$

where

$$\begin{aligned} W\{\boldsymbol{\gamma},\boldsymbol{\chi}\} &= \frac{\mu+\alpha}{2}\gamma_{ij}\gamma_{ij}+\frac{\mu-\alpha}{2}\gamma_{ij}\gamma_{ji}+\frac{\lambda}{2}\gamma_{kk}\gamma_{nn} \\ &+\frac{\gamma+\epsilon}{2}\chi_{ij}\chi_{ij}+\frac{\gamma-\epsilon}{2}\chi_{ij}\chi_{ji}+\frac{\beta}{2}\chi_{kk}\chi_{nn}, \end{aligned} \tag{2.13}$$

then the constitutive relations (2.5) - (2.6) can be written in the form:

$$\boldsymbol{\sigma} = \mathbf{C}_{\boldsymbol{\sigma}}\left[W\right] = \nabla_{\boldsymbol{\gamma}} W \text{ and } \boldsymbol{\mu} = \mathbf{C}_{\boldsymbol{\mu}}\left[W\right] = \nabla_{\boldsymbol{\chi}} W. \tag{2.14}$$

The function W is non-negative if and only if [59], [60]

$$\begin{aligned} \mu &> 0, \quad 3\lambda+2\mu>0, \\ \gamma &> 0, \quad 3\beta+2\gamma>0, \\ \alpha &> 0, \quad \mu+\alpha>0, \\ \epsilon &> 0, \quad \gamma+\epsilon>0. \end{aligned} \tag{2.15}$$

For future convenience, we present the stress energy

$$U_K = \int_{B_0} \Phi\left\{\boldsymbol{\sigma},\boldsymbol{\mu}\right\} dv,$$

where

$$\begin{aligned} \Phi\left\{\boldsymbol{\sigma},\boldsymbol{\mu}\right\} &= \frac{\mu'+\alpha'}{2}\sigma_{ij}\sigma_{ij}+\frac{\mu'-\alpha'}{2}\sigma_{ij}\sigma_{ji}+\frac{\lambda'}{2}\sigma_{kk}\sigma_{nn} \\ &+\frac{\gamma'+\epsilon'}{2}\mu_{ij}\mu_{ij}+\frac{\gamma'-\epsilon'}{2}\mu_{ij}\mu_{ji}+\frac{\beta'}{2}\mu_{kk}\mu_{nn}. \end{aligned} \tag{2.16}$$

The reversed constitutive relations (2.7) - (2.8) can be also written in form:

$$\boldsymbol{\gamma} = \mathbf{K}_{\gamma}\left[\boldsymbol{\sigma}\right] = \frac{\partial\Phi}{\partial\boldsymbol{\sigma}}, \ \boldsymbol{\chi} = \boldsymbol{K}_{\chi}\left[\boldsymbol{\mu}\right] = \frac{\partial\Phi}{\partial\boldsymbol{\mu}}. \tag{2.17}$$

The total internal work done by the stresses $\boldsymbol{\sigma}$ and $\boldsymbol{\mu}$ over the strains $\boldsymbol{\gamma}$ and $\boldsymbol{\chi}$ for the body B_0 [59] is

$$U = \int_{B_0} \left[\boldsymbol{\sigma}\cdot\boldsymbol{\gamma}+\boldsymbol{\mu}\cdot\boldsymbol{\chi}\right] dv \tag{2.18}$$

and

$$U = U_K = U_C$$

provided the constitutive relations (2.5) - (2.6) hold.

2.2.3 The Generalized Hellinger-Prange-Reissner Principle

The HPR principle [61] in the case of Cosserat elasticity states, that for any set $\mathscr{A}$ of all admissible states $\mathfrak{s} = [\hat{\mathbf{u}}, \hat{\boldsymbol{\varphi}}, \boldsymbol{\gamma}, \boldsymbol{\chi}, \boldsymbol{\sigma}, \boldsymbol{\mu}]$ that satisfy the strain-displacement and torsion-rotation relations (2.3) - (2.4), the zero variation

$$\delta\Theta(\mathfrak{s}) = 0$$

of the functional

$$\begin{aligned} \Theta(\mathfrak{s}) &= U_K - \int_{B_0} [\boldsymbol{\sigma}\cdot\boldsymbol{\gamma} + \boldsymbol{\mu}\cdot\boldsymbol{\chi}]\, dv \\ &+ \int_{\mathscr{G}_1} [\hat{\boldsymbol{\sigma}}_{\hat{\mathbf{n}}}\cdot(\hat{\mathbf{u}} - \hat{\mathbf{u}}_0) + \hat{\boldsymbol{\mu}}_{\hat{\mathbf{n}}}\,(\hat{\boldsymbol{\varphi}} - \hat{\boldsymbol{\varphi}}_0)]\, da + \int_{\mathscr{G}_2} [\hat{\boldsymbol{\sigma}}_0\cdot\hat{\mathbf{u}} + \hat{\boldsymbol{\mu}}_0\cdot\hat{\boldsymbol{\varphi}}]\, da \end{aligned} \tag{2.19}$$

at $\mathfrak{s} \in \mathscr{A}$ is equivalent of $\mathfrak{s}$ to be a solution of the system of equilibrium equations (2.1) - (2.2), constitutive relations (2.7) - (2.8), which satisfies the mixed boundary conditions (2.9) - (2.11). The proof is similar to the proof for HPR principle for classic linear elasticity [61].

2.3 The Cosserat Plate Assumptions

In this section we formulate our stress, couple stress and kinematic assumptions of the Cosserat plate. We consider the thin plate P where h is the thickness of the plate and $x_3 = 0$ contains its middle plane. The sets T and B are the top and bottom surfaces contained in the planes $x_3 = h/2$, $x_3 = -h/2$ respectively and the curve Γ is the boundary of the middle plane of the plate.

The set of points $P = \big(\Gamma \times [-\frac{h}{2}, \frac{h}{2}]\big) \cup T \cup B$ forms the entire surface of the plate and $\Gamma_u \times [-\frac{h}{2}, \frac{h}{2}]$ is the lateral part of the boundary where displacements and microrotations are prescribed. The notation $\Gamma_\sigma = \Gamma \backslash \Gamma_u$ of the remainder we use to describe the lateral part of the boundary edge $\Gamma_\sigma \times [-\frac{h}{2}, \frac{h}{2}]$ where stress and couple stress are prescribed. We also use notation P_0 for the middle plane internal domain of the plate.

In our case we consider the vertical load and pure twisting momentum boundary conditions at the top and bottom of the plate, which can be written in the form:

$$\sigma_{33}(x_1, x_2, h/2) = \sigma^t(x_1, x_2),\ \sigma_{33}(x_1, x_2, -h/2) = \sigma^b(x_1, x_2), \tag{2.20}$$

$$\sigma_{3\beta}(x_1, x_2, \pm h/2) = 0, \tag{2.21}$$

$$\mu_{33}(x_1, x_2, h/2) = \mu^t(x_1, x_2),\ \mu_{33}(x_1, x_2, -h/2) = \mu^b(x_1, x_2), \tag{2.22}$$

$$\mu_{3\beta}(x_1, x_2, \pm h/2) = 0, \tag{2.23}$$

where $(x_1, x_2) \in P_0$.

2.3.1 Stress and Couple Stress Assumptions

Our approach, which is a generalization of the theories of plates [35] and [36], assumes that the variation of stress σ_{kl} and couple stress μ_{kl} components across the thickness can be represented by means of polynomials of x_3 in such way that it will be consistent with the equilibrium equations (2.1) and (2.2).

First, as it is assumed in the standard theory of plates, we use expressions for the stress components in the following form [37]:

$$\sigma_{\alpha\beta} = \frac{h}{2}\zeta m_{\alpha\beta}(x_1, x_2), \tag{2.24}$$

where $\zeta = \frac{2}{h}x_3$, and $\alpha, \beta \in \{1, 2\}$. Based on (2.24) and by means of the first two equations of stress equilibrium (2.1) written in the component form

$$\sigma_{j\beta,j} = 0$$

we obtain for the shear stress components

$$\sigma_{3\beta} = q_\beta(x_1, x_2)\left(1 - \zeta^2\right), \tag{2.25}$$

We use expression for the stress components [37]:

$$\sigma_{\beta 3} = q^*_\beta(x_1, x_2)\left(1 - \zeta^2\right) + \hat{q}_\beta(x_1, x_2). \tag{2.26}$$

Substituting equations (2.26) in the remaining equilibrium differential equation for stress

$$\sigma_{j3,j} = 0$$

we obtain the expression for the transverse normal stress

$$\sigma_{33} = \zeta\left(\frac{1}{3}\zeta^2 - 1\right)k^*(x_1, x_2) + \zeta l^*(x_1, x_2) + m^*(x_1, x_2). \tag{2.27}$$

The next step is to accommodate approximations (2.27) to the boundary conditions (2.20). By direct substitution to (2.20) it easy to obtain that

$$\sigma_{33} = -\frac{3}{4}\left(\frac{1}{3}\zeta^3 - \zeta\right)p_1(x_1, x_2) + \zeta p_2(x_1, x_2) + \sigma_0(x_1, x_2), \tag{2.28}$$

where

$$p_1(x_1, x_2) + 2p_2(x_1, x_2) = p(x_1, x_2)$$

We consider the parametric solution of the last equation in the form:

$$\begin{aligned} p_1(x_1, x_2) &= \eta p(x_1, x_2), \\ p_2(x_1, x_2) &= \frac{(1-\eta)}{2}p(x_1, x_2) \end{aligned}$$

and η is a parameter, which we call the **splitting parameter**. This allows us to split the bending pressure on the plate $p(x_1, x_2)$ into two parts corresponding to different orders of stress approximation. The optimal value of the splitting parameter shows the contribution of different types of approximation in the plate bending. This approach gives a more accurate description of the mechanical phenomenon of bending.

Note that for

$$\begin{aligned} p(x_1, x_2) &= \sigma^t(x_1, x_2) - \sigma^b(x_1, x_2) \\ \sigma_0(x_1, x_2) &= \frac{1}{2}\left(\sigma^t(x_1, x_2) + \sigma^b(x_1, x_2)\right) \end{aligned}$$

the expression (2.28) satisfies the boundary condition requirements. Note that in the case of $\eta = 1$ expression (2.28) is identical to the expression of σ_{33} given in [36].

We use the following approximation for the couple stress components [37]:

$$\mu_{\alpha\beta} = \left(1 - \zeta^2\right) r_{\alpha\beta}(x_1, x_2) + r^*_{\alpha\beta}(x_1, x_2). \tag{2.29}$$

and couple stress:

$$\mu_{\beta 3} = \zeta s^*_\beta(x_1, x_2). \tag{2.30}$$

Note that the first two equations of (2.2) can be written in the form

$$\epsilon_{\beta jk}\sigma_{jk} + \mu_{j\beta,j} = 0, \tag{2.31}$$

and substituting the couple stress (2.29) in (2.31) and taking into account (2.25) and (2.26) we obtain the expression for the transverse shear couple stress:

$$\mu_{3\beta} = \left(\frac{1}{3}\zeta^3 - \zeta\right) s_\beta(x_1, x_2). \tag{2.32}$$

Substituting (2.32) to boundary conditions (2.23) we obtain that

$$s_\beta(x_1, x_2) = 0,$$

i.e. the transverse shear couple stress [36]:

$$\mu_{3\beta} = 0. \tag{2.33}$$

We use the assumption from [36], i.e. μ_{33} is a first order polynomial:

$$\mu_{33} = \zeta b^*(x_1, x_2) + c^*(x_1, x_2). \tag{2.34}$$

which satisfies the remaining differential equation of the equilibrium of angular momentum (2.2)

$$\epsilon_{3jk}\sigma_{jk} + \mu_{j3,j} = 0. \tag{2.35}$$

This assumption is also consistent with the equilibrium equation (2.35) and allows us to proceed as we did for the determination of transverse loading stress (2.28) from the stress boundary conditions. The boundary conditions (2.22) are sufficient to determine μ_{33}, which must be of the form [36]

$$\mu_{33} = \zeta v + t, \tag{2.36}$$

where the functions $v(x_1, x_2)$ and $t(x_1, x_2)$ are given as

$$\begin{aligned} v(x_1, x_2) &= \frac{1}{2}\left(\mu^t(x_1, x_2) - \mu^b(x_1, x_2)\right), \\ t(x_1, x_2) &= \frac{1}{2}\left(\mu^t(x_1, x_2) + \mu^b(x_1, x_2)\right). \end{aligned}$$

2.3.2 Kinematic Assumptions

The choice of kinematic assumptions is based on simplicity and their compatibility with the constitutive relationships of stress and couple stress assumptions

[37]:

$$u_\alpha = \zeta V_\alpha(x_1, x_2), \tag{2.37}$$

$$u_3 = w(x_1, x_2) + \left(1 - \zeta^2\right) w^*(x_1, x_2), \tag{2.38}$$

We also use the microrotation φ_α in the following form [37]:

$$\varphi_\alpha = \Theta_\alpha^0(x_1, x_2)\left(1 - \zeta^2\right) + \hat{\Theta}_\alpha(x_1, x_2), \tag{2.39}$$

$$\varphi_3 = \zeta\left(1 - \frac{1}{3}\zeta^2\right)\Theta_3(x_1, x_2). \tag{2.40}$$

The constitutive formulas motivate us to chose the forms (2.39) and (2.40), which produce expressions for $\varphi_{\alpha,\beta}$ and $\varphi_{3,3}$ similar to what we have for couple stress approximations (2.29).

2.4 HPR Variational Principle for Cosserat Plate

The HPR variational principle for a Cosserat plate is most appropriately expressed in terms of corresponding integrands calculated across the whole thickness. We also introduce the weighted characteristics of displacements, microrotations, strains and stresses of the plate, which will be used to produce the explicit forms of these integrands.

2.4.1 The Cosserat plate stress energy density

We define the plate stress energy density by the formula

$$\Phi(\mathscr{S}) = \frac{h}{2}\int_{-1}^{1} \Phi\left\{\sigma, \mu\right\} d\zeta_3. \tag{2.41}$$

Taking into account the stress and couple stress assumptions (2.24) - (2.36) and by the integrating $\Phi\left\{\sigma, \mu\right\}$ with respect ζ_3 in $[-1, 1]$ we obtain the explicit plate stress energy density expression in the form:

$$
\begin{aligned}
\Phi(\mathscr{S},\eta) \quad = \quad & -\frac{3\lambda}{h^3\mu(3\lambda+2\mu)}\left(M_{\alpha\alpha}M_{\beta\beta}+\frac{\alpha+\mu}{2h^3\alpha\mu}3M_{\alpha\beta}^2\right) \\
& +\frac{3\,(\alpha+\mu)}{160h^3\alpha\mu}\left[8\hat{Q}_\alpha\hat{Q}_\alpha+15Q_\alpha\hat{Q}_\alpha+20\hat{Q}_\alpha Q_\alpha^*+8Q_\alpha^*Q_\alpha^*\right] \\
& +\frac{\alpha-\mu}{2h^3\alpha\mu}3M_{\alpha\beta}^2+\frac{\alpha-\mu}{280h^3\alpha\mu}\left[21Q_\alpha\left(5\hat{Q}_\alpha+4Q_\alpha^*\right)\right] \\
& -\frac{\gamma-\epsilon}{160h\gamma\epsilon}\left[24R_{\alpha\alpha}^2+45R_{\alpha\alpha}^*+60R_{\alpha\beta}R_{\alpha\beta}^*+48R_{12}R_{21}\right] \\
& +\frac{\gamma+\epsilon}{2h^3\gamma\epsilon}3S_\alpha^*S_\alpha^*+\frac{\lambda}{560h\mu(3\lambda+2\mu)}\frac{5+3\eta}{(1+\eta)}pM_{\alpha\alpha} \\
& +\frac{\gamma+\epsilon}{160h^3\gamma\epsilon}\left[8R_{\alpha\beta}^2+15R_{\alpha\beta}^*R_{\alpha\beta}^*+20R_{\alpha\beta}R_{\alpha\beta}^*\right] \\
& +\frac{3\beta}{80h\gamma(3\beta+2\gamma)}\left[8R_{\alpha\alpha}R_{\beta\beta}+15R_{\alpha\alpha}^*R_{\beta\beta}^*+20R_{\alpha\alpha}R_{\alpha\alpha}^*\right] \\
& -\frac{\beta}{4\gamma(3\beta+2\gamma)}\left[(2R_{\alpha\alpha}+3R_{\alpha\alpha}^*)t-h\left(v^2+t^2\right)\right] \\
& +\frac{(\lambda+\mu)\,h}{840\mu(3\lambda+2\mu)}\left(\frac{140+168\eta+51\eta^2}{4(1+\eta)^2}\right)p^2 \\
& +\frac{(\lambda+\mu)\,h}{2\mu(3\lambda+2\mu)}\sigma_0^2+\frac{\epsilon h}{12h\gamma\epsilon}\left(3t^2+v^2\right)
\end{aligned}
\tag{2.42}
$$

where $\mathscr{S}$ the Cosserat stress set

$$
\mathscr{S}=\left[M_{\alpha\beta},Q_\alpha,Q_\alpha^*,\hat{Q}_\alpha,R_{\alpha\beta},R_{\alpha\beta}^*,S_\beta^*\right]
\tag{2.43}
$$

Here we define the variables

$$\begin{aligned}
M_{\alpha\beta} &= \left(\frac{h}{2}\right)^2 \int_{-1}^{1} \zeta_3 \sigma_{\alpha\beta} d\zeta_3 = \frac{h^3}{12} m_{\alpha\beta}, \\
Q_\alpha &= \frac{h}{2} \int_{-1}^{1} \sigma_{3\alpha} d\zeta_3 = \frac{2h}{3} q_\alpha, \\
Q_\alpha^* &= \frac{h}{2} \int_{-1}^{1} q_\alpha^* \left(1 - \zeta^2\right) d\zeta_3 = \frac{2h}{3} q_\alpha^*, \\
\hat{Q}_\alpha &= \frac{h}{2} \int_{-1}^{1} \hat{q}_\alpha \left(1 - \zeta^2\right) d\zeta_3 = \frac{2h}{3} \hat{q}_\alpha \\
R_{\alpha\beta} &= \frac{h}{2} \int_{-1}^{1} r_{\alpha\beta} \left(1 - \zeta^2\right) d\zeta_3 = \frac{2h}{3} r_{\alpha\beta}, \\
R_{\alpha\beta}^* &= \frac{h}{2} \int_{-1}^{1} r_{\alpha\beta}^* \left(1 - \zeta^2\right) d\zeta_3 = \frac{2h}{3} r_{\alpha\beta}^*, \\
S_\alpha^* &= \left(\frac{h}{2}\right)^2 \int_{-1}^{1} \zeta_3 \mu_{\alpha 3} d\zeta_3 = \frac{h^3}{12} s_\alpha^*.
\end{aligned}$$

Here M_{11} and M_{22} are the bending moments, M_{12} and M_{21} – twisting moments, Q_α – shear forces, Q_α^*, $\hat{Q}_\alpha$ – transverse shear forces, R_{11}, R_{22}, R_{11}^*, R_{22}^* – micropolar bending moments, R_{12}, R_{21}, R_{12}^* ,R_{21}^* – micropolar twisting moments, S_α^* – micropolar couple moments, all defined per unit length.

Then the stress energy of the plate P

$$U_K^{\mathscr{S}} = \int_{P_0} \Phi(\mathscr{S}, \eta) da, \tag{2.44}$$

where P_0 is the internal domain of the middle plane of the plate P.

2.4.2 The density of the work over the plate boundary

In the following consideration we also assume that the proposed stress, couple stress, and kinematic assumptions are valid for the lateral boundary of the plate P as well.

We evaluate the density of the work over the boundary $\Gamma_u \times [-h/2, h/2]$

$$\mathscr{W}_1 = \frac{h}{2}\int_{-1}^{1} [\sigma_{\mathbf{n}} \cdot \mathbf{u} + \mu_{\mathbf{n}} \cdot \varphi]\, d\zeta_3. \tag{2.45}$$

Taking into account the stress and couple stress assumptions (2.24) - (2.36) and kinematic assumptions (2.37) - (2.40) we are able to represent $\mathscr{W}_1$ by the following expression:

$$\mathscr{W}_1 = \mathscr{S}_n \cdot \mathscr{U} = \check{M}_\alpha \Psi_\alpha + \check{Q}_\alpha^* W + \check{Q}_\alpha^{\hat{}} W^* + \check{R}_\alpha \Omega_\alpha^0 + \check{R}_\alpha^* \hat{\Omega}_\alpha^0 + \check{S}^* \Omega_3, \tag{2.46}$$

where the set $\mathscr{S}_n$ is defined as

$$\mathscr{S}_n \;=\; \left[\check{M}_\alpha, \check{Q}^*, \check{Q}_\alpha^{\hat{}}, \check{R}_\alpha, \check{R}_\alpha^*, \check{S}^*\right],$$

and

$$\begin{aligned}
\check{M}_\alpha &= M_{\alpha\beta} n_\beta,\ \check{Q}^* = Q_\beta^* n_\beta,\ \check{R}_\alpha = R_{\alpha\beta} n_\beta,\\
\check{S}^* &= S_\beta^* n_\beta, \check{Q}^{\hat{}} = \check{Q}_\beta^{\hat{}} n_\beta,\ \check{R}_\alpha^* = \check{R}_{\alpha\beta}^* n_\beta.
\end{aligned}$$

In the above n_β is the outward unit normal vector to Γ_u and

$$\begin{aligned}
\Psi_\alpha &= \frac{3}{h}\int_{-1}^{1} \zeta_3 u_\alpha d\zeta_3,\\
W &= \frac{3}{4}\int_{-1}^{1} \left(1-\zeta^2\right) w d\zeta_3,\\
W^* &= \frac{3}{4}\left(1-\zeta^2\right)^2 w^* d\zeta_3,\\
\Omega_\alpha^0 &= \frac{3}{4}\int_{-1}^{1} \left(1-\zeta^2\right) \Theta_\alpha^0 d\zeta_3,\\
\hat{\Omega}_\alpha &= \frac{3}{4}\int_{-1}^{1} \left(1-\zeta^2\right) \hat{\Theta}_\alpha^0 d\zeta_3,\\
\Omega_3 &= \frac{3}{h}\int_{-1}^{1} \zeta_3 \varphi_3 d\zeta_3,
\end{aligned}$$

Here Ψ_α are the rotations of the middle plane around x_α axis, $W + W^*$ the vertical deflection of the middle plate, $\Omega_k^0 + \widehat{\Omega}_\alpha$ the microrotations in the middle plate around

x_k axis, U_α is the in-plane displacements of the middle plane along x_a axis, Ω_3 the rate of change of the microrotation φ_3 along x_3.

Therefore we can introduce the set of kinematic variables defined as

$$\mathscr{U} = \left[\Psi_\alpha, W, \Theta_3, \Theta_\alpha^0, W^*, \hat{\Theta}_\alpha\right]^T,$$

We also obtain the correspondence between the weighted displacements and the microrotations and the kinematic variables:

$$\begin{aligned}
\Psi_\alpha &= V_\alpha(x_1,x_2), W = w(x_1,x_2),\ W^* = w^*(x_1,x_2),\\
\Omega_\alpha^0 &= k_1\Theta_\alpha^0(x_1,x_2),\ \hat{\Omega}_\alpha = \hat{\Theta}_\alpha(x_1,x_2),\ \Omega_3 = \frac{k_2}{h}\Theta_3(x_1,x_2),\\
U_\alpha &= U_\alpha(x_1,x_2),\ \Omega_3^0 = \Theta_3^0(x_1,x_2),
\end{aligned}$$

where coefficients k_1 and k_2 depend on the variation of microrotations. Under the conditions (2.40) we have that $k_1 = \frac{4}{5}$ and $k_2 = \frac{8}{5}$.

The density of the work over the boundary $\Gamma_\sigma \times [-h/2, h/2]$

$$\mathscr{W}_2 = \frac{h}{2}\int_{-1}^{1}\left(\sigma_{o\alpha}u_\alpha + m_{o\alpha}\varphi_\alpha\right)n_\alpha d\zeta_3$$

can be presented in the form

$$\mathscr{W}_2 = \mathscr{S}_o\cdot\mathscr{U} = \Pi_{o\alpha}\Psi_\alpha + \Pi_{o3}W + \Pi_{o3}^*W^* + M_{o\alpha}\Omega_\alpha^0 + M_{o\alpha}^*\hat{\Omega}_\alpha + M_{o3}^*\Omega_3,$$

where

$$\begin{aligned}
M_{\alpha\beta}n_\beta &= \Pi_{o\alpha},\ R_{\alpha\beta}n_\beta = M_{o\alpha},\\
Q_\alpha^*n_\alpha &= \Pi_{o3},\ S_\alpha^*n_\alpha = M_{o3}^*,\\
\hat{Q}_\alpha n_\alpha &= \Pi_{o3}^*,\ R_{\alpha\beta}^*n_\beta = M_{o\alpha}^*.
\end{aligned}$$

Now n_β is the outward unit normal vector to Γ_σ, and

$$\begin{aligned}
\Pi_{o\alpha} &= \left(\frac{h}{2}\right)^2 \int_{-1}^{1} \zeta_3 \sigma_{o\alpha} d\zeta_3, \;\; M_{o\alpha} = \frac{h}{2}\int_{-1}^{1} \mu_{o\alpha} d\zeta_3, \\
\Pi_{o3} &= \frac{h}{2}\int_{-1}^{1} (\sigma_{o3} - \sigma_0)\, d\zeta_3, \;\; M^*_{o3} = \frac{h}{2}\int_{-1}^{1} (\mu_{o3} - t n_3) d\zeta_3, \\
\Pi^*_{o3} &= \frac{h}{2}\int_{-1}^{1} (\sigma_{o3} - \sigma_0)\, d\zeta_3, \;\; M^*_{o\alpha} = \frac{h}{2}\int_{-1}^{1} \mu_{o\alpha} d\zeta_3.
\end{aligned} \tag{2.47}$$

We are able to evaluate the work done at the top and bottom of the Cosserat plate by using boundary conditions (2.20) and (2.22)

$$\int_{T\cup B} (\sigma_{o3} u_3 + m_{o3}\varphi_{o3})\, n_3 da = \int_{P_0} (pW + v\Omega_3^0) da.$$

2.4.3 The Cosserat plate internal work density

Here we define the density of the work done by the stress and couple stress over the Cosserat strain field:

$$\mathscr{W}_3 = \frac{h}{2}\int_{-1}^{1} (\sigma\cdot\gamma + \mu\cdot\chi)\, d\zeta_3. \tag{2.48}$$

Substituting stress and couple stress assumptions (2.24) - (2.36) and integrating expression (2.48) we obtain the following expression:

$$\mathscr{W}_3 = \mathscr{S}\cdot\mathscr{E} \;\; = \;\; M_{\alpha\beta} e_{\alpha\beta} + Q_\alpha \omega_\alpha + Q^*_{3\alpha}\omega^*_\alpha + \hat{Q}_\alpha \hat{\omega}_\alpha + R_{\alpha\beta}\tau_{\alpha\beta} + R^*_{\alpha\beta}\tau^*_{\alpha\beta} + S^*_\alpha \tau_{3\alpha},$$

where $\mathscr{E}$ is the Cosserat plate strain set of the the weighted averages of strain and torsion tensors

$$\mathscr{E} = \left[e_{\alpha\beta}, \omega_\beta, \omega^*_\alpha, \hat{\omega}_\alpha, \tau_{3\alpha}, \tau_{\alpha\beta}, \tau^*_{\alpha\beta}\right].$$

Here the components of $\mathscr{E}$ are

$$e_{\alpha\beta} = \frac{3}{h}\int_{-1}^{1} \zeta_3\gamma_{\alpha\beta}d\zeta_3, \tag{2.49}$$

$$\omega_\alpha = \frac{3}{4}\int_{-1}^{1} \gamma_{3\alpha}\left(1-\zeta^2\right)d\zeta_3, \tag{2.50}$$

$$\omega_\alpha^* = \frac{3}{4}\int_{-1}^{1} \gamma_{\alpha 3}\left(1-\zeta^2\right)d\zeta_3, \tag{2.51}$$

$$\hat{\omega}_\alpha = \frac{3}{4}\int_{-1}^{1} \gamma_{\alpha 3}d\zeta_3, \tag{2.52}$$

$$\tau_{3\alpha} = \frac{3}{h}\int_{-1}^{1} \zeta_3\chi_{3\alpha}d\zeta_3, \tag{2.53}$$

$$\tau_{\alpha\beta} = \frac{3}{4}\int_{-1}^{1} \chi_{\alpha\beta}\left(1-\zeta^2\right)d\zeta_3, \tag{2.54}$$

$$\tau_{\alpha\beta}^* = \frac{3}{4}\int_{-1}^{1} \chi_{\alpha\beta}d\zeta_3. \tag{2.55}$$

The components of Cosserat plate strain (2.49)-(2.55) can also be represented in terms of the components of set $\mathscr{U}$ by the following formulas:

$$e_{\alpha\beta} = \Psi_{\beta,\alpha} + \varepsilon_{3\alpha\beta}\Omega_3, \tag{2.56}$$

$$\omega_\alpha = \Psi_\alpha + \varepsilon_{3\alpha\beta}\left(\Omega_\beta^0 + \hat{\Omega}_\beta\right), \tag{2.57}$$

$$\omega_\alpha^* = W_{,\alpha} + \frac{4}{5}W_{,\alpha}^* + \varepsilon_{3\alpha\beta}\left(\Omega_\beta^0 + \hat{\Omega}_\beta\right), \tag{2.58}$$

$$\hat{\omega}_\alpha = \frac{3}{2}W_{,\alpha} + W_{,\alpha}^* + \varepsilon_{3\alpha\beta}\left(\frac{5}{4}\Omega_\beta^0 + \frac{3}{2}\hat{\Omega}_\beta\right), \tag{2.59}$$

$$\tau_{3\alpha} = \Omega_{3,\alpha}, \tag{2.60}$$

$$\tau_{\alpha\beta} = \Omega_{\beta,\alpha}^0 + \hat{\Omega}_{\beta,\alpha}, \tag{2.61}$$

$$\tau_{\alpha\beta}^* = \frac{5}{4}\Omega_{\beta,\alpha}^0 + \frac{3}{2}\hat{\Omega}_{\beta,\alpha}, \tag{2.62}$$

We call the relations (2.56) - (2.62) the Cosserat plate strain-displacement relation.

2.5 Cosserat Plate HPR Principle

It is natural now to reformulate HPR variational principle for the Cosserat plate.

Theorem 1. *Let $\mathscr{A}$ denote the set of all admissible states that satisfy the Cosserat plate strain-displacement relations (2.56) - (2.62) and let Θ be a HPR functional on $\mathscr{A}$ defined by*

$$\begin{aligned}\Theta(s,\eta) &= U_K^S(\eta) - \int\limits_{P_0} (\mathscr{S}\cdot\mathscr{E} - P\cdot\mathscr{W} + \upsilon\Omega_3^0)da \\ &\quad + \int_{\Gamma_\sigma} \mathscr{S}_o\cdot(\mathscr{U} - \mathscr{U}_o)\, ds + \int_{\Gamma_u} \mathscr{S}_n\cdot\mathscr{U}\, ds, \end{aligned} \tag{2.63}$$

for every $s = [\mathscr{U}, \mathscr{E}, \mathscr{S}] \in \mathscr{A}$. Here $P = (\hat{p}_1, \hat{p}_2)$ and $\mathscr{W} = (W, W^*)$.

The optimization

$$\delta\Theta(s,\eta) = 0$$

is equivalent to the following [37]:

A. The equilibrium system of equations for the plate bending

$$M_{\alpha\beta,\alpha} - Q_\beta = 0, \tag{2.64}$$

$$Q^*_{\alpha,\alpha} + \hat{p}_1 = 0, \tag{2.65}$$

$$R_{\alpha\beta,\alpha} + \varepsilon_{3\beta\gamma}\left(Q^*_\gamma - Q_\gamma\right) = 0, \tag{2.66}$$

$$\varepsilon_{3\beta\gamma}M_{\beta\gamma} + S^*_{\alpha,\alpha} = 0, \tag{2.67}$$

$$\hat{Q}_{\alpha,\alpha} + \hat{p}_2 = 0, \tag{2.68}$$

$$R^*_{\alpha\beta,\alpha} + \varepsilon_{3\beta\gamma}\hat{Q}_\gamma = 0, \tag{2.69}$$

where $\hat{p}_1 = \eta p$, $\hat{p}_2 = \frac{2}{3}(1-\eta)\,p$ and η is the splitting parameter, with the resultant traction boundary conditions :

$$M_{\alpha\beta}n_{\beta} = \Pi_{o\alpha},\ R_{\alpha\beta}n_{\beta} = M_{o\alpha}, \tag{2.70}$$

$$Q^*_{\alpha}n_{\alpha} = \Pi_{o3},\ S^*_{\alpha}n_{\alpha} = \Upsilon_{o3}, \tag{2.71}$$

at the part Γ_σ and he resultant displacement boundary conditions

$$\Psi_\alpha = \Psi_{o\alpha},\ W = W_o,\ \Omega^0_\alpha = \Omega^0_{o\alpha},\ \Omega_3 = \Omega_{o3}, \tag{2.72}$$

at the part Γ_u.

B. The zero variation of the stress energy with respect to the splitting parameter

$$\delta U^S_K(\eta) = 0;$$

C: The constitutive formulas:

$$\begin{aligned} e_{\alpha\alpha} &= \frac{\partial\Phi}{\partial M_{\alpha\alpha}} = \frac{12(\lambda+\mu)}{h^3\mu(3\lambda+2\mu)}M_{\alpha\alpha} - \\ &\quad |\varepsilon_{\alpha\beta3}|\frac{6\lambda}{h^3\mu(3\lambda+2\mu)}M_{\beta\beta} - \frac{\lambda\,(3p_1+5p_2)}{5h\mu(3\lambda+2\mu)}, \end{aligned} \tag{2.73}$$

$$e_{\alpha\beta} = \frac{\partial\Phi}{\partial M_{\alpha\beta}} = \frac{3(\alpha+\mu)}{h^3\alpha\mu}M_{\alpha\beta} + \frac{3(\alpha-\mu)}{h^3\alpha\mu}M_{\beta\alpha},\ \alpha\neq\beta \tag{2.74}$$

$$\omega_\alpha = \frac{\partial\Phi}{\partial Q_\alpha} = \frac{3(\alpha-\mu)}{10h\alpha\mu}Q^*_\alpha + \frac{3(\alpha+\mu)}{10h\alpha\mu}Q_\alpha + \frac{3(\alpha-\mu)}{8h\alpha\mu}\hat{Q}_\alpha, \tag{2.75}$$

$$\omega^*_\alpha = \frac{\partial\Phi}{\partial Q^*_\alpha} = \frac{3(\alpha-\mu)}{10h\alpha\mu}Q_\alpha + \frac{3(\alpha+\mu)}{10h\alpha\mu}Q^*_\alpha + \frac{3(\alpha+\mu)}{8h\alpha\mu}\hat{Q}_\alpha, \tag{2.76}$$

$$\begin{aligned}
\tau^0_{\alpha\alpha} &= \frac{\partial \Phi}{\partial R_{\alpha\alpha}} = \frac{6(\beta+\gamma)}{5h\gamma(3\beta+2\gamma)} R_{\alpha\alpha} - |\varepsilon_{\alpha\beta 3}| \frac{3\beta}{5h\gamma(3\beta+2\gamma)} R^*_{\beta\beta} \\
&\quad + \frac{3(\beta+\gamma)}{2h\gamma(3\beta+2\gamma)} R^*_{\alpha\alpha} - |\varepsilon_{\alpha\beta 3}| \frac{3\beta}{4h\gamma(3\beta+2\gamma)} R_{\beta\beta}, \qquad (2.77) \\
\tau^0_{\alpha\beta} &= \frac{\partial \Phi}{\partial R_{\beta\alpha}} = \frac{3(\epsilon+\gamma)}{10h\gamma\epsilon} R_{\alpha\beta} - \frac{3(\gamma-\epsilon)}{10h\gamma\epsilon} R_{\beta\alpha} \\
&\quad + \frac{3(\epsilon+\gamma)}{8h\gamma\epsilon} R^*_{\alpha\beta} - \frac{3(\gamma-\epsilon)}{8h\gamma\epsilon} R^*_{\beta\alpha}, \;\; \alpha \neq \beta \qquad (2.78) \\
\widehat{\omega^*_\alpha} &= \frac{\partial \Phi}{\partial \widehat{Q_\alpha}} = \frac{3(\alpha-\mu)}{8h\alpha\mu} Q_\alpha + \frac{3(\alpha+\mu)}{8h\alpha\mu} Q^*_\alpha + \frac{9(\alpha+\mu)}{16h\alpha\mu} \hat{Q}_\alpha, \qquad (2.79) \\
\tau^*_{\alpha\alpha} &= \frac{\partial \Phi}{\partial R^*_{\alpha\alpha}} = \frac{3(\beta+\gamma)}{2h\gamma(3\beta+2\gamma)} R_{\alpha\alpha} - |\varepsilon_{\alpha\beta 3}| \frac{9\beta}{8h\gamma(3\beta+2\gamma)} R^*_{\beta\beta} \\
&\quad + \frac{3(\beta+\gamma)}{4h\gamma(3\beta+2\gamma)} R^*_{\alpha\alpha} |\varepsilon_{\alpha\beta 3}| \frac{3\beta}{4h\gamma(3\beta+2\gamma)} R_{\beta\beta}, \qquad (2.80) \\
\tau^*_{\alpha\beta} &= \frac{\partial \Phi}{\partial R^*_{\alpha\beta}} = \frac{3(\epsilon+\gamma)}{8h\gamma\epsilon} R_{\alpha\beta} - \frac{3(\gamma-\epsilon)}{8h\gamma\epsilon} R_{\beta\alpha} \\
&\quad + \frac{3(\epsilon+\gamma)}{16h\gamma\epsilon} R^*_{\alpha\beta} - \frac{3(\gamma-\epsilon)}{16h\gamma\epsilon} R^*_{\beta\alpha}, \;\; \alpha \neq \beta \qquad (2.81)
\end{aligned}$$

$$\tau_{3\alpha} = \frac{\partial \Phi}{\partial S^*_\alpha} = \frac{3(\gamma+\epsilon)}{h^3\gamma\epsilon} S^*_\alpha. \qquad (2.82)$$

Proof 1. *The variation of* $\Theta(s)$

$$\begin{aligned}
\delta\Theta(s) &= \delta U^S_K(\eta) + \int_{P_0} \left\{ (\mathscr{K}[\mathscr{S}] - \mathscr{E}) \cdot \delta\mathscr{S} - \mathscr{S}\delta\mathscr{E} + p\delta W + v\delta\Omega^0_3 \right\} da \\
&\quad + \int_{\Gamma_\sigma} \{\delta\mathscr{S}_o \cdot (\mathscr{U} - \mathscr{U}_o) + \mathscr{S}_o \cdot \delta\mathscr{U}\}\, ds + \int_{\Gamma_u} \mathscr{S}_n \cdot \delta\mathscr{U}\, ds.
\end{aligned}$$

We apply Green's theorem and integration by parts for $\mathscr{S}$ *and* $\delta\mathscr{U}$ *[61] to the expression:*

$$\begin{aligned}\int\limits_{P_0} \mathscr{S}\cdot\delta\mathscr{E}da &= \int\limits_{\partial P_0} \mathscr{S}_o\delta\cdot\mathscr{U}\ ds - \int\limits_{P_0} \{(M_{\alpha\beta,\alpha}-Q_\beta)\,\delta\Psi_\beta + Q^*_{\alpha,\alpha}\delta W \\ &+ \left(R_{\alpha\beta,\alpha} + \varepsilon_{3\beta\gamma}\left(Q^*_\gamma - Q_\gamma\right)R_{\alpha\beta,\alpha}\right)\delta\Omega^0_\beta \\ &+ \left(S^*_{\alpha,\alpha} + \epsilon_{3\beta\gamma}M_{\beta\gamma}\right)\delta\Omega_3\}da.\end{aligned}$$

Then based on the fact that $\delta\mathscr{U}$ *and* $\delta\mathscr{E}$ *satisfy the Cosserat plate strain-displacement relation, we obtain*

$$\begin{aligned}\delta\Theta(s,\eta) &= \delta U^S_K(\eta) + \int\limits_{P_0} \{(\mathscr{K}[\mathscr{S}]-\mathscr{E})\cdot\delta\mathscr{S} - \mathscr{S}\delta\mathscr{E}\}\,da \\ &+ \int\limits_{P_0} \{(M_{\alpha\beta,\alpha}-Q_\beta)\,\delta\Psi_\beta + \left(Q^*_{\alpha,\alpha}+\hat{p}_1\right)\delta W + \left(\hat{Q}_{\alpha,\alpha}+\hat{p}_2\right)\delta W \\ &+ \left(R_{\alpha\beta,\alpha} + \varepsilon_{3\beta\gamma}\left(Q^*_\gamma - Q_\gamma\right)R_{\alpha\beta,\alpha}\right)\delta\Omega^0_\beta \\ &+ \left(R^*_{\alpha\beta,\alpha} + \varepsilon_{3\beta\gamma}\hat{Q}_\gamma\right)\delta\Omega^0_\beta \\ &+ \left(S^*_{\alpha,\alpha} + \epsilon_{3\beta\gamma}M_{\beta\gamma}\right)\delta\Omega_3\}da \\ &+ \int_{\Gamma_\sigma} \delta\mathscr{S}_o\cdot(\mathscr{U}-\mathscr{U}_o)\,ds + \int_{\Gamma_u} (\mathscr{S}_o - \mathscr{S}_n)\cdot\delta\mathscr{U}\,ds.\end{aligned}$$

If s *is a solution of the mixed problem, then*

$$\delta\Theta(s,\eta) = 0.$$

On the other hand, some extensions of the fundamental lemma of calculus of variations [61] together with the fact that $\mathscr{U}$ *and* $\mathscr{E}$ *satisfy the Cosserat plate strain-displacement relations (2.56) - (2.62) imply that* $\mathscr{S}$ *is a solution of the A and B mixed problems.* ■

Remark. The above equilibrium equations and boundary conditions for the Cosserat plate can also be obtained by substituting polynomial approximations of stress and couple stress directly to the elastic equilibrium (2.1) - (2.2) and the boundary conditions (2.20) - (2.23) and collecting and equating to zero all coefficients of the resulting polynomials with respect to variable x_3.

The constitutive formulas can also be given in the following reverse form[1]

$$M_{\alpha\alpha} = \frac{h^3\mu(\lambda+\mu)}{3(\lambda+2\mu)}\Psi_{\alpha,\alpha} + \frac{\lambda\mu h^3}{6(\lambda+2\mu)}\Psi_{\beta,\beta} + \frac{(3p_1+5p_2)\,\lambda h^2}{30(\lambda+2\mu)}, \tag{2.83}$$

$$M_{\beta\alpha} = \frac{(\mu-\alpha)\,h^3}{12}\Psi_{\alpha,\beta} + \frac{h^3(\alpha+\mu)}{12}\Psi_{\beta,\alpha} + (-1)^{\beta}\frac{\alpha h^3}{6}\Omega_3, \tag{2.84}$$

$$R_{\beta\alpha} = \frac{5\,(\gamma-\epsilon)\,h}{6}\Omega^0_{\beta,\alpha} + \frac{5h\,(\gamma+\epsilon)}{6}\Omega^0_{\alpha,\beta}, \tag{2.85}$$

$$R_{\alpha\alpha} = \frac{10h\gamma\,(\beta+\gamma)}{3\,(\beta+2\gamma)}\Omega^0_{\alpha,\alpha} + \frac{5h\beta\gamma}{3(\beta+2\gamma)}\Omega^0_{\beta,\beta}, \tag{2.86}$$

$$R^*_{\beta\alpha} = \frac{2\,(\gamma-\epsilon)\,h}{3}\hat{\Omega}_{\beta,\alpha} + \frac{2\,(\gamma+\epsilon)\,h}{3}\hat{\Omega}_{\alpha,\beta}, \tag{2.87}$$

$$R^*_{\alpha\alpha} = \frac{8\gamma\,(\gamma+\beta)\,h}{3(\beta+2\gamma)}\hat{\Omega}_{\alpha,\alpha} + \frac{4\gamma\beta h}{3(\beta+2\gamma)}\hat{\Omega}_{\beta,\beta}, \tag{2.88}$$

$$\begin{aligned} Q_\alpha &= \frac{5h(\alpha+\mu)}{6}\Psi_\alpha + \frac{5\,(\mu-\alpha)\,h}{6}W_{,\alpha} + \frac{2\,(\mu-\alpha)\,h}{3}W^*_{,\alpha} \\ &\quad + (-1)^{\beta}\frac{5h\alpha}{3}\left(\Omega^0_\beta + \hat{\Omega}_\beta\right), \end{aligned} \tag{2.89}$$

$$\begin{aligned} Q^*_\alpha &= \frac{5\,(\mu-\alpha)\,h}{6}\Psi_\alpha + \frac{5\,(\mu-\alpha)^2\,h}{6\,(\mu+\alpha)}W_{,\alpha} + \frac{2\,(\mu+\alpha)\,h}{3}W^*_{,\alpha} \\ &\quad + (-1)^{\alpha}\frac{5h\alpha}{3}\left(\Omega^0_\beta + \frac{(\mu-\alpha)}{(\mu+\alpha)}\hat{\Omega}_\beta\right), \end{aligned} \tag{2.90}$$

$$\hat{Q}_\alpha = \frac{8\alpha\mu h}{3\,(\mu+\alpha)}W_{,\alpha} + (-1)^{\alpha}\frac{8\alpha\mu h}{3\,(\mu+\alpha)}\hat{\Omega}_\beta, \tag{2.91}$$

$$S^*_\alpha = \frac{5\gamma\epsilon h^3}{3\,(\gamma+\epsilon)}\Omega_{3,\alpha}. \tag{2.92}$$

[1] In the following formulas a subindex $\beta = 1$ iff $\alpha = 2$ and $\beta = 2$ iff $\alpha = 1$

2.6 Solution Uniqueness

Here we prove that if there is a solution for the deformation of a Cosserat elastic plate, which satisfies the equilibrium equations (2.64) - (2.69), constitutive (2.73) - (2.82), and kinematics formulas (2.56) - (2.62) with boundary conditions (2.70), (2.71) at Γ_σ and (2.72) at Γ_u then this elastic solution must be unique. We also assume that all functions and the plate middle plane region P_0 satisfy Green - Gauss theorem requirements.

We present a proof by contradiction. Let us assume that the solution of the Cosserat plate is not unique in terms of the stresses and strains, i.e. there would be two different solutions of (2.64) - (2.69), both of which satisfy the same boundary conditions (2.70), (2.71) at Γ_σ and (2.72) at Γ_u. Due to linearity of the proposed model, the difference between these two different solutions is also a solution of the same system of equations with the following zero boundary conditions:

$$M_{\alpha\beta}n_\beta = 0, \; R_{\alpha\beta}n_\beta = 0, \tag{2.93}$$

$$R^*_{\alpha\beta}n_\beta = 0, \; \hat{Q}_\alpha n_\alpha = 0, \tag{2.94}$$

$$Q^*_\alpha n_\alpha = 0, \; S^*_\alpha n_\alpha = 0, \tag{2.95}$$

It can be shown that for zero loads, the internal work U can be expressed by applying integration by parts as follows:

$$\begin{aligned} U = & \int_{P_0} \mathscr{S} \cdot \mathscr{E} da = \int_{P_0} ((\check{M}_{\alpha\beta}\Psi_\alpha + \check{Q}^*_\beta W + \check{Q}\hat{}_\beta W^* \\ & + \check{R}_{\alpha\beta}\Omega^0_\alpha + \check{R}^*_{\alpha\beta}\hat{\Omega}^0_\alpha + \check{S}^*_\beta \Omega_3 + \check{N}_{\alpha\beta}U_\alpha + \check{M}^*_\beta \Omega^0_3)_{,\beta} \\ & - (M_{\alpha\beta,\alpha} - Q_\beta)\Psi_\beta - Q^*_{\alpha,\alpha}W - \hat{Q}_{\alpha,\alpha}W^* \\ & - \left(R_{\alpha\beta,\alpha} + \varepsilon_{3\beta\gamma}\left(Q^*_\gamma - Q_\gamma\right) R_{\alpha\beta,\alpha}\right)\Omega^0_\beta \\ & -(R^*_{\alpha\beta,\alpha} + \varepsilon_{3\beta\gamma}\hat{Q}_\gamma)\hat{\Omega}^0_\alpha \\ & - \left(S^*_{\alpha,\alpha} + \epsilon_{3\beta\gamma}M_{\beta\gamma}\right)\Omega_3)da. \end{aligned}$$

Taking into account Green's theorem, the equilibrium equations (2.64) - (2.69), the upper expression is reduced to the following line integral:

$$\begin{aligned} U &= \oint_\Gamma \mathscr{S}_n \cdot \mathscr{U}\, ds = \oint_\Gamma (\check{M}_{\alpha\beta\alpha\beta}\Psi_\alpha + \check{Q}^*_\beta W + \check{Q}\hat{_\beta} W^* \\ &\quad + \check{R}_{\alpha\beta}\Omega^0_\alpha + \check{R}^*_{\alpha\beta}\hat{\Omega}^0_\alpha + \check{S}^*_\beta \Omega_3) ds = 0, \end{aligned} \tag{2.96}$$

which vanishes because of the zero boundary conditions (2.93) - (2.95).

Using the constitutive equations in the reversible form (2.83) - (2.92), the positive definite quadratic form strain energy density (2.42) can be represented in terms of the Cosserat plate strain set $\mathscr{E}$, which components in this case should be zeros. Thus the difference between any two deformations and microrotations of the plate, having the same boundary conditions, represents changes of the plate as a rigid body. So the solutions are identical in terms of stress and strain components. This contradiction completes the proof of uniqueness.

2.7 Cosserat Plate Field Equations

In order to obtain the micropolar plate bending field equations in terms of the kinematic variables, we substitute the constitutive formulas in the reverse form (2.83) - (2.92) into the bending system of equations (2.64) - (2.69). The micropolar plate bending field equations can be written in the following form [46]:

$$L\mathscr{U} = f\,(\eta) \tag{2.97}$$

where

$$L = \begin{bmatrix} L_{11} & L_{12} & L_{13} & L_{14} & 0 & L_{16} & k_1 L_{13} & 0 & L_{16} \\ L_{12} & L_{22} & L_{23} & L_{24} & L_{16} & 0 & k_1 L_{23} & L_{16} & 0 \\ -L_{13} & -L_{23} & L_{33} & 0 & L_{35} & L_{36} & k_1 L_{77} & L_{38} & L_{39} \\ L_{41} & L_{42} & 0 & L_{44} & 0 & 0 & 0 & 0 & 0 \\ 0 & -L_{16} & -L_{38} & 0 & L_{55} & L_{56} & -k_1 L_{35} & L_{58} & 0 \\ L_{16} & 0 & -L_{39} & 0 & L_{56} & L_{66} & -k_1 L_{36} & 0 & L_{58} \\ -L_{13} & -L_{14} & L_{73} & 0 & L_{35} & L_{36} & k_1 L_{77} & L_{78} & L_{79} \\ 0 & -L_{16} & -L_{78} & 0 & L_{85} & L_{56} & -k_1 L_{35} & k_1 L_{88} & k_1 L_{56} \\ L_{16} & 0 & -L_{79} & 0 & L_{56} & L_{55} & -k_1 L_{36} & k_1 L_{56} & k_1 L_{99} \end{bmatrix},$$

$$\mathscr{U} = \begin{bmatrix} \Psi_1, & \Psi_2, & W, & \Omega_3, & \Omega_1^0, & \Omega_2^0, & W^*, & \Omega_1^0, & \Omega_2^0 \end{bmatrix}^T,$$

$$f(\eta) = \begin{bmatrix} -\frac{h^2\lambda(3p_{1,1}+5p_{2,1})}{30(\lambda+2\mu)}, & -\frac{h^2\lambda(3p_{1,2}+5p_{2,2})}{30(\lambda+2\mu)}, & -p_1, & 0, & 0, & 0, & \frac{h^2(3p_1+4p_2)}{24}, & 0, & 0 \end{bmatrix}^T. \tag{2.98}$$

The operators L_{ij} are defined as follows $L_{11} = c_1 \frac{\partial^2}{\partial x_1^2} + c_2 \frac{\partial^2}{\partial x_2^2} - c_3, L_{12} = (c_1 - c_2)\frac{\partial^2}{\partial x_1 x_2}, L_{13} = c_{11}\frac{\partial}{\partial x_1}, L_{14} = c_{12}\frac{\partial}{\partial x_2}, L_{16} = c_{13}, L_{17} = k_1 c_{11}\frac{\partial}{\partial x_1}, L_{22} = c_2\frac{\partial^2}{\partial x_1^2} + c_1\frac{\partial^2}{\partial x_2^2} - c_3, L_{23} = c_{11}\frac{\partial}{\partial x_2}, L_{24} = -c_{12}\frac{\partial}{\partial x_1}, L_{33} = c_3(\frac{\partial^2}{\partial x_1^2} + \frac{\partial^2}{\partial x_2^2}), L_{35} = -c_{13}\frac{\partial}{\partial x_2}, L_{36} = c_{13}\frac{\partial}{\partial x_1}, L_{38} = -c_{10}\frac{\partial}{\partial x_2}, L_{39} = c_{10}\frac{\partial}{\partial x_1}, L_{41} = -c_{12}\frac{\partial}{\partial x_2}, L_{42} = c_{12}\frac{\partial}{\partial x_1}, L_{44} = c_6\left(\frac{\partial^2}{\partial x_1^2} + \frac{\partial^2}{\partial x_2^2}\right) - 2c_{12}, L_{55} = c_7\frac{\partial^2}{\partial x_1^2} + c_8\frac{\partial^2}{\partial x_2^2} - 2c_{13}, L_{56} = (c_7 - c_8)\frac{\partial^2}{\partial x_1 x_2}, L_{58} = -c_9, L_{66} = c_8\frac{\partial^2}{\partial x_1^2} + c_7\frac{\partial^2}{\partial x_2^2} - 2c_{13}, L_{73} = c_5(\frac{\partial^2}{\partial x_1^2} + \frac{\partial^2}{\partial x_2^2}), L_{77} = c_4(\frac{\partial^2}{\partial x_1^2} + \frac{\partial^2}{\partial x_2^2}), L_{78} = -c_{14}\frac{\partial}{\partial x_2}, L_{79} = c_{14}\frac{\partial}{\partial x_1}, L_{85} = c_7\frac{\partial^2}{\partial x_1^2} + c_8\frac{\partial^2}{\partial x_2^2} - 2c_{13}, L_{88} = c_7\frac{\partial^2}{\partial x_1^2} + c_8\frac{\partial^2}{\partial x_2^2} - c_{15}, L_{99} = c_8\frac{\partial^2}{\partial x_1^2} + c_7\frac{\partial^2}{\partial x_2^2} - c_{15}$

where

$$
\begin{aligned}
c_1 &= \frac{h^3\mu(\lambda+\mu)}{3(\lambda+2\mu)}, c_2 = \frac{h^3(\alpha+\mu)}{12}, c_3 = \frac{5h(\alpha+\mu)}{6}, c_4 = \frac{5h(\alpha-\mu)^2}{6(\alpha+\mu)}, \\
c_5 &= \frac{h(5\alpha^2+6\alpha\mu+5\mu^2)}{6(\alpha+\mu)}, c_6 = \frac{h^3\gamma\epsilon}{3(\gamma+\epsilon)}, c_7 = \frac{10h\gamma\,(\beta+\gamma)}{3\,(\beta+2\gamma)}, \\
c_8 &= \frac{5h\,(\gamma+\epsilon)}{6} c_9 = \frac{10h\alpha^2}{3(\alpha+\mu)}, c_{10} = \frac{5h\alpha(\alpha-\mu)}{3(\alpha+\mu)}, c_{11} = \frac{5h(\alpha-\mu)}{6}, \\
c_{12} &= \frac{h^3\alpha}{6}, c_{13} = \frac{5h\alpha}{3}, c_{14} = \frac{h\alpha(5\alpha+3\mu)}{3(\alpha+\mu)}, c_{15} = \frac{2h\alpha(5\alpha+4\mu)}{3(\alpha+\mu)}.
\end{aligned}
$$

The parametric system (2.97) is an elliptic order two system of nine partial differential equations, where L is a linear differential operator acting on the set of kinematic variables $\mathscr{U}$.

The ellipticity of the operator L follows from the invertibility of its principle symbol $L(\xi)$ for all $\xi \neq 0$ $(\xi \in \mathbb{R}^2)$ [62] and since

$$\det L\,(\xi) = \frac{256\alpha\mu}{375(\alpha+\mu)} c_1 c_2 c_3 c_6 c_7^2 \,|\xi|^2$$

the operator L is elliptic for positive elastic constants.

2.8 Optimal Value of the Splitting Parameter

The equlibrium systems of partial differential equations correspond to a state of the system (2.97) where the minimum of the energy is reached. The optimization of the splitting parameter appears as a result of the Generalized Hellinger-Prange-Reissner (HPR) principle for the Cosserat elastic plate (2.63). The bending system of equations depends on the splitting parameter and therefore its solution is parametric. The minimization procedure for the elastic energy allows us to find the optimal value of this parameter, which corresponds to the unique solution of the bending problem [46].

Let us find an explicit expression for the optimal value of the splitting parameter η that minimizes the micropolar plate stress energy density. Taking advantage of the linearity of the system (2.97) we consider two cases:

$$L\mathscr{U}_0 = f(0), \tag{2.99}$$

$$L\mathscr{U}_1 = f(1), \tag{2.100}$$

where $\mathscr{U}_0$ is a solution of the bending system of equations (2.97) when $\eta = 0$, and $\mathscr{U}_1$ when $\eta = 1$.

Let us define $\mathscr{U}_\eta$ as a linear combination of $\mathscr{U}_0$ and $\mathscr{U}_1$:

$$\mathscr{U}_\eta = (1-\eta)\,\mathscr{U}_0 + \eta\mathscr{U}_1 \tag{2.101}$$

Notice that since $p_1(x_1, x_2) = \eta p(x_1, x_2)$ and $p_2(x_1, x_2) = \frac{(1-\eta)}{2} p(x_1, x_2)$

$$f(\eta) = (1-\eta)\, f(0) + \eta f(1)$$

and therefore due to the linearity of system (2.97)

$$\begin{aligned} L\mathscr{U}_\eta &= L\left((1-\eta)\,\mathscr{U}_0 + \eta\mathscr{U}_1\right) = (1-\eta)\, L\mathscr{U}_0 + \eta L\mathscr{U}_1 = \\ &= (1-\eta)\, f(0) + \eta f(1) = f(\eta) \end{aligned}$$

The set of kinematic variables $\mathscr{U}_\eta$ defined as (2.101) is a solution of the micropolar plate bending system of equations (2.97).

The optimal value of the splitting parameter η is a minimizer of the density of the work $\mathscr{W}^{(\eta)}$ done by the stress and couple stress over the micropolar strain field. Let us obtain an explicit expression for the optimal value of the parameter η.

Let us represent each component of the stress set $\mathscr{S}^{(\eta)}$ and strain set $\mathscr{E}^{(\eta)}$ as a linear combinations of the stress sets $\mathscr{S}^{(0)}$ and $\mathscr{S}^{(1)}$, and the strain sets $\mathscr{E}^{(0)}$ and

$\mathscr{E}^{(1)}$ respectively:

$$\begin{aligned}\mathscr{S}^{(\eta)} &= (1-\eta)\,\mathscr{S}^{(0)} + \eta\mathscr{S}^{(1)}\\ \mathscr{E}^{(\eta)} &= (1-\eta)\,\mathscr{E}^{(0)} + \eta\mathscr{E}^{(1)}\end{aligned}$$

Therefore

$$\mathscr{W}^{(\eta)} = \mathscr{S}^{(\eta)} \cdot \mathscr{E}^{(\eta)} = \left((1-\eta)\,\mathscr{S}^{(0)} + \eta\mathscr{S}^{(1)}\right) \cdot \left((1-\eta)\,\mathscr{E}^{(0)} + \eta\mathscr{E}^{(1)}\right)$$

The zero of the derivation $\frac{\partial\mathscr{W}^{(\eta)}}{\partial\eta}$ gives the optimal value η_0 of the splitting parameter η [46]:

$$\frac{\partial\mathscr{W}^{(\eta)}}{\partial\eta} = \left(-\mathscr{S}^{(0)} + \mathscr{S}^{(1)}\right)\cdot\left((1-\eta)\,\mathscr{E}^{(0)} + \eta\mathscr{E}^{(1)}\right) + \left((1-\eta)\,\mathscr{S}^{(0)} + \eta\mathscr{S}^{(1)}\right)\cdot\left(\mathscr{E}^{(1)} - \mathscr{E}^{(0)}\right)$$

and the optimal value

$$\eta_0 = \frac{2\mathscr{W}^{(00)} - \mathscr{W}^{(10)} - \mathscr{W}^{(01)}}{2\left(\mathscr{W}^{(11)} + \mathscr{W}^{(00)} - \mathscr{W}^{(10)} - \mathscr{W}^{(01)}\right)}, \tag{2.102}$$

where

$$\mathscr{W}^{(00)} = \mathscr{S}^{(0)}\cdot\mathscr{E}^{(0)} \tag{2.103}$$

$$\mathscr{W}^{(01)} = \mathscr{S}^{(0)}\cdot\mathscr{E}^{(1)} \tag{2.104}$$

$$\mathscr{W}^{(10)} = \mathscr{S}^{(1)}\cdot\mathscr{E}^{(0)} \tag{2.105}$$

$$\mathscr{W}^{(11)} = \mathscr{S}^{(1)}\cdot\mathscr{E}^{(1)} \tag{2.106}$$

This result allow us to use in our numerical modeling the following effective algorithm for the optimal value of the splitting parameter η, which will be used for the plates of different shapes in Chapters 3 and 4.

Algorithm 1. *Optimal Value of the Splitting Parameter*

1. *Solve the systems (2.99) and (2.100) for $\mathscr{U}_0$ and $\mathscr{U}_1$ respectively.*

2. Calculate the components of the micropolar plate stress sets $\mathscr{S}^{(0)}$ and $\mathscr{S}^{(1)}$ from the sets of kinematic variables $\mathscr{U}_0$ and $\mathscr{U}_1$, using the constitutive formulas in the reverse form (2.83) - (2.92).

3. Calculate the components of the micropolar plate strain sets $\mathscr{E}^{(0)}$ and $\mathscr{E}^{(1)}$ from the sets of kinematic variables $\mathscr{U}_0$ and $\mathscr{U}_1$, using the strain-displacement relations (2.56) - (2.62).

4. Find the work densities $\mathscr{W}^{(00)}$, $\mathscr{W}^{(11)}$, $\mathscr{W}^{(10)}$ and $\mathscr{W}^{(01)}$ by substituting the micropolar plate stress and strain sets $\mathscr{S}^{(0)}$, $\mathscr{S}^{(1)}$, $\mathscr{E}^{(0)}$ and $\mathscr{E}^{(1)}$ into the definitions (2.103) - (2.106).

5. Substitute the values of the work densities $\mathscr{W}^{(00)}$, $\mathscr{W}^{(11)}$, $\mathscr{W}^{(10)}$ and $\mathscr{W}^{(01)}$ into the expression for the optimal value of the splitting parameter η_0 (4.19).

The above algorithm can be efficiently used to find the solution of the system of equations (2.97). Indeed, once the optimal value of the splitting parameter η_0 is found, the solution $\mathscr{U}_{\eta_0}$ of the bending system of equations (2.97) is found from (2.101) as a linear combination of the sets of kinematic variables $\mathscr{U}_0$ and $\mathscr{U}_1$:

$$\mathscr{U}_{\eta_0} = (1 - \eta_0)\,\mathscr{U}_0 + \eta_0 \mathscr{U}_1 \tag{2.107}$$

Chapter 3

Validation of the Mathematical Model for Cosserat Elastic Plates

3.1 Scope of the Chapter

In this chapter we present the validation of the proposed mathematical model for Cosserat elastic plates. We provide the three-dimensional analytical solution for the simply supported Cosserat square plate and compare it with the analytical solution based on the mathematical model for Cosserat elastic plates. We present the numerical comparison of the displacements, microrotations, stresses and couple stresses. We also provide the numerical results of the minimization of the total plate energy with respect to the splitting parameter η. The comparison between Cosserat and classical elasticity plates and the convergence of the solution of the proposed mathematical model to the corresponding Reissner solution, and such important feature of the Cosserat plate theory as size effect are also discussed.

3.2 Three-Dimensional Analytical Solution for Cosserat Elastic Square Plate

Let us consider the plate B_0 being a rectangular cuboid $[0,a]\times[0,a]\times[-\frac{h}{2},\frac{h}{2}]$. Let the sets T and B be the top and the bottom surfaces contained in the planes $x_3=\frac{h}{2}$ and $x_3=-\frac{h}{2}$ respectively, and the curve $\Gamma=\Gamma_1\cup\Gamma_2$ be the lateral part of the boundary:

$$\begin{aligned}\Gamma_1 &= \left\{(x_1,x_2,x_3) : x_1\in\{0,a\}, x_2\in[0,a], x_3\in\left[-\frac{h}{2},\frac{h}{2}\right]\right\},\\ \Gamma_2 &= \left\{(x_1,x_2,x_3) : x_1\in[0,a], x_2\in\{0,a\}, x_3\in\left[-\frac{h}{2},\frac{h}{2}\right]\right\},\end{aligned}$$

We solve the three-dimensional Cosserat equilibrium equations without body forces and body moments (2.1) - (2.2) accompanied by the constitutive equations (2.5) - (2.6) and strain-displacement and torsion-rotation relations (2.3) - (2.4) complemented by the following boundary conditions:

$$\Gamma_1 \ : \ u_2=0,\ u_3=0,\ \varphi_1=0, \tag{3.1}$$

$$\Gamma_1 \ : \ \sigma_{11}=0,\ \mu_{12}=0,\ \mu_{13}=0; \tag{3.2}$$

$$\Gamma_2 \ : \ u_1=0,\ u_3=0,\ \varphi_2=0, \tag{3.3}$$

$$\Gamma_2 \ : \ \sigma_{22}=0,\ \mu_{21}=0,\ \mu_{23}=0; \tag{3.4}$$

$$T \ : \ \sigma_{33}=p(x_1,x_2),\ \mu_{33}=0; \tag{3.5}$$

$$B \ : \ \sigma_{33}=0,\ \mu_{33}=0. \tag{3.6}$$

where the initial distribution of the pressure is given as

$$p(x_1,x_2)=\sin\left(\frac{\pi x_1}{a}\right)\sin\left(\frac{\pi x_2}{a}\right)$$

Using the method of separation of variables and taking into account the boundary conditions (3.1) - (3.4), we express the kinematic variables in the form:

$$u_1 = \cos\left(\frac{\pi x_1}{a}\right)\sin\left(\frac{\pi x_2}{a}\right) z_1\left(x_3\right), \tag{3.7}$$

$$u_2 = \sin\left(\frac{\pi x_1}{a}\right)\cos\left(\frac{\pi x_2}{a}\right) z_1\left(x_3\right), \tag{3.8}$$

$$u_3 = \sin\left(\frac{\pi x_1}{a}\right)\sin\left(\frac{\pi x_2}{a}\right) z_2\left(x_3\right), \tag{3.9}$$

$$\varphi_1 = \sin\left(\frac{\pi x_1}{a}\right)\cos\left(\frac{\pi x_2}{a}\right) z_3\left(x_3\right), \tag{3.10}$$

$$\varphi_2 = -\cos\left(\frac{\pi x_1}{a}\right)\sin\left(\frac{\pi x_2}{a}\right) z_3\left(x_3\right) \tag{3.11}$$

$$\varphi_3 = 0, \tag{3.12}$$

where the functions $z_1(x_3)$, $z_2(x_3)$ and $z_3(x_3)$ represent the transverse variations of the kinematic variables.

If we substitute the expressions (3.7) - (3.12) into (2.3) - (2.4) and then into (2.5) - (2.6) and (2.1) - (2.2) we will obtain the following second order linear system of three ordinary differential equations in terms of z_1, z_2 and z_3:

$$a^2(\mu+\alpha) z_1'' + a(\mu-\alpha+\lambda) z_2' + 2a^2\alpha z_3' - 2\pi^2(\lambda+2\mu) z_1 = 0 \tag{3.13}$$

$$a^2(\lambda+2\mu) z_2'' - 2a\pi(\mu-\alpha+\lambda) z_1' - 2\pi(\mu+\alpha) z_2 + 4a\pi z_3 = 0 \tag{3.14}$$

$$a^2(\epsilon+\gamma) z_3'' - 2a^2\alpha z_1' + 2a\alpha\pi z_2 - 2\left(2a^2\alpha + (\epsilon+\gamma)\pi^2\right) z_3 = 0 \tag{3.15}$$

complemented by the boundary conditions

$$\begin{aligned} x_3 = \frac{h}{2} \quad &: \quad a(\mu+\alpha) z_1' + (\mu-\alpha)\pi z_2 = 0, \\ &\quad\;\; a(\lambda+2\mu) z_2' - 2\pi\lambda z_1 = a, \\ &\quad\;\; z_3 = 0; \\ x_3 = -\frac{h}{2} \quad &: \quad a(\mu+\alpha) z_1' + (\mu-\alpha)\pi z_2 = 0, \\ &\quad\;\; a(\lambda+2\mu) z_2' - 2\pi\lambda z_1 = 0, \\ &\quad\;\; z_3 = 0, \end{aligned}$$

Now let us make the following substitution:

$$\begin{aligned} \kappa_1(x_3) &= z_1(x_3) \\ \kappa_2(x_3) &= z_2(x_3) \\ \kappa_3(x_3) &= z_3(x_3) \\ \kappa_4(x_3) &= z_1'(x_3) \\ \kappa_5(x_3) &= z_2'(x_3) \\ \kappa_6(x_3) &= z_3'(x_3) \end{aligned}$$

The system of equations (3.13) - (3.15) can be therefore rewritten as a first order linear system of six ordinary differential equations in terms of κ_i $(i = 1, ..., 6)$:

$$\hat{\boldsymbol{\kappa}}'(x_3) = \mathbf{K} \cdot \hat{\boldsymbol{\kappa}}(x_3) \tag{3.16}$$

or equivalently in the matrix form:

$$\begin{bmatrix} \kappa_1' \\ \kappa_2' \\ \kappa_3' \\ \kappa_4' \\ \kappa_5' \\ \kappa_6' \end{bmatrix} = \begin{bmatrix} 0 & 0 & 0 & 1 & 0 & 0 \\ 0 & 0 & 0 & 0 & 1 & 0 \\ 0 & 0 & 0 & 0 & 0 & 1 \\ K_{41} & 0 & 0 & 0 & K_{45} & K_{46} \\ 0 & K_{52} & K_{53} & K_{54} & 0 & 0 \\ 0 & K_{62} & K_{63} & K_{64} & 0 & 0 \end{bmatrix} \begin{bmatrix} \kappa_1 \\ \kappa_2 \\ \kappa_3 \\ \kappa_4 \\ \kappa_5 \\ \kappa_6 \end{bmatrix}$$

where $K_{41} = \frac{2\pi^2(\lambda+2\mu)}{a^2(\alpha+\mu)}$, $K_{45} = \frac{\pi(\alpha-\lambda-\mu)}{a(\alpha+\mu)}$, $K_{46} = -\frac{2a}{(\alpha+\mu)}$, $K_{52} = \frac{2\pi^2(\alpha+\mu)}{a^2(\lambda+2\mu)}$, $K_{53} = -\frac{4\pi\alpha}{a(\lambda+2\mu)}$, $K_{54} = \frac{2\pi(-\alpha+\lambda+\mu)}{a(\lambda+2\mu)}$, $K_{62} = -\frac{2\pi\alpha}{a(\gamma+\epsilon)}$, $K_{63} = \frac{2\left(2a^2\alpha+\pi^2(\gamma+\epsilon)\right)}{a^2(\gamma+\epsilon)}$, $K_{64} = \frac{2\alpha}{\gamma+\epsilon}$.

The system is complemented by the boundary conditions at $x_3 = \pm\frac{h}{2}$:

$$a(\mu+\alpha)\kappa_4 + (\mu-\alpha)\pi\kappa_2 = 0, \tag{3.17}$$

$$a(\lambda+2\mu)\kappa_5 - 2\pi\lambda\kappa_1 = a, \tag{3.18}$$

$$\kappa_3 = 0; \tag{3.19}$$

The general solution of the system of six ordinary differential equations given above is found as

$$\hat{\boldsymbol{\kappa}}\left(x_3\right) = c_i e^{r_i x_3} \hat{\boldsymbol{\theta}_i^T}, \tag{3.20}$$

where r_i are the eigenvalues of the matrix $\mathbf{K}$, θ_i are the corresponding eigenvectors of the matrix $\mathbf{K}$ and c_i are some constants that can be determined from the boundary conditions (3.17) - (3.19). Note that since $z_i = \kappa_i$ for $(i = 1, 2, 3)$, therefore the general solution for the variables z_i is also of the form (3.20) (see [63], [64] for details).

The eigenvalues r_i of the matrix $\mathbf{K}$ are given as

$$\begin{aligned}
r_1 &= -\frac{\sqrt{2}\pi}{a}, \\
r_2 &= \frac{\sqrt{2}\pi}{a}, \\
r_3 &= -\sqrt{\frac{4\alpha\mu}{(\gamma+\epsilon)(\alpha+\mu)} + \frac{2\pi^2}{a^2}}, \\
r_4 &= \sqrt{\frac{4\alpha\mu}{(\gamma+\epsilon)(\alpha+\mu)} + \frac{2\pi^2}{a^2}}.
\end{aligned}$$

The corresponding eigenvectors θ_i of the matrix $\mathbf{K}$ are given as

$$\begin{aligned}
\theta_1 &= \left[\frac{a}{2\pi}, -\frac{a}{\sqrt{2}\pi}, 0, -\frac{1}{\sqrt{2}}, 1, 0\right], \\
\theta_2 &= \left[\frac{a}{2\pi}, \frac{a}{\sqrt{2}\pi}, 0, \frac{1}{\sqrt{2}}, 1, 0\right], \\
\theta_3 &= \left[-\frac{\gamma+\epsilon}{2\mu}, \frac{\pi(\gamma+\epsilon)}{a\mu r_4}, -\frac{1}{r_4}, \frac{(\gamma+\epsilon)r_4}{\mu}, -\frac{\pi(\gamma+\epsilon)}{a\mu}, 1\right], \\
\theta_4 &= \left[-\frac{\gamma+\epsilon}{2\mu}, -\frac{\pi(\gamma+\epsilon)}{a\mu r_4}, \frac{1}{r_4}, -\frac{(\gamma+\epsilon)r_4}{\mu}, -\frac{\pi(\gamma+\epsilon)}{a\mu}, 1\right],
\end{aligned}$$

We will provide the numerical values of the variables z_j $(j = 1, 2, 3)$ for the square plate made of polyurethane foam in the comparison section.

3.3 Analytical Solution for Cosserat Elastic Square Plate Based on the Proposed Mathematical Model

The body B_0 can viewed as a square plate of size $[0,a]\times[0,a]$, having thickness h and $x_3 = 0$ containing its middle plane (see Figure 3–1). The boundary $G = G_1 \cup G_2 \cup G_3 \cup G_4$ is given by

$$\begin{aligned}
G_1 &= \{(x_1,x_2) : x_1 = 0, x_2 \in [0,a]\}\,, \\
G_2 &= \{(x_1,x_2) : x_1 = a, x_2 \in [0,a]\}\,, \\
G_3 &= \{(x_1,x_2) : x_1 \in [0,a]\,, x_2 = 0\}\,, \\
G_4 &= \{(x_1,x_2) : x_1 \in [0,a]\,, x_2 = a\}\,,
\end{aligned}$$

Let us consider the following hard simply supported boundary conditions similar to [65] and [66]:

$$W = 0, W^* = 0, \mathbf{\Psi}\cdot\hat{\mathbf{s}} = 0, \hat{\mathbf{n}}\cdot\mathbf{M}\hat{\mathbf{n}} = 0, \hat{\mathbf{s}}\cdot\mathbf{R}\hat{\mathbf{n}} = 0, \tag{3.21}$$

$$\hat{\mathbf{s}}\cdot\mathbf{R}^*\hat{\mathbf{n}} = 0, \mathbf{S}^*\cdot\hat{\mathbf{n}} = 0, \hat{\mathbf{Q}}\cdot\hat{\mathbf{s}} = 0, \mathbf{Q}^*\cdot\hat{\mathbf{s}} = 0, \tag{3.22}$$

where $\hat{\mathbf{n}}$ and $\hat{\mathbf{s}}$ are the normal and the tangent vectors to the boundary G.

The initial distribution of the pressure is sinusoidal and given as

$$p\,(x_1,x_2) = \sin\left(\frac{\pi x_1}{a}\right)\sin\left(\frac{\pi x_2}{a}\right)$$

Let us rewrite the boundary conditions (3.21) - (3.22) in terms of the kinematic variables. Let us show how it can be done for one part of the boundary, for example G_2. The other parts of the boundary can be analyzed in a similar manner.

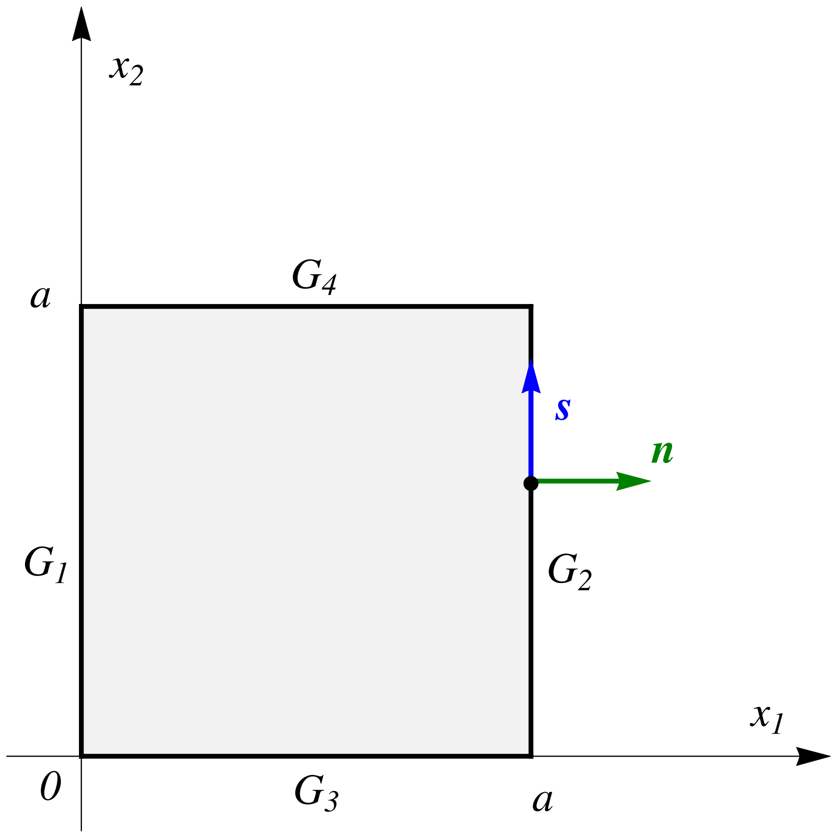

Figure 3–1: Square plate of size $[0, a] \times [0, a]$ *(top view)*

The normal and tangent vectors to G_2 are $\hat{\mathbf{n}} = \langle 1, 0 \rangle$ and $\hat{\mathbf{s}} = \langle 0, 1 \rangle$ respectively. Note that the boundary conditions $W = 0$ and $W^* = 0$ are already written in terms of the kinematic variables and therefore

$$
\begin{aligned}
W &= 0 \text{ on } G_2 \\
W^* &= 0 \text{ on } G_2
\end{aligned}
$$

The boundary condition $\mathbf{\Psi} \cdot \hat{\mathbf{s}} = 0$ implies $\mathbf{\Psi} \cdot \langle 0, 1 \rangle = 0$ and therefore:

$$\Psi_2 = 0 \text{ on } G_2$$

The boundary condition $\mathbf{S}^* \cdot \hat{\mathbf{n}} = 0$ implies $\mathbf{S}^* \cdot \langle 1, 0 \rangle = 0$ and therefore:

$$S_1^* = 0$$

From the constitutive formulas in the reverse form (2.92) $S_1^* = 0$ is equivalent to

$$\Omega_{3,1} = 0 \text{ on } G_2$$

The boundary condition $\hat{\mathbf{n}} \cdot \mathbf{M}\hat{\mathbf{n}} = 0$ implies $\langle 1, 0\rangle \cdot \mathbf{M} \langle 1, 0\rangle^T = 0$ and therefore:

$$M_{11} = 0$$

From the constitutive formulas in the reverse form (2.83) $M_{11} = 0$ is equivalent to

$$\frac{h^3\mu(\lambda+\mu)}{3(\lambda+2\mu)}\Psi_{1,1} + \frac{\lambda\mu h^3}{6(\lambda+2\mu)}\Psi_{2,2} + \frac{(3p_1+5p_2)\,\lambda h^2}{30(\lambda+2\mu)} = 0$$

Note that $p(x_1, x_2)$ is zero on the boundary and that $p_1(x_1, x_2) = \eta p(x_1, x_2)$ and therefore so are $p_2(x_1, x_2) = \frac{(1-\eta)}{2}p(x_1, x_2)$ and thus

$$\frac{(3p_1+5p_2)\,\lambda h^2}{30(\lambda+2\mu)} = 0$$

and since $\Psi_2 = 0$ and then $\Psi_{2,2} = 0$ we have that $M_{11} = 0$ is equivalent to

$$\Psi_{1,1} = 0 \text{ on } G_2$$

The boundary condition $\hat{\mathbf{Q}} \cdot \hat{\mathbf{s}} = 0$ implies $\hat{\mathbf{Q}} \cdot \langle 0, 1\rangle = 0$ and therefore:

$$\hat{Q}_2 = 0$$

From the constitutive formulas in the reverse form (2.91) $\hat{Q}_2 = 0$ is equivalent to

$$\frac{8\alpha\mu h}{3\,(\mu+\alpha)}W_{,2} + (-1)^2\frac{8\alpha\mu h}{3\,(\mu+\alpha)}\hat{\Omega}_1 = 0$$

and since $W = 0$ and then also $W_{,2} = 0$, we have that $\hat{Q}_2 = 0$ is equivalent to

$$\hat{\Omega}_1 = 0 \text{ on } G_2$$

The boundary condition $\hat{\mathbf{s}} \cdot \mathbf{R}^* \hat{\mathbf{n}} = 0$, implies $\langle 0,1 \rangle \cdot \mathbf{R}^* \langle 1,0 \rangle^T = 0$ and therefore:

$$R^*_{21} = 0$$

From the constitutive formulas in the reverse form (2.87) $\hat{R}_{21} = 0$ is equivalent to

$$\frac{2(\gamma - \epsilon) h}{3} \hat{\Omega}_{2,1} + \frac{2(\gamma + \epsilon) h}{3} \hat{\Omega}_{1,2} = 0$$

and since $\hat{\Omega}_1 = 0$ and then also $\hat{\Omega}_{1,2} = 0$, we have that $R^*_{21} = 0$ is equivalent to

$$\hat{\Omega}_{2,1} = 0 \text{ on } G_2$$

The boundary condition $\mathbf{Q}^* \cdot \hat{\mathbf{s}} = 0$ implies $\mathbf{Q}^* \cdot \langle 0,1 \rangle = 0$ and therefore:

$$Q^*_2 = 0$$

From the constitutive formulas in the reverse form (2.90) $Q^*_2 = 0$ is equivalent to

$$\begin{aligned} \frac{5(\mu - \alpha) h}{6} \Psi_2 \quad &+ \quad \frac{5(\mu - \alpha)^2 h}{6(\mu + \alpha)} W_{,2} + \frac{2(\mu + \alpha) h}{3} W^*_{,2} \\ &+ \quad (-1)^\alpha \frac{5h\alpha}{3} \left(\Omega^0_1 + \frac{(\mu - \alpha)}{(\mu + \alpha)} \hat{\Omega}_1 \right) = 0 \end{aligned}$$

and since $\Psi_2 = 0$, $W_{,2} = 0$, $W^*_{,2} = 0$ and $\hat{\Omega}_1 = 0$ we have that $Q^*_2 = 0$ is equivalent to

$$\Omega^0_1 = 0 \text{ on } G_2$$

The boundary condition $\hat{\mathbf{s}} \cdot \mathbf{R} \hat{\mathbf{n}} = 0$, implies $\langle 0,1 \rangle \cdot \mathbf{R} \langle 1,0 \rangle^T = 0$ and therefore:

$$R_{21} = 0$$

From the constitutive formulas in the reverse form (2.85) $R_{21} = 0$ is equivalent to

$$\frac{5(\gamma - \epsilon) h}{6} \Omega^0_{2,1} + \frac{5h(\gamma + \epsilon)}{6} \Omega^0_{1,2} = 0$$

and since $\Omega_1^0 = 0$ and then $\Omega_{1,2}^0 = 0$ we have that $R_{21} = 0$ is equivalent to

$$\Omega_{2,1}^0 = 0 \text{ on } G_2$$

The analysis of other parts of the boundary is similar to the one provided above. The hard simply supported boundary conditions therefore can be written in the mixed Dirichlet-Neumann form:

$$\begin{aligned} G_1 \cup G_2 \quad &: \quad W = 0,\ W^* = 0,\ \Psi_2 = 0,\ \Omega_1^0 = 0,\ \hat{\Omega}_1^0 = 0, \\ &\quad \frac{\partial \Omega_3}{\partial n} = 0,\ \frac{\partial \Psi_1}{\partial n} = 0,\ \frac{\partial \Omega_2^0}{\partial n} = 0,\ \frac{\partial \hat{\Omega}_2^0}{\partial n} = 0; \end{aligned} \tag{3.23}$$

$$\begin{aligned} G_3 \cup G_4 \quad &: \quad W = 0,\ W^* = 0,\ \Psi_1 = 0,\ \Omega_2^0 = 0,\ ,\hat{\Omega}_2^0 = 0 \\ &\quad \frac{\partial \Omega_3}{\partial n} = 0,\ \frac{\partial \Psi_2}{\partial n} = 0,\ \frac{\partial \Omega_1^0}{\partial n} = 0,\ \frac{\partial \hat{\Omega}_1^0}{\partial n} = 0. \end{aligned} \tag{3.24}$$

We solve the two-dimensional bending equilibrium system of equations (2.97) by applying the method of separation of variables similar to how it was performed in detail in [44]. Taking into account the boundary conditions (3.23) - (3.24) we obtain the kinematic variables in the following form:

$$\Psi_1 = A_1 \cos\left(\frac{\pi x_1}{a}\right) \sin\left(\frac{\pi x_2}{a}\right), \tag{3.25}$$

$$\Psi_2 = A_2 \sin\left(\frac{\pi x_1}{a}\right) \cos\left(\frac{\pi x_2}{a}\right), \tag{3.26}$$

$$W = A_3 \sin\left(\frac{\pi x_1}{a}\right) \sin\left(\frac{\pi x_2}{a}\right), \tag{3.27}$$

$$\Omega_3 = A_4 \cos\left(\frac{\pi x_1}{a}\right) \cos\left(\frac{\pi x_2}{a}\right), \tag{3.28}$$

$$\Omega_1^0 = A_5 \sin\left(\frac{\pi x_1}{a}\right) \cos\left(\frac{\pi x_2}{a}\right), \tag{3.29}$$

$$\Omega_2^0 = A_6 \cos\left(\frac{\pi x_1}{a}\right) \sin\left(\frac{\pi x_2}{a}\right), \tag{3.30}$$

$$W^* = A_7 \sin\left(\frac{\pi x_1}{a}\right) \sin\left(\frac{\pi x_2}{a}\right), \tag{3.31}$$

$$\hat{\Omega}_1^0 = A_8 \sin\left(\frac{\pi x_1}{a}\right) \cos\left(\frac{\pi x_2}{a}\right), \tag{3.32}$$

$$\hat{\Omega}_2^0 = A_9 \cos\left(\frac{\pi x_1}{a}\right) \sin\left(\frac{\pi x_2}{a}\right). \tag{3.33}$$

where $A_i \in \mathbb{R}$ are some constants.

We find A_i by substituting the expressions (3.25) - (3.33) into the system of equations (2.97) and solving the obtained system of 9 linear equations for A_i.

Note that since the right-hand side of the system of equations (2.97) depends on the splitting parameter η therefore A_i will also in general depend on the splitting parameter η $(i = 1, ..., 9)$. The numerical values for A_i correspond to the optimal value of the splitting parameter η, which minimizes the free stress energy (2.16). We obtain its value by applying the algorithm for the optimal value of the splitting parameter described in the Chapter 3. We find the solution for the two-dimensional problem by solving the field equations (2.97) for $\eta = 0$ and $\eta = 1$ and then calculate the optimal solution as their linear combination (2.107). We will provide the numerical values of the kinematic variables for the square plate made of polyurethane foam in the comparison section.

3.4 Comparison of the Analytical Solutions

In this section we provide the results of the validation of the proposed mathematical model. The validation is given for the case of square Cosserat elastic plate, which is compared to the analytical solution of the three-dimensional Cosserat Elasticity.

In our calculations we will use the following technical parameters: the Young's modulus E, the Poisson's ratio ν, the characteristic length for bending l_b, the characteristic length for torsion l_t and the coupling number N.

The conversion formulas between the technical constants and elastic parameters are given as in [12]

$$
\begin{aligned}
E &= \frac{\mu(3\lambda + 2\mu)}{\lambda + \mu}, \\
\nu &= \frac{\lambda}{2(\lambda + \mu)}, \\
l_b &= \frac{1}{2}\sqrt{\frac{\gamma + \epsilon}{\mu}}, \\
l_t &= \sqrt{\frac{\gamma}{\mu}}, \\
N &= \sqrt{\frac{\alpha}{\mu + \alpha}},
\end{aligned}
$$

and imply the following inverse conversion formulas

$$
\begin{aligned}
\lambda &= \frac{E\nu}{2\nu^2 + \nu - 1}, \\
\mu &= \frac{E}{2\left(\nu + 1\right)}, \\
\alpha &= \frac{EN^2}{2\left(\nu + 1\right)\left(N^2 - 1\right)}, \\
\beta &= \frac{El_t}{2\left(\nu + 1\right)}, \\
\gamma &= \frac{El_t^2}{2\left(\nu + 1\right)}, \\
\epsilon &= \frac{E\left(4l_b^2 - l_t^2\right)}{2\left(\nu + 1\right)}.
\end{aligned}
$$

In our computations we consider plates made of polyurethane foam – a material reported in the literature to be Cosserat and the values of the technical elastic parameters are presented in [16]:

$$\begin{aligned} E &= 299.5 \text{ MPa}, \\ \nu &= 0.44, \\ l_t &= 0.62 \text{ mm}, \\ l_b &= 0.327, \\ N^2 &= 0.04. \end{aligned}$$

Taking into account that the ratio β/γ is equal to 1 for bending [16], these values of the technical constants correspond to the following values of Lamé and asymmetric parameters:

$$\begin{aligned} \lambda &= 762.616 \text{ MPa}, \\ \mu &= 103.993 \text{ MPa}, \\ \alpha &= 4.333 \text{ MPa}, \\ \beta &= 39.975 \text{ MPa}, \\ \gamma &= 39.975 \text{ MPa}, \\ \epsilon &= 4.505 \text{ MPa}, \end{aligned}$$

Since the typical thickness to width ratio of a plate structure is less than 0.1, we will consider the thickness of the plate $h = 0.1$m and the ratio a/h varying from 10 to 30.

We provide the numerical values for the kinematic variables obtained by solving the proposed two-dimensional Cosserat plate bending problem and the three-dimensional Cosserat Elasticity for a plate made of polyurethane foam. Because of the symmetry of the square plate the values of the displacements u_1 and u_2 are identical, and the absolute values of the microrotations φ_1 and φ_2 are identical. Tables 3–1, 3–2 and 3–3 represents the numerical comparisons of the maximum values

Table 3–1: Comparison of the Maximum Vertical Deflection u_3 of the Polyurethane Foam Square Plate

a/h	10	15	20	25	30
Optimal value of η	0.238315	0.128047	0.079566	0.054878	0.040799
Cosserat Plate Model (m)	0.023630	0.062281	0.120595	0.201153	0.307674
Cosserat 3D Elasticity (m)	0.023744	0.062428	0.120762	0.201336	0.307870
Relative Error (%)	**0.47**	**0.23**	**0.13**	**0.09**	**0.06**

Table 3–2: Comparison of the Maximum Microrotation φ_1 of the Polyurethane Foam Square Plate

a/h	10	15	20	25	30
Optimal value of η	0.238315	0.128047	0.079566	0.054878	0.040799
Cosserat Plate Model	0.001336	0.005256	0.013236	0.026625	0.046770
Cosserat 3D Elasticity	0.001343	0.005268	0.013254	0.026649	0.046799
Relative Error (%)	**0.48**	**0.23**	**0.14**	**0.09**	**0.06**

of the main kinematic variables obtained by solving the proposed two-dimensional Cosserat plate bending problem and the three-dimensional Cosserat Elasticity – vertical deflection u_3, microrotation φ_1 and shear displacement u_1 respectively.

The qualitative comparisons of the transverse variations of the displacement and microrotation for the proposed model and the three-dimensional Cosserat Elasticity, are given in the Figures 3–2 and 3–3, where the ratio a/h is equal to 30.

Table 3–3: Comparison of the Maximum Displacement u_1 of the Polyurethane Foam Square Plate

a/h	10	15	20	25	30
Optimal value of η	0.238315	0.128047	0.079566	0.054878	0.040799
Cosserat Plate Model (m)	0.003192	0.005837	0.008615	0.011604	0.014892
Cosserat 3D Elasticity (m)	0.003063	0.005617	0.008305	0.011206	0.014407
Relative Error (%)	**4.21**	**3.93**	**3.74**	**3.55**	**3.36**

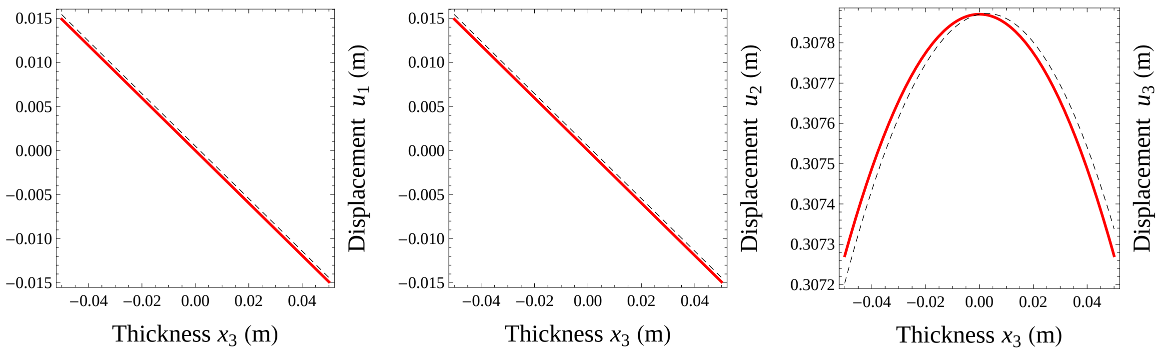

Figure 3–2: The comparison of the transverse variation of the displacement components: solid line - the proposed model, dashed line - three-dimensional Cosserat Elasticity (a/h = 30)

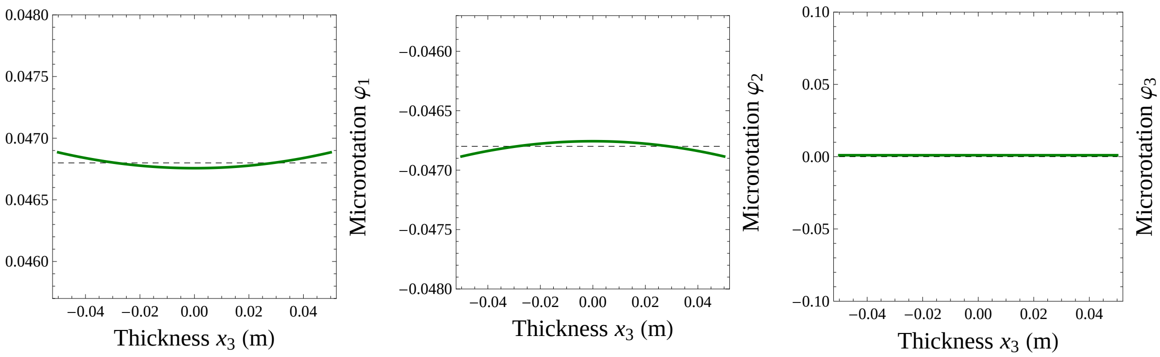

Figure 3–3: The comparison of the transverse variation of the microrotation components: solid line - the proposed model, dashed line - three-dimensional Cosserat Elasticity (a/h = 30)

The qualitative comparisons of the transverse variations of the stress and couple–stress components for the proposed model and the three-dimensional Cosserat Elasticity, are given in the Figures 3–4 and 3–5, where the ratio a/h is equal to 30.

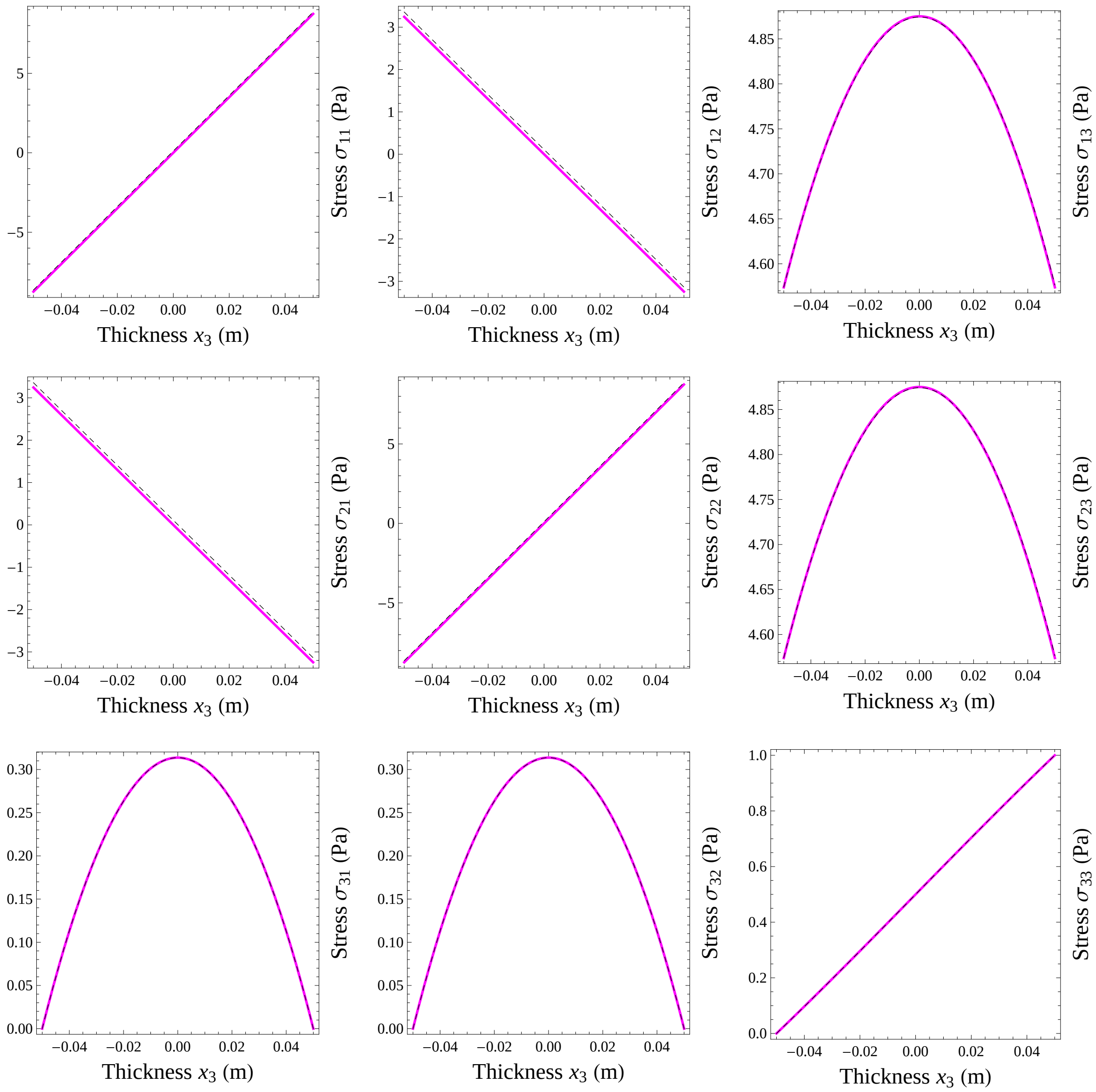

Figure 3–4: The comparison of the transverse variation of the stress components: solid line - the proposed model, dashed line - three-dimensional Cosserat Elasticity (a/h = 30)

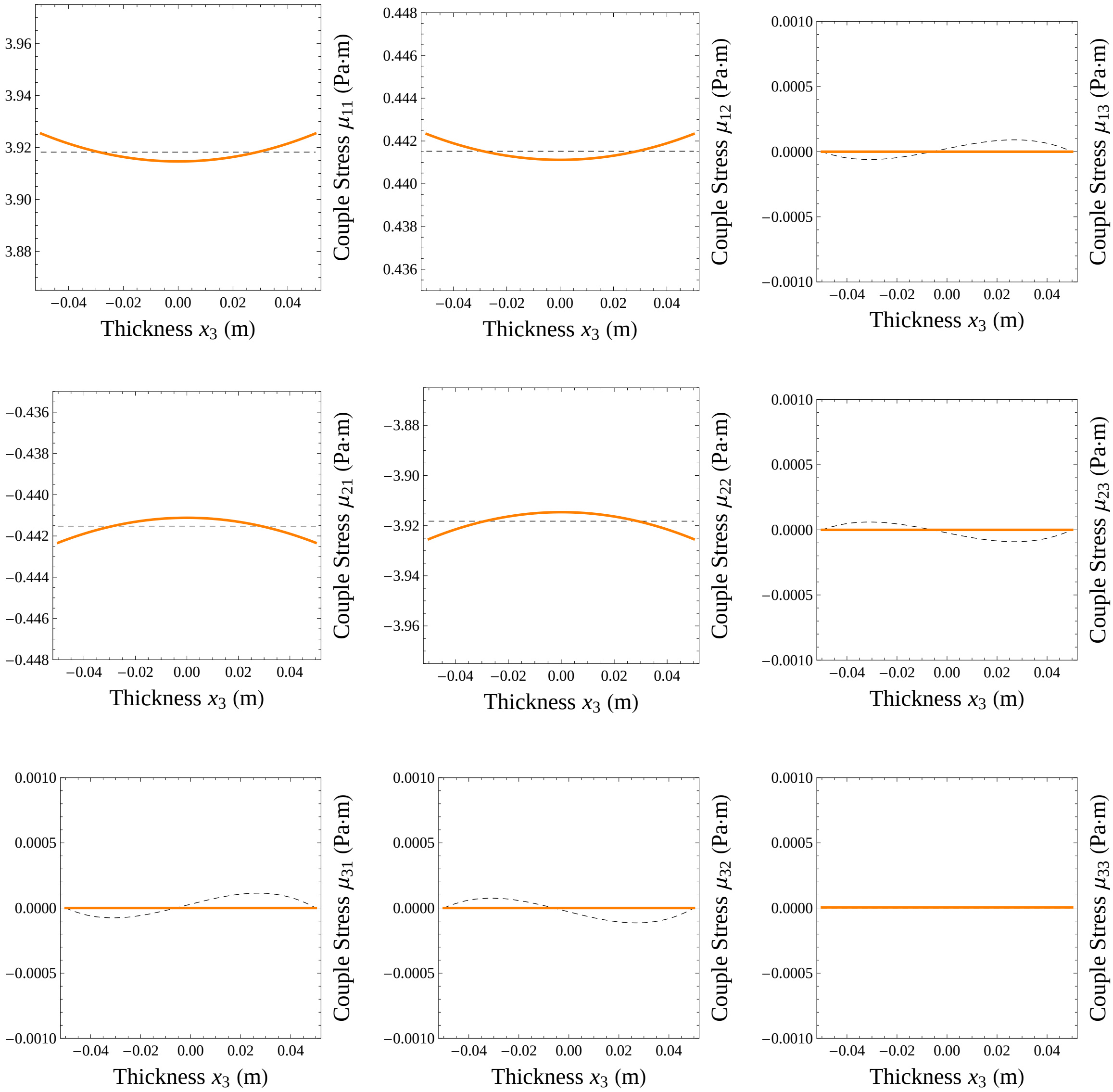

Figure 3–5: The comparison of the transverse variation of the couple stress components: solid line - the proposed model, dashed line - three-dimensional Cosserat Elasticity (a/h = 30)

The comparison of the numerical values of the kinematic variables for the square plate made of dense polyurethane foam with the analytical solution of the three-dimensional Cosserat elasticity confirms the high order of approximation of three-dimensional (exact) solution. The relative error of order 1% for the maximum vertical deflection is compatible with the precision of the Reissner plate theory [38] (see Figure 3–6).

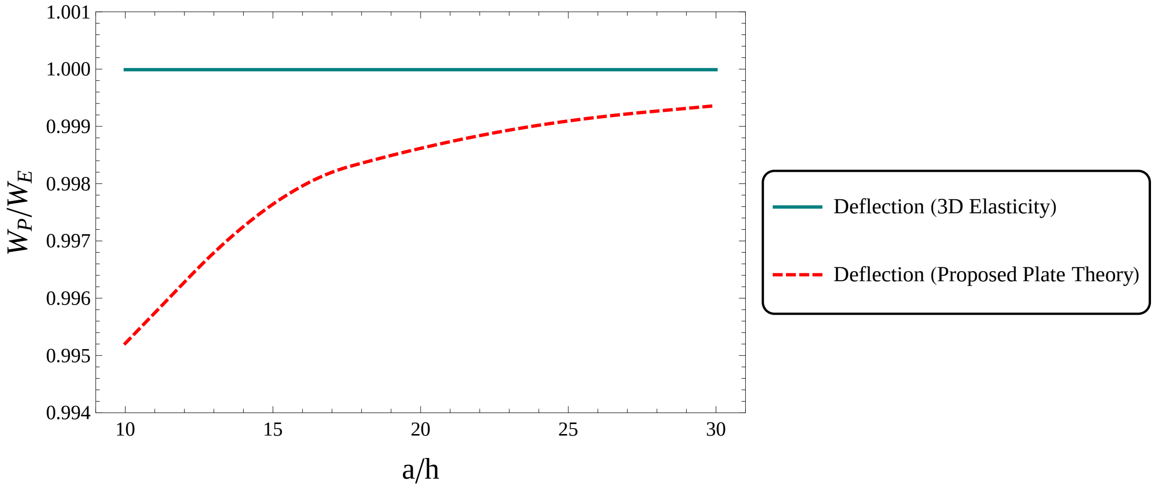

Figure 3–6: Comparison of the vertical deflection for the square plate made of dense polyurethane foam: analytical solution of the proposed plate theory W_P and the analytical solution of the three-dimensional Cosserat elasticity W_E

The graph in Figure 3–7 represents the total plate energy depending on the splitting parameter η. The figure shows the optimal value of η which minimizes the plate stress energy and the relative error for the vertical deflection calculated using three-dimensional Cosserat elasticity $(a/h = 30\ )$.

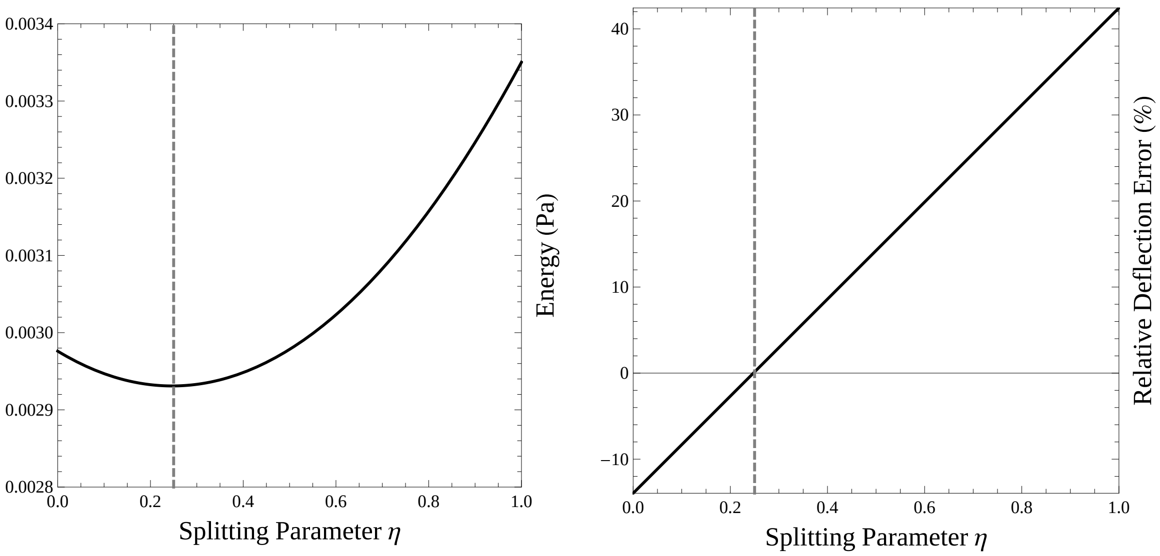

Figure 3–7: Elastic energy approximation (left) and the vertical deflection relative error (right) depending on the values of the splitting parameter η $(a/h = 10)$: Optimal value of the splitting parameter corresponds to the minimum of the elastic energy $(\eta = 0.25)$

Figure 3–8 provides information for comparison between Cosserat and classical elasticity. The energy of microrotation becomes a part of the total elastic energy. This causes the redistribution of the elastic energy depending on the value of the asymmetric part. We perform computations for different levels of the asymmetric microstructure by reducing the values of the elastic asymmetric parameters. In the case when 0.1% of real values of asymmetric parameters are used, i.e. the microstructure is almost irrelevant, the solution of the proposed model converges to the corresponding Reissner solution.

Figure 3–8 also illustrates such important feature of the Cosserat plate theory as the size effect. The Cosserat elasticity predicts that plates of smaller thickness will be more rigid than would be expected on the basis of the Reissner plate theory. This can be clearly seen as the relative deflection declines with thickness of the plate. Similar experimental behavior was reported in [16] for torsion and bending of cylindrical Cosserat rods.

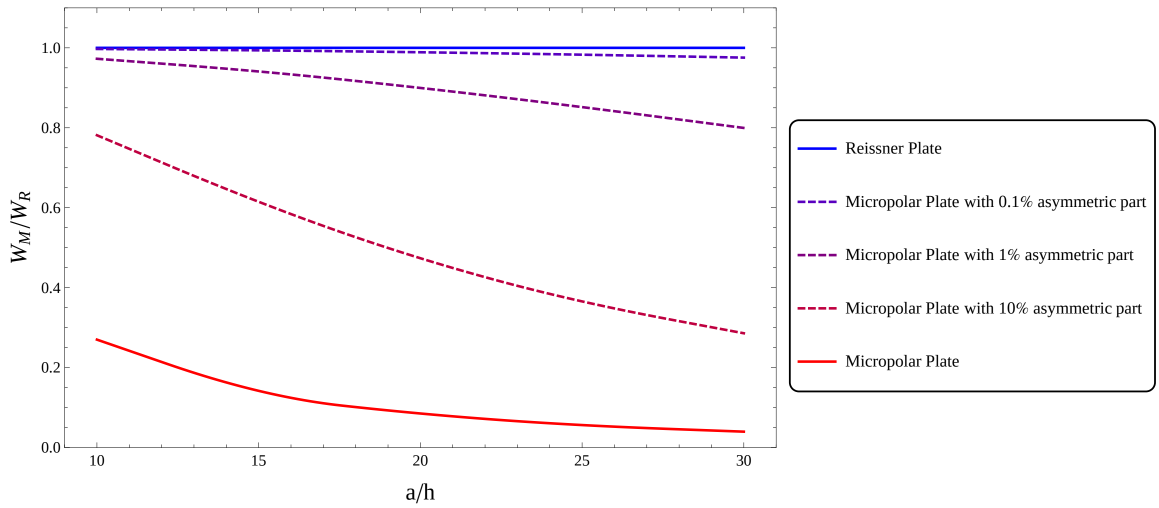

Figure 3–8: Comparison of the vertical deflections of the Cosserat plate W_M and Reissner plate W_R, which illustrates the influence of the microstructure of the Cosserat plate

Chapter 4

Finite Element Computation of Cosserat Elastic Plates

4.1 Scope of the Chapter

In this chapter we develop the Finite Element Method for Cosserat elastic plates based on the calculation of the optimal value of the splitting parameter. We discuss the existence and uniqueness of the weak solution and the convergence of the proposed FEM. We present the Finite Element analysis of the clamped Cosserat plates of different shapes under different loads. We also provide the numerical validation of the proposed FEM by estimating the order of convergence, when comparing the main kinematic variables with the analytical solution developed in the Chapter 3 for simply supported square plate.

4.2 Formulation of the Clamped Cosserat Plate Bending Problem

The field equations (2.97) can be represented as an elliptic system of nine partial differential equations:

$$Lu = f(\eta),$$

where L is a linear differential operator acting on the vector of nine kinematic variables u and $f(\eta)$ is the right-hand side vector defined as (2.98), that in general depends on η.

Let us consider the following hard clamped boundary conditions similar to [65]:

$$W = 0, W^* = 0, \mathbf{\Psi} \cdot \hat{\mathbf{s}} = 0, \mathbf{\Psi} \cdot \hat{\mathbf{n}} = 0, \Omega_3 = 0, \tag{4.1}$$

$$\mathbf{\Omega^0} \cdot \hat{\mathbf{s}} = 0, \mathbf{\Omega^0} \cdot \hat{\mathbf{n}} = 0, \hat{\mathbf{\Omega}} \cdot \hat{\mathbf{s}} = 0, \hat{\mathbf{\Omega}} \cdot \hat{\mathbf{n}} = 0, \tag{4.2}$$

where $\hat{\mathbf{n}}$ and $\hat{\mathbf{s}}$ are the normal and the tangent vectors to the boundary. These conditions represent homogeneous Dirichlet type boundary conditions for the kinematic variables:

$$W = 0,\ W^* = 0,\ \Psi_1 = 0,\ \Psi_2 = 0,\ \Omega_3 = 0, \tag{4.3}$$

$$\hat{\Omega}_1^0 = 0,\ \hat{\Omega}_2^0 = 0,\ \hat{\Omega}_1^0 = 0,\ \hat{\Omega}_2^0 = 0. \tag{4.4}$$

Clamped plate boundary conditions correspond to the boundary conditions (2.9) for the three-dimensional Cosserat solid introduced in the Chapter 3.

4.3 Finite Element Algorithm for Cosserat Elastic Plates

The right-hand side of the system (4.2) depends on the splitting parameter η and so does the solution. Therefore the solution of the Cosserat elastic plate bending problem requires not only solving the system (2.97), but also an additonal technique for the calculation of the value of the splitting parameter, that corresponds to the unique solution. Considering that the elliptic systems of partial differential equations correspond to a state where the minimum of the energy is reached, the optimal value of the splitting parameter should minimize the elastic plate energy (2.63) [67].

We propose the Finite Element Method for Cosserat elastic plates based on the algorithm for the optimal value of the splitting parameter presented in the Chapter 3. This algorithm requires solving the system (2.97) for two different values of the splitting parameter η, numerical calculation of stresses, strains and the corresponding work densities.

The proposed Finite Element Method for Cosserat elastic plates consists of the following phases:

1. Use classic Galerkin FEM to solve two elliptic systems:

$$Lu_0 = f\,(0)$$

$$Lu_1 = f\,(1)$$

for u_0 and u_1 respectively.

2. Calculate numerically the stress sets $\mathscr{S}^{(0)}$ and $\mathscr{S}^{(1)}$ from the solutions u_0 and u_1 respectively, using (2.83) - (2.92).

3. Calculate numerically the strain sets $\mathscr{E}^{(0)}$ and $\mathscr{E}^{(1)}$ from the solutions u_0 and u_1 respectively, using (2.56) - (2.62).

4. Calculate numerically the work densities $\mathscr{W}^{(ij)}$ as $\mathscr{S}^{(i)} \cdot \mathscr{E}^{(j)}$.

5. Calculate the optimal value of the splitting parameter η_0 using (4.19).

6. Calculate the optimal solution u_{η_0} of the Cosserat plate bending problem from (2.107)

4.4 Weak Formulation of the Clamped Cosserat Plate Bending Problem

Let us denote by $\mathbf{L}^2(B_0)$ the standard space of square-integrable functions defined everywhere on B_0:

$$\mathbf{L}^2(B_0) = \left\{ v : \int_{B_0} v^2 ds < \infty \right\}$$

and by $\mathbf{H}^1(B_0)$ the Hilbert space of functions that are square-integrable together with their first partial derivatives:

$$\mathbf{H}^1(B_0) = \left\{ v : v \in L^2(B_0), \partial_i v \in L^2(B_0) \right\}$$

Let us denote the Hilbert space of functions from $\mathbf{H}^1(B_0)$ that vanish on the boundary as in [68]:

$$\mathbf{H}^1_0(B_0) = \left\{ v \in \mathbf{H}^1(B_0), v = 0 \text{ on } \partial B_0 \right\}$$

The space $\mathbf{H}^1_0(B_0)$ is equipped with the inner product:

$$\langle u, v \rangle_{\mathbf{H}^1_0} = \int_{B_0} (uv + \partial_i u \partial_i v)\, ds \text{ for } u, v \in \mathbf{H}^1_0(B_0)$$

Taking into account that the boundary conditions for all variables are of the same homogeneous Dirichlet type, we look for the solution in the function space $\mathscr{H}(B_0)$ defined as

$$\mathscr{H} = \mathbf{H}^1_0(B_0)^9 . \tag{4.5}$$

The space $\mathscr{H}$ is equipped with the inner product $\langle u, v \rangle_{\mathscr{H}}$:

$$\langle u, v \rangle_{\mathscr{H}} = \sum_{i=1}^{9} \langle u_i, v_i \rangle_{\mathbf{H}^1_0} \text{ for } u, v \in \mathscr{H}$$

and relative to the metric

$$d(u, v) = \|u - v\|_{\mathscr{H}} \text{ for } u, v \in \mathscr{H},$$

induced by the norm $\|x\| = \sqrt{\langle x, x\rangle_{\mathscr{H}}}$, the space $\mathscr{H}$ is a complete metric space and therefore is a Hilbert space [69].

Let us consider a dot product of both sides of the system of the field equations (4.2) and an arbitrary function $v \in \mathscr{H}$:

$$v \cdot Lu = v \cdot f(\eta)$$

and then integrate both sides of the obtained scalar equation over the plate B_0:

$$\int_{B_0} (v \cdot Lu)\, ds = \int_{B_0} (v \cdot f(\eta))\, ds.$$

Let us introduce a bilinear form $a(u,v) : \mathscr{H} \times \mathscr{H} \to \mathbb{R}$ and a linear form $b_{(\eta)}(v) : \mathscr{H} \to \mathbb{R}$ defined as

$$\begin{aligned} a(u,v) &= \int_{B_0} (v \cdot Lu)\, ds, \\ b_{(\eta)}(v) &= \int_{B_0} (v \cdot f(\eta))\, ds. \end{aligned} \tag{4.6}$$

The expression for $a(u,v)$

$$a(v,u) = \int_{B_0} (v_i L_{ij} u_j)\, ds$$

is a summation over the terms of the form

$$a^{ij}(v_m, u_n) = \int_{B_0} \left(v_m \hat{L} u_n\right) ds,$$

where $v_m \in \mathscr{H}_m$, $u_n \in \mathscr{H}_n$ and $\hat{L}$ is a scalar differential operator.

There are 3 types of linear operators present in the field equations (2.97) – operators of order zero, one and two, which are constant multiples of the following differential operators:

$$
\begin{aligned}
L^{(0)} &= \mathbb{1}, && (4.7)\\
L^{(1)} &= \frac{\partial}{\partial x_\alpha}, && (4.8)\\
L^{(2)} &= -\nabla \cdot A\nabla, && (4.9)
\end{aligned}
$$

These operators act on the components of the vector u and are multiplied by the components of the vector v and the obtained expressions are then integrated over B_0:

$$
\begin{aligned}
\int_{B_0} \left(v_m L^{(0)} u_n\right) ds &= \int_{B_0} \left(v_m u_n\right) ds && (4.10)\\
\int_{B_0} \left(v_m L^{(1)} u_n\right) ds &= \int_{B_0} \left(v_m \frac{\partial u_n}{\partial x_\alpha}\right) ds && (4.11)\\
\int_{B_0} \left(v_m L^{(2)} u_n\right) ds &= -\int_{B_0} \left(v_m (\nabla \cdot A\nabla) u_n\right) ds
\end{aligned}
$$

where $v_m \in \mathscr{H}_m$ and $u_n \in \mathscr{H}_n$.

The weak form of the second order operator is obtained by performing the corresponding integration by parts and taking into account that the test functions v_m vanish on the boundary ∂B_0:

$$
\begin{aligned}
\int_{B_0} \left(v_m L^{(2)} u_n\right) ds &= -\int_{B_0} \left(v_m (\nabla \cdot A\nabla u_n)\right) ds\\
&= -\int_{\partial B_0} \left(A\nabla u_n \cdot n\right) v_m d\tau + \int_{B_0} \left(A\nabla u_n \cdot \nabla v_m\right) ds\\
&= \int_{B_0} \left(A\nabla u_n \cdot \nabla v_m\right) ds && (4.12)
\end{aligned}
$$

The expression for $b_{(\eta)}\left(v\right)$:

$$
b_{(\eta)}\left(v\right) = \int_{B_0} v_i f_i\left(\eta\right) ds
$$

represents a summation over the terms of the form:

$$
\int_{B_0} v_m \hat{f}\left(\eta\right) ds,
$$

Taking into account that the optimal solution of the field equations (4.2) minimizes the stress plate energy (2.44), we can give the weak formulation for the clamped Cosserat plate bending problem.

Weak Formulation of the Clamped Cosserat Plate Bending Problem

Find all $u \in \mathscr{H}$ *and* $\eta \in \mathbb{R}$ *that minimize the stress plate energy* $U_K^{\mathscr{S}}(u, \eta)$ *defined as (2.44) subject to*

$$a(v, u) = b_{(\eta)}(v) \;\; \textit{for all } v \in \mathscr{H} \tag{4.13}$$

4.5 Construction of the Finite Element Spaces

Let us construct the finite element space, i.e. finite-dimensional subspace $\mathscr{H}_h$ of the space $\mathscr{H}$, where we will be looking for an approximate Finite Element solution of the weak formulation (4.13).

Let us assume that the boundary ∂B_0 is a polygonal curve. Let us make a triangulation of the domain B_0 by subdividing B_0 into l non-overlapping triangles K_i with m vertices N_j:

$$B_0 = \bigcup_{i=1}^{l} K_i = K_1 \cup K_2 \cup ... \cup K_l$$

such that no vertex of the triangular element lies on the edge of another triangle (see Figure 4–1).

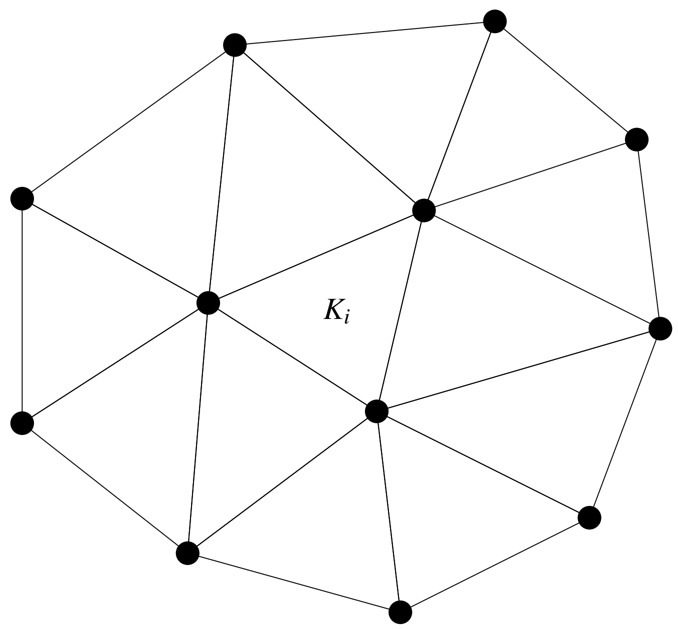

Figure 4–1: Example of the Finite Element triangulation of the domain B_0

Let us introduce the mesh parameter h as the greatest diameter among the elements K_i:

$$h = \max_{i=\overline{1,l}} d\left(K_i\right),$$

which for the triangular elements corresponds to the length of the longest side of the triangle.

We now define the finite dimensional space $\hat{\mathscr{H}_h}$ as a space of all continuous functions that are linear on each element K_j and vanish on the boundary:

$$\hat{\mathscr{H}_h} = \mathscr{H}_i^h = \left\{v : v \in C\left(B_0\right), v \text{ is linear on every } K_j, v = 0 \text{ on } \partial B_0\right\}.$$

By definition $\mathscr{H}_i^h \subset \mathscr{H}_i$, and the finite element space $\mathscr{H}_h$ is then defined as:

$$\mathscr{H}_h = \hat{\mathscr{H}_h}^9 \tag{4.14}$$

The approximate weak solution u^h can be found from the Galerkin formulation of the clamped Cosserat plate bending problem [70], [71].

Galerkin Formulation of the Clamped Cosserat Plate Bending Problem

Find all $u^h \in \mathscr{H}_h$ and $\eta \in \mathbb{R}$ that minimize the stress plate energy $U_K^{\mathscr{S}}\left(u^h, \eta\right)$ defined as (2.44) subject to

$$a\left(v^h, u^h\right) = b_{(\eta)}\left(v^h\right) \text{ for all } v^h \in \mathscr{H}_h \tag{4.15}$$

The description of the function $v_i^h \in \mathscr{H}_i^h$ is provided by the values $v_i^h\left(N_k\right)$ at the nodes N_k $(k = \overline{1, m})$.

Let us define the set of basis functions $\{\phi_1, \phi_2, ..., \phi_m\}$ of each space $\mathscr{H}_i^h$ as

$$\phi_j\left(N_k\right) = \delta_{jk}, \;\; j, k = \overline{1, m}$$

excluding the points N_k on the boundary ∂B_0.

Therefore

$$\mathscr{H}_i^h = span\left\{\phi_1, \phi_2, ..., \phi_m\right\} = \left\{v : v = \sum_{j=1}^{m} \alpha_j^{(i)} \phi_j\right\}$$

and the functions ϕ_j is non-zero only at the node N_j and those that belong to the specified boundary and the support of ϕ_j consists of all triangles K_i with the common node N_j (see the Figure 4–2).

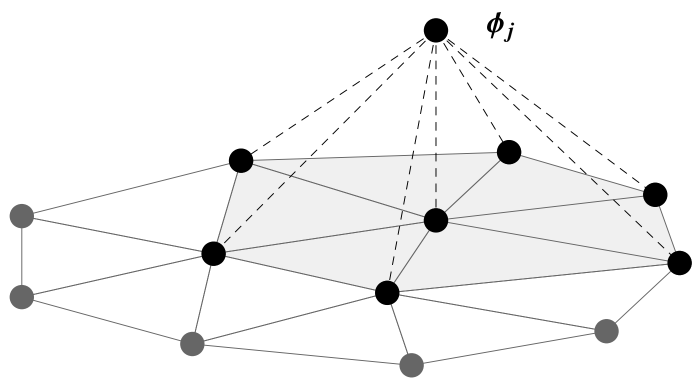

Figure 4–2: Example of the Finite Element basis function

Since the spaces $\mathscr{H}_i^h$ are identical they will also have identical sets of basis functions ϕ_j $(j = \overline{1,m})$. Sometimes we will need to distinguish between the basis functions of different spaces assigning the superscript of the functions space to the basis function, i.e. the basis functions for the space $\mathscr{H}_i^h$ are ϕ_j^i. For computational purposes these superscripts will be droped.

4.6 Calculation of the Stiffness Matrix and the Load Vector

The bilinear form of the Galerkin formulation (4.15) is given as

$$a\left(v^h, u^h\right) = a^{ij}\left(v_i^h, u_j^h\right) = \int_{B_0} v_i^h L_{ij} u_j^h ds \tag{4.16}$$

Since $u_j^h \in \mathscr{H}_j^h$ then there exist such constants $\alpha_p^{(j)} \in \mathbb{R}$ that

$$u_j^h = \alpha_p^{(j)} \phi_p^{(i)}$$

Since the equation (4.16) is satisfied for all $v_i^h \in \mathscr{H}_i^h$ then it is also satisfied for all basis functions $\phi_k^{(i)}$ $(k = \overline{1,m})$:

$$a^{ij}\left(v_i^h, u_j^h\right) = a^{ij}\left(\phi_k^{(i)}, \alpha_p^{(j)} \phi_p^{(j)}\right) = \alpha_p^{(j)} a^{ij}\left(\phi_k^{(i)}, \phi_p^{(j)}\right)$$

where

$$a^{ij}(v,u) = \int_{B_0} v L_{ij} u ds \tag{4.17}$$

Following [71] we define the block stiffness matrices K^{ij} $(i,j = \overline{1,9})$:

$$K^{ij} = \begin{bmatrix} a^{ij}\left(\phi_1^{(i)}, \phi_1^{(j)}\right) & \dots & a^{ij}\left(\phi_1^{(i)}, \phi_m^{(j)}\right) \\ \vdots & \ddots & \vdots \\ a^{ij}\left(\phi_m^{(i)}, \phi_1^{(j)}\right) & \dots & a^{ij}\left(\phi_m^{(i)}, \phi_m^{(j)}\right) \end{bmatrix}$$

For computational purposes the superscripts of the basis functions can be droped and the block stiffness matrices K^{ij} can be calculated as

$$K^{ij} = \begin{bmatrix} a^{ij}(\phi_1, \phi_1) & \dots & a^{ij}(\phi_1, \phi_m) \\ \vdots & \ddots & \vdots \\ a^{ij}(\phi_m, \phi_1) & \dots & a^{ij}(\phi_m, \phi_m) \end{bmatrix}$$

Let us define the block load vectors $F^i(\eta)$ $(i = \overline{1,9})$:

$$F^i(\eta) = \begin{bmatrix} b^i_{(\eta)}(\phi_1) \\ \vdots \\ b^i_{(\eta)}(\phi_m) \end{bmatrix}$$

and the solution block vectors α^i corresponding to the variable u_i^h $(i = \overline{1,9})$:

$$\alpha^i = \begin{bmatrix} \alpha^i_1 \\ \vdots \\ \alpha^i_m \end{bmatrix}$$

The equation (4.15) of the Galerkin formulation can be rewritten as

$$\left(K^{ij}\right)\alpha^i = F^j(\eta) \tag{4.18}$$

The global stiffness matrix consists of 81 block stiffness matrices K^{ij}, the global load vector consists of 9 block load vectors $F^i(\eta)$ and the global displacement vector is represented by the 9 blocks of coefficients α^i. The entries of the block matrices K^{ij} and the block vectors $F^i(\eta)$ can be calculated as

$$\begin{aligned} K^{ij}_{mn} &= \int_{B_0} \phi_m L_{ij} \phi_n ds \\ F^i_m(\eta) &= \int_{B_0} \phi_m f_i(\eta)\, ds \end{aligned}$$

The block matrix form of the equation (4.15) is given as

$$\begin{bmatrix} \boxed{K^{11}} & \boxed{K^{12}} & \cdots & \boxed{K^{19}} \\ \boxed{K^{21}} & \boxed{K^{22}} & \cdots & \boxed{K^{29}} \\ \vdots & \vdots & \ddots & \vdots \\ \boxed{K^{91}} & \boxed{K^{92}} & \cdots & \boxed{K^{99}} \end{bmatrix} \begin{bmatrix} \boxed{\alpha^{1}} \\ \boxed{\alpha^{2}} \\ \vdots \\ \boxed{\alpha^{9}} \end{bmatrix} = \begin{bmatrix} \boxed{F^{1}(\eta)} \\ \boxed{F^{2}(\eta)} \\ \vdots \\ \boxed{F^{9}(\eta)} \end{bmatrix}$$

4.7 Existence and Uniqueness of the Weak Solution

We will follow [72] and [73], where the analysis of the analytic regularity for the linear elliptic systems and their general treatment were recently presented.

Let us consider the bilinear form $a(\cdot,\cdot)$ defined in (4.6):

$$a\,(u,v) = \int_{B_0} v_i L_{ij} u_j ds$$

where L_{ij} are linear differential operators of at most second order. Employing integration by parts for the second order operators L_{ij} the bilinear form $a(\cdot,\cdot)$ can be rewritten in the following form:

$$a\,(u,v) = \sum_{|\beta|,|\gamma|\leq 1} \int_{B_0} c_{ij} \partial^{\beta} v_i \partial^{\gamma} u_j ds$$

where β and γ are multi-indices.

Since coefficients c_{ij} are constant and therefore bounded on B_0, the bilinear form $a(\cdot,\cdot)$ is continuous over $\mathscr{H}$ [72], i.e. there exists a constant $C > 0$ such that

$$|a(v,u)| \leq C \|v\|_{\mathscr{H}} \|u\|_{\mathscr{H}} \qquad \forall u, v \in \mathscr{H}.$$

Since the operator L is strong elliptic on B_0 the bilinear form $a(\cdot,\cdot)$ is V-elliptic on $\mathscr{H}$ [72], [67], i.e. there exists a constant $\alpha > 0$ such that

$$a(u,u) \geq \alpha \|u\|^2_{\mathscr{H}} \qquad \forall v \in \mathscr{H}$$

The strong ellipticity of the operator L follows from the positive definiteness of its principal symbol $L(\xi)$ for all $\xi \in \mathbb{R}^2$ [74], [75]:

$$\begin{aligned} \tau^T L(\xi)\, \tau \;\; = \;\; & c_1 (\xi_1\tau_1 + \xi_2\tau_2)^2 + c_2 (\xi_1\tau_2 - \xi_2\tau_1)^2 + \left(\xi_1^2 + \xi_2^2\right)\left(c_3\tau_3^2 + c_5\tau_4^2 + c_4\tau_7^2\right) \\ & + (c_7 + c_8)(\xi_1\tau_5 + \xi_2\tau_6)^2 + (c_7 + c_8)(\xi_1\tau_5 + \xi_2\tau_6)(\xi_1\tau_9 - \xi_2\tau_8) \\ & + \frac{4}{5}(c_7 + c_8)(\xi_1\tau_9 - \xi_2\tau_8)^2 + (c_7 + c_8)(\xi_1\tau_5 - \xi_2\tau_6)^2 \\ & + (c_7 + c_8)(\xi_1\tau_5 - \xi_2\tau_6)(\xi_1\tau_9 + \xi_2\tau_8) + \frac{4}{5}(c_7 + c_8)(\xi_1\tau_9 + \xi_2\tau_8)^2 > 0 \end{aligned}$$

The existence of the solution of the weak problem (4.13) and its uniqueness are the consequences of the Lax-Milgram Theorem [76], [47].

Lax-Milgram Theorem

Given a Hilbert space V, a bilinear form $a(\cdot,\cdot) : V \times V \to \mathbb{R}$ that is continuous and V-elliptic, and a continuous linear form $f : V \to \mathbb{R}$, then there exists a unique $u \in V$ such that

$$a(v,u) = f(v) \qquad \forall v \in V$$

and the solution u depends continuously on the data f:

$$\|u\|_V \leq \frac{1}{\alpha} \|f\|_{V'}$$

where α is the V-ellipticity constant and V' is the dual space of V.

Note that the existence and uniqueness of the Galerkin weak problem (4.15) is also a consequence of the Lax-Milgram theorem, since the bilinear form $a(\cdot,\cdot)$ restricted on $\mathscr{H}^h$ obviously remains bilinear, continuous and V-elliptic [67]. Lax-Milgram theorem also states that the solution is bounded by the right hand side which represents the stability condition for the Galerkin method.

4.8 Convergence of the Galerkin Method

The convergence of the Galerkin approximation follows from Céa's lemma and an additional convergence theorem [77], [67].

Céa's Lemma

Let $u \in V$ be the solution of the weak problem

$$a(v,u) = F(v) \qquad \forall v \in V$$

and $u^h \in V^h$ be the solution of the corresponding Galerkin weak problem

$$a(v^h,u^h) = F(v^h) \qquad \forall v^h \in V^h$$

where V and V^h are Hilbert spaces such that $V^h \subset V$, and a bilinear form $a(\cdot,\cdot)$ is continuous and coercive on V, then

$$\left\|u - u^h\right\|_V \leq \frac{C}{\alpha} \inf_{v \in V^h} \left\|u - v\right\|_V$$

where C and α are the continuity and the coercivity constants.

The inequality in the Céa's lemma will imply convergence of the approximate Galerkin solution u^h to the weak solution u if the finite element spaces V^h approximate the space V [67].

Galerkin Method Convergence Theorem

Let V be a Hilbert space and $V_1 \subset V_2 \subset ... \subset V$ a sequence of its finite-dimensional subspaces such that

$$\overline{\bigcup_{n=1}^{\infty} V_n} = V$$

Let $a(\cdot,\cdot)$ be a continuous and coercive on V and let $u \in V$ be the solution of the weak problem

$$a(v,u) = F(v) \qquad \forall v \in V$$

and $u^n \in V^n$ be the solution of the corresponding Galerkin weak problem

$$a(v^n,u^n) = F(v^n) \qquad \forall v^n \in V^n$$

then

$$\lim_{n\to\infty} \|u - u^n\|_V = 0$$

i.e. the Galerkin method converges.

On the polygonal domains the sequence of subspaces of $\mathscr{H} = \mathbf{H}_0^1(B_0)^9$ can be obtained by the successive uniform refinement of the initial mesh using the midpoints as new nodes thus subdividing every triangle into 4 congruent triangles. Therefore $\mathscr{H}_n \subset \mathscr{H}_{n+1}$ for every $n \in \mathbb{N}$ and the sequence of spaces $\mathscr{H}^n$ is dense in $\mathscr{H}$ [78], and thus

$$\overline{\bigcup_{n=1}^{\infty} \mathscr{H}_n} = \mathscr{H}$$

and u^n converges to u as $n \to \infty$ [67], [79].

It was shown that there exists a sequence of triangulations that ensures optimal rates of convergence in $\mathbf{H}^1$-norm for the FEM approximation of the second order strongly elliptic system with zero Dirichlet boundary condition on polyhedron domain with continuous, piecewise polynomials of degree m [80].

4.9 Calculation of the Optimal Value of the Splitting Parameter

We perform the calculation of the optimal value of the splitting parameter according to the algorithm presented in the Chapter 3. The optimal value of the splitting parameter is given as

$$\eta_0 = \frac{2\mathscr{W}^{(00)} - \mathscr{W}^{(10)} - \mathscr{W}^{(01)}}{2\left(\mathscr{W}^{(11)} + \mathscr{W}^{(00)} - \mathscr{W}^{(10)} - \mathscr{W}^{(01)}\right)}, \tag{4.19}$$

where $\mathscr{W}^{(ij)} = \mathscr{S}^{(i)} \cdot \mathscr{E}^{(j)}$.

It requires the calculation of the stress and strain sets $\mathscr{S}^{(i)}$ and $\mathscr{E}^{(i)}$, and the Cosserat plate internal work densities done by the stress and couple stress over the Cosserat strain field $\mathscr{W}^{(ij)}$ for two different solutions of the system (2.97).

The calculation of the stress and strain components from the solution vector can be done using the constitutive formulas in reverse form (2.83) - (2.92). These formulas imply the necessity of the approximation of the partial derivatives of the kinematic variables. Since the kinematic variables are piecewise linear, first we calculate the vector $\hat{\mathbf{n}} = n_i \hat{\mathbf{e}}_i$ normal to the solution at each element and then calculate the tangent plane. The approximate value of the partial derivative at the particular element is the negative of the quotient of the corresponding components of the normal vector:

$$\begin{aligned} &-\frac{n_1}{n_3} \text{ for the derivative by } x_1 \\ &-\frac{n_2}{n_3} \text{ for the derivative by } x_2 \end{aligned}$$

Once the partial derivatives are approximated we can calculate the components of stresses and strains on each element by adding the corresponding approximation sets of values at each node.

4.10 Implementation

In our implementation of the Finite Element method to solve the Galerkin formulation (4.18), we use the MATLAB environment to carry out the following procedure.

1. Implement the class `mesh`

We implement the class `mesh`, whose objects will contain such information as the list of vertices and their coordinates, indices of the vertices in the triangular element, boundary edges, mappings to the reference element, etc.

The class `mesh` contains the following properties:

- `obj.nvertices` – number of vertices
- `obj.x` – array of x-coordinates of the vertices
- `obj.y` – array of y-coordinates of the vertices
- `obj.nelements` – number of triangular elements
- `obj.vertex1` – array of the indices of the first vertices of each element
- `obj.vertex2` – array of the indices of the second vertices of each element
- `obj.vertex3` – array of the indices of the third vertices of each element
- `obj.nedges` – number of boundary edges
- `obj.start` – list of the start vertex indices of the boundary edges
- `obj.finish` – list of the finish vertex indices of the boundary edges
- `obj.condition` – list of the boundary types of the boundary edges

The class `mesh` also contains the following methods:

- `display(obj)` – draws given triangulation
- `adjelements(obj,vertexindex)` – returns the list of indices of the elements containing the given vertex `vertexindex`

- `obj.adjvertices(obj,vertexindex)` – returns the list of indices of the vertices adjacent to the given vertex `vertexindex`
- `obj.mapping1d(obj,edgeindex,iks)` – mapping between the segment $[0, 1]$ and the boundary edge `edgeindex`
- `obj.mapping2d(obj,elementindex,iks,igrek)` – mapping between the reference element and the element `elementindex`
- `obj.jacobianmatrix(obj,elementindex,localvertexindex)` – returns the jacobian of the transformation of the reference element to the element `cellindex`

2. Generate the triangulation of the plate B_0.

We implement the function `meshrecognizer` responsible for the generation of the triangular mesh on the specified domain and its recognition into the object of the class `mesh`.

We start by specifying the domain in the function `domain` in terms of the inequalities. The output of `domain` is the set formula `sf` and the name space matrix `ns`. The function `ortdomain` returns the parameter `gd` – the Constructive Solid Geometry model (CSG model) specified in `domain`. Now the parameters `gd`, `sf` and `ns` are used as the input for the standard MATLAB function `decsg(gd,sf,ns)`. It analyzes the CSG model `gd`, constructs a set of disjoint minimal regions that evaluate to true for the set formula sf, bounded by boundary segments and border segments, and decomposes `gd` into the decomposed geometry `dl`. The name space matrix `ns` is a text matrix that relates the columns in `gd` to variable names in `sf`.

In order to obtain the triangular mesh for the specified domain we call the standard MATLAB function

```
[p,e,t] = initmesh(dl)
```

using the geometry specification function `dl` as an input. The function `initmesh(dl)` uses a Delaunay triangulation algorithm. The size of the triangles, the mesh growth rate and the jiggling of the mesh can be controlled. The output parameters are: the point matrix `p`, the edge matrix `e` and the triangle matrix `t` are the mesh data. In the point matrix `p`, the first and second columns x-coordinates and y-coordinates of the points in the mesh. In the edge matrix `e`, the first and second columns contain indices of the starting and ending point. In the triangle matrix `t`, the first three columns contain indices to the corner points, given in counter clockwise order.

In order to refine the initial triangular mesh we call the standard MATLAB function

```
[ p, e, t] = refinemesh ( dl, p, e, t, 'regular' )
```

which returns a refined version of the triangular mesh specified by the geometry `g`, point matrix `p`, edge matrix `e`, and triangle matrix `t`, performing a regular refinement, where all of the specified triangles are divided into four triangles of the same shape.

3. Implement Numerical Integration.

We implement the function `quadrature` responsible for the numerical integration on the reference domain by employing a Gauss quadrature [81].

Let us define the triangle K_{ref} with the vertices $(0,0)$, $(0,1)$ and $(1,0)$ to be a reference element. We need to perform the following integration:

$$\int_{K_{ref}} f(x,y)dxdy$$

We use the function

```
[x,y,wx,wy] = triquad(n,v)
```

which computes the n^2 nodes with coordinates provided in `x` and `y`, and weights provided in `wx` and `wy` for a triangle with vertices given by the 3×2 vector `v`. The nodes are produced by collapsing the square to a triangle.

Since the basis functions are linear, then the choice of $n = 2$ is sufficient for the numerical integration to be exact.

The numerical integration of

$$\int_{K_{ref}} f(x, y) dx dy$$

therefore is performed as

```
wx' * F * wy
```

where the matrix `F` is given as

$$F = \begin{bmatrix} f(x_{11}, y_{11}) & f(x_{12}, y_{12}) \\ f(x_{21}, y_{21}) & f(x_{22}, y_{22}) \end{bmatrix}.$$

4. Generate the stiffness matrix.

We implement the function `stiffnessmatrix` responsible for the calculation of the global stiffness matrix.

The stiffness matrix consists of 81 block stiffness matrices ($\check{a}^{ij}$). Each block matrix is defines as

$$\check{a}_{ij} = \begin{bmatrix} a^{ij}\left(\phi_1^{(i)}, \phi_1^{(j)}\right) & \dots & a^{ij}\left(\phi_1^{(i)}, \phi_m^{(j)}\right) \\ \vdots & \ddots & \vdots \\ a^{ij}\left(\phi_m^{(i)}, \phi_1^{(j)}\right) & \dots & a^{ij}\left(\phi_m^{(i)}, \phi_m^{(j)}\right) \end{bmatrix}$$

where each entry is of the form

$$a^{ij}\left(\phi_k^{(i)}, \phi_p^{(j)}\right) = \int_{B_0} \phi_k^{(i)} L_{ij} \phi_p^{(j)} ds$$

We define the stiffness matrix as sparse using the MATLAB function `sparse`. We note that there are three types of operators among L_{ij}: order zero, order one and order two. Since many of these operators differ only on a constant we will calculate the stiffness block matrices for each of the operators only once and then fill the block multiplies by the corresponding constants. In order to calculate the stiffness block matrices we employ the functions `phi` and `phider` which return the values of the basis function and its gradient.

The entry of the block stiffness matrix of the operator of order zero is calculated as:

```
1/det ( phiinv ) * ( wx' * F * wy )
```

where `det(phiinv)` is the inverse of the jacobian of the transformation to the reference element and

```
F(i,j) = phi(ver1,x(i,j),y(i,j)) * phi(ver2,x(i,j),y(i,j))
```

The entry of the block stiffness matrix of the operators of order one $\frac{\partial}{\partial x}$ and $\frac{\partial}{\partial y}$ are calculated in the same manner and the matrix `F` given as

```
F(i,j) = phider(ver2) * phiinv * m * phi(ver1,x(i,j),y(i,j))
```

where $m = [1, 0]^T$ for the operator $\frac{\partial}{\partial x}$ and $m = [0, 1]^T$ for the operator $\frac{\partial}{\partial y}$.

The entry of the block stiffness matrix of the operators of order two $\nabla \cdot A\nabla$ are calculated in the same manner and the matrix `F` is given as

```
F(i,j) = phider(ver1) * phiinv * A * phiinv' * phider(ver2)'
```

5. Generate the load vectors.

We implement the function `loadvector` responsible for the calculation of the global load vector.

The load vector consists of 9 load block vectors ($\check{a}^{ij}$). Each block vector is defines as

$$\check{b}^i_\eta = \begin{bmatrix} b^i_\eta(\phi_1) \\ \vdots \\ b^i_\eta(\phi_m) \end{bmatrix}$$

where each entry is of the form

$$b^i_\eta(\phi_k) = \int_{B_0} \phi_k f_i ds$$

The entry of the block load vector is calculated as:

```
1/det ( phiinv ) * ( wx' * F * wy )
```

where `det(phiinv)` is the inverse of the jacobian of the transformation to the reference element and

```
F(i,j) = f(t,eta,x(i,j),y(i,j)) * phi(1,x(i,j),y(i,j))
```

where `f` returns the value of the right-hand side function f_t.

6. Impose the boundary values.

We implement the function `boundaryfix` responsible for imposing the values at the boundary. It employs the function `blockboundaryfix`, which treats stiffness block matrices. For the diagonal block-matrix the cycle consists of substituting the entries of the row that corresponds to the edge-vertex i of the stiffness matrix for 1 if the entry is diagonal and 0 otherwise. We also substitute the entries of the load vector that correspond to the edge-vertex i by the value prescribed by the Dirichlet boundary condition . For the non-diagonal block matrix the cycle consists only of substituting the row that corresponds to the edge-vertex i of the stiffness matrix for 0.

The implementation of the weak formulation of the clamped Cosserat plate is similar to the implementation of the Cosserat simply supported plate. The treatment is different when the boundary conditions are taken into account. This is done on the stage of evaluating the `boundaryfix` function. For the clamped plate we employ the same technique used for the block matrices corresponding to the Dirichlet boundary conditions. The diagonal block matrices are treated differently than the non-diagonal ones.

For the diagonal block matrices the cycle consists of two parts:

```
for i = 1:obj.nedges
      matrix (obj.start(i),1:obj.npoints) = 0;
      matrix (obj.start(i),obj.start(i)) = 1;
      matrix (obj.finish(i),1:obj.npoints) = 0;
      matrix (obj.finish(i),obj.finish(i)) = 1;
      xs = obj.x(obj.start(i))
      ys = obj.y(obj.start(i))
      xf = obj.x(obj.finish(i))
      yf = obj.y(obj.finish(i))
      vector(obj.start(i)) = f(s,xs,ys);
      vector(obj.finish(i)) = f(s,xf,yf);
end
```

which substitutes the edge-vertex `i` entries of the `matrix` for 1 if they are diagonal and 0 otherwise, and substitutes the elements of the `vector` for the value of the right-hand side function f_i evaluated in the coordinates of the edge vertex. For the

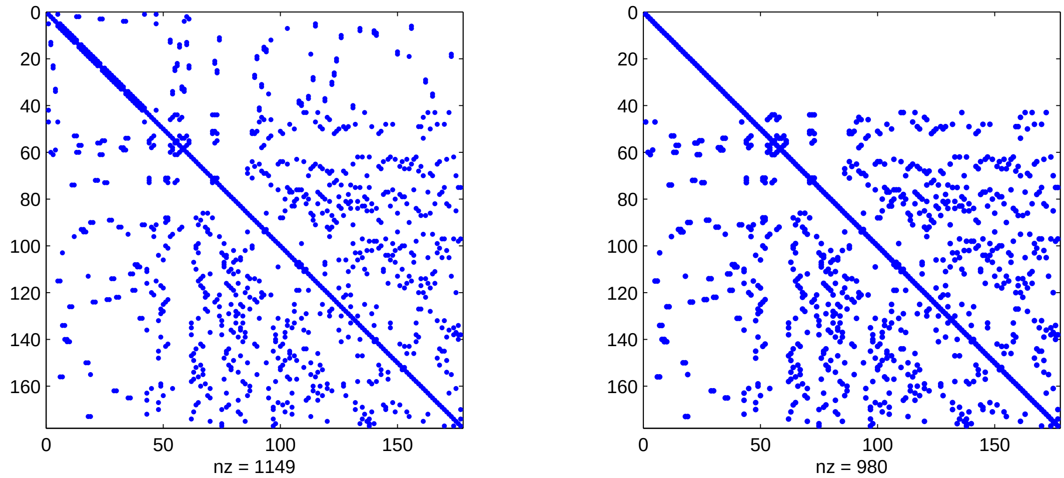

Figure 4–3: Stiffness matrix before and after imposing the boundary values

non-diagonal block matrices the cycle consists only of substituting

```
for i = 1:obj.nedges
      matrix ( obj.start(i), 1:obj.npoints ) = 0;
      matrix ( obj.finish(i), 1:obj.npoints ) = 0;
end
```

7. Solve the systems of linear equations.

We implement the function `systemsolve` responsible for solving the system of linear equations.

We solve the systems of linear equations using the standard MATLAB function `mldivide`, which employs different algorithms to handle different kinds of coefficient matrices. For the case of the nonsymmetric matrices it performs a general triangular factorization using LU decomposition with partial pivoting. We also calculate the relative residual as

```
norm(b-A*z)/norm(b)
```

8. Calculate the optimal value of the splitting parameter η.

We implement the function `eta` responsible for the calculation of the optimal value `etaoptimal` of the splitting parameter η. The function imploys the *Algorithm for the Optimal Value of the Splitting Parameter* discussed in the Chapter 3. Function `eta` imploys the functions `strainset` and `stressset`, which calculate the stress and strain sets respectively. The stress and strain sets are calculated from the solution sets for a specific value of the parameter η. After the stress and strain sets are calculated the optimal value of the splitting parameter η_0 is calculated using the formula (4.19).

9. Calculate the optimal solution.

The optimal solution is calculated as a linear combination of the 9 blocks of solution vectors $\breve{\alpha}^i_{(0)}$ and $\breve{\alpha}^i_{(1)}$ represented by `veta0` and `veta1`:

```
v = veta0*(1-etaoptimal) + veta1*(etaoptimal)
```

10. Visualize the results.

We implement the function `graphsolution` responsible for the visualization of the results. The function uses the MATLAB function `plot3` that displays a three-dimensional plot of a set of data points. It also has an option for creating a density plot and generating the output for *Mathematica* computation system.

11. Estimate the Error.

We implement the function `errorestimation` responsible for the estimation of the error in both $\mathbf{H}^1$ and L_2 norms. It calculates the error of the approximation performing the numerical integration over each triangular element and then adding the results of the integration.

4.11 Numerical Validation of the Proposed Finite Element Method

Since the proposed FEM is based on the classical FEM we will estimate the rate of its convergence for Dirichlet and mixed Neumann-Dirichlet boundary conditions and the rate of convergence of the proposed FEM for simply supported plates.

4.11.1 Validation of the FEM for Different Boundary Conditions

Let us consider the plate B_0 to be a square plate of size $[0,a]\times[0,a]$ with the boundary $G=G_1\cup G_2\cup G_3\cup G_4$ and the hard simply supported boundary conditions written in terms of the kinematic variables in the mixed Dirichlet-Neumann:

$$\begin{aligned}
G_1\cup G_2 \quad &: \quad W=0,\ W^*=0,\ \Psi_2=0,\ \Omega_1^0=0,\ \hat{\Omega}_1^0=0,\\
&\qquad \frac{\partial\Omega_3}{\partial n}=0,\ \frac{\partial\Psi_1}{\partial n}=0,\ \frac{\partial\Omega_2^0}{\partial n}=0,\ \frac{\partial\hat{\Omega}_2^0}{\partial n}=0;\\
G_3\cup G_4 \quad &: \quad W=0,\ W^*=0,\ \Psi_1=0,\ \Omega_2^0=0,\ ,\hat{\Omega}_2^0=0,\\
&\qquad \frac{\partial\Omega_3}{\partial n}=0,\ \frac{\partial\Psi_2}{\partial n}=0,\ \frac{\partial\Omega_1^0}{\partial n}=0,\ \frac{\partial\hat{\Omega}_1^0}{\partial n}=0.
\end{aligned}$$

where

$$\begin{aligned}
G_1 &= \{(x_1,x_2): x_1=0, x_2\in[0,a]\},\\
G_2 &= \{(x_1,x_2): x_1=a, x_2\in[0,a]\},\\
G_3 &= \{(x_1,x_2): x_1\in[0,a], x_2=0\},\\
G_4 &= \{(x_1,x_2): x_1\in[0,a], x_2=a\},
\end{aligned}$$

The existence of a sequence of triangulations that ensures the optimal rates of convergence for the Finite Element approximation of the solution of a second order strongly elliptic system with homogeneous Dirichlet boundary condition on polyhedron domain with continuous piecewise polynomials was shown in [80]. For the case of piecewise linear polynomials the optimal rate of convergence in $\mathbf{H}^1$-norm is linear.

We propose to use the uniform refinement to form the sequence of triangulations and estimate the order of the error of approximation of the proposed FEM in $\mathbf{H}^1$-norm and L_2-norm.

Let us consider homogeneous Dirichlet boundary conditions. We will assume the solution u of the form:

$$u_i = U_i \sin\left(\frac{\pi x_1}{a}\right) \sin\left(\frac{\pi x_2}{a}\right), \qquad U_i \in \mathbb{R}, i = \overline{1,9}, \tag{4.20}$$

which automatically satisfies homogeneous Dirichlet boundary conditions. Substituting the solution (4.20) into the system of field equations (4.2) we can find the corresponding right-hand side function f. The results of the error estimation of the FEM approximation in $\mathbf{H}^1$ and L_2 norms performed for the elastic parameters corresponding to the polyurethane foam are given in the Tables 4–1 and 4–2 respectively.

Let us consider mixed Neumann-Dirichlet boundary conditions. Simply supported boundary conditions (3.23) - (3.24) represent this type of boundary conditions and therefore the FEM approximation can be compared with the analytical solution developed in the Chapter 3 for some fixed value of the parameter η. The results of the error estimation of the FEM approximation in $\mathbf{H}^1$ and L_2 norms performed for the elastic parameters corresponding to the polyurethane foam are given in the Tables 4–3 and 4–4 respectively.

Table 4–1: Order of Convergence in $\mathbf{H}^1$-norm for Homogeneous Dirichlet BC

Refinements	Number of Nodes	Diameter	Error in $\mathbf{H}^1$-norm	Convergence Rate
0	177	0.302456	1.620369	
1	663	0.151228	0.711098	**1.19**
2	2565	0.075614	0.322016	**1.14**
3	10089	0.037807	0.150149	**1.10**
4	40017	0.018903	0.073481	**1.03**
5	159393	0.009451	0.036512	**1.01**

Table 4–2: Order of Convergence in L_2-norm for Homogeneous Dirichlet BC

Refinements	Number of Nodes	Diameter	Error in L_2-norm	Convergence Rate
0	177	0.302456	0.279484	
1	663	0.151228	0.069632	**2.00**
2	2565	0.075614	0.018175	**1.94**
3	10089	0.037807	0.004598	**1.98**
4	40017	0.018903	0.001153	**2.00**
5	159393	0.009451	0.000288	**2.00**

Table 4–3: Order of Convergence in $\mathbf{H}^1$-norm for Mixed Neumann-Dirichlet BC

Refinements	Number of Nodes	Diameter	Error in $\mathbf{H}^1$-norm	Convergence Rate
0	177	0.302456	0.236791	
1	663	0.151228	0.115809	**1.03**
2	2565	0.075614	0.054195	**1.09**
3	10089	0.037807	0.026233	**1.05**
4	40017	0.018903	0.012986	**1.01**
5	159393	0.009451	0.006475	**1.00**

Table 4–4: Order of Convergence in L_2-norm for Mixed Neumann-Dirichlet BC

Refinements	Number of Nodes	Diameter	Error in L_2-norm	Convergence Rate
0	177	0.302456	6.214×10^{-2}	
1	663	0.151228	1.638×10^{-2}	**1.92**
2	2565	0.075614	4.219×10^{-3}	**1.96**
3	10089	0.037807	1.065×10^{-3}	**1.99**
4	40017	0.018903	2.678×10^{-4}	**1.99**
5	159393	0.009451	6.772×10^{-5}	**1.98**

4.11.2 Validation of the proposed FEM for Simply Supported Cosserat Elastic Plate

The boundary condition for the variable Ω_3 is a Neumann-type boundary condition:

$$\frac{\partial \Omega_3}{\partial n} = 0 \text{ on } G$$

and thus we will look for Ω_3 in the space $\mathbf{H}^1(\Delta, B_0)$, where.

$$\mathbf{H}^1(\Delta, B_0) = \left\{u \in \mathbf{H}^1(B_0) : \Delta u \in L_2(B_0)\right\}$$

The boundary condition for the variables W and W^* is a Dirichlet-type boundary condition:

$$\begin{aligned} W &= 0 \text{ on } G \\ W^* &= 0 \text{ on } G \end{aligned}$$

and thus we will look for W and W^* in the space $\mathbf{H}_0^1(B_0)$ defined as [68]:

$$\mathbf{H}_0^1(B_0) = \left\{v \in \mathbf{H}^1(B_0), v = 0 \text{ on } G\right\}$$

The boundary condition for the variables Ψ_1, Ω_2^0 and $\hat{\Omega}_2^0$ is of mixed Dirichlet-Neumann type:

$$\begin{aligned} \frac{\partial \Psi_1}{\partial n} = 0, \frac{\partial \Omega_2^0}{\partial n} = 0, \frac{\partial \hat{\Omega}_2^0}{\partial n} = 0 \qquad & \text{on } G_1 \cup G_2 \\ \Psi_1 = 0, \Omega_2^0 = 0, \hat{\Omega}_2^0 = 0 \qquad & \text{on } G_3 \cup G_4 \end{aligned}$$

and thus we will look for Ψ_1, Ω_2^0 and $\hat{\Omega}_2^0$ in the following space [68]:

$$\mathbf{H}_V^1 = \left\{v \in \mathbf{H}^1(\Delta, B_0), v = 0 \text{ on } G_3 \cup G_4\right\}$$

The boundary condition for the variables Ψ_2, Ω_1^0 and $\hat{\Omega}_1^0$ is of mixed Dirichlet-Neumann type:

$$\begin{aligned} \Psi_2 = 0, \Omega_1^0 = 0, \hat{\Omega}_1^0 = 0 \qquad & \text{on } G_1 \cup G_2 \\ \frac{\partial \Psi_2}{\partial n} = 0, \frac{\partial \Omega_1^0}{\partial n} = 0, \frac{\partial \hat{\Omega}_1^0}{\partial n} = 0 \qquad & \text{on } G_3 \cup G_4 \end{aligned}$$

and thus we will look for Ψ_2, Ω_1^0 and $\hat{\Omega}_1^0$ in the following space [68]:

$$\mathbf{H}_H^1 = \left\{v \in \mathbf{H}^1(\Delta, B_0), v = 0 \text{ on } G_1 \cup G_2\right\}$$

Therefore we will look for the solution

$$\left[\Psi_1, \Psi_2, W, \Omega_3, \Omega_1^0, \Omega_2^0, W^*, \hat{\Omega}_1, \hat{\Omega}_2\right]^T$$

of the Cosserat plate field equations (2.97) in the space $\mathscr{H}$ defined as

$$\mathscr{H} = \mathscr{H}_1 \times \mathscr{H}_2 \times \mathscr{H}_3 \times \mathscr{H}_4 \times \mathscr{H}_5 \times \mathscr{H}_6 \times \mathscr{H}_7 \times \mathscr{H}_8 \times \mathscr{H}_9 \tag{4.21}$$

where

$$\mathscr{H}_1 = \mathscr{H}_6 = \mathscr{H}_9 = \mathbf{H}_V^1\left(B_0\right),$$

$$\mathscr{H}_2 = \mathscr{H}_5 = \mathscr{H}_8 = \mathbf{H}_H^1\left(B_0\right),$$

$$\mathscr{H}_3 = \mathscr{H}_7 = \mathbf{H}_0^1\left(B_0\right),$$

$$\mathscr{H}_4 = \mathbf{H}^1\left(\Delta, B_0\right).$$

The space $\mathscr{H}$ is a Hilbert space equipped with the inner product $\langle u, v\rangle_{\mathscr{H}}$ on defined on $\mathscr{H}$ as follows:

$$\langle u, v\rangle_{\mathscr{H}} = \sum_{i=1}^{9} \langle u_i, v_i\rangle_{\mathscr{H}_i} \text{ for } u, v \in \mathscr{H}$$

where $\langle u, v\rangle_{\mathscr{H}_i}$ is an inner product defined on the Hilbert space $\mathscr{H}_i$ respectively.

Taking into account the essential boundary conditions we define the finite element spaces $\mathscr{H}_i^h$ as follows:

$$\mathscr{H}_1^h = \mathscr{H}_6^h = \mathscr{H}_9^h = \left\{v : v \in C\left(B_0\right), v \text{ is linear on every } K_j, v = 0 \text{ on } G_1 \cup G_2\right\},$$

$$\mathscr{H}_2^h = \mathscr{H}_5^h = \mathscr{H}_8^h = \left\{v : v \in C\left(B_0\right), v \text{ is linear on every } K_j, v = 0 \text{ on } G_3 \cup G_4\right\},$$

$$\mathscr{H}_3^h = \mathscr{H}_7^h = \left\{v : v \in C\left(B_0\right), v \text{ is linear on every } K_j, v = 0 \text{ on } G\right\},$$

$$\mathscr{H}_4^h = \left\{v : v \in C\left(B_0\right), v \text{ is linear on every } K_j\right\}.$$

The finite dimensional space $\mathscr{H}^h$ is then defined as

$$\mathscr{H}^h = \mathscr{H}_1^h \times \mathscr{H}_2^h \times \mathscr{H}_3^h \times \mathscr{H}_4^h \times \mathscr{H}_5^h \times \mathscr{H}_6^h \times \mathscr{H}_7^h \times \mathscr{H}_8^h \times \mathscr{H}_9^h \tag{4.22}$$

Table 4–5: Order of Convergence in $\mathbf{H}^1$-norm for Simply Supported Plate

Refinements	Nodes Number	Diameter	Error in $\mathbf{H}^1$-norm	Convergence Rate
0	177	0.302456	0.256965	
1	663	0.151228	0.119234	**1.11**
2	2565	0.075614	0.054701	**1.12**
3	10089	0.037807	0.026301	**1.05**
4	40017	0.018903	0.012994	**1.01**
5	159393	0.009451	0.006476	**1.00**

Table 4–6: Order of Convergence in L_2-norm for Simply Supported Plate

Refinements	Nodes Number	Diameter	Error in L_2-norm	Convergence Rate
0	177	0.302456	8.253×10^{-2}	
1	663	0.151228	2.260×10^{-2}	**1.87**
2	2565	0.075614	5.860×10^{-3}	**1.95**
3	10089	0.037807	1.482×10^{-3}	**1.98**
4	40017	0.018903	3.720×10^{-4}	**1.99**
5	159393	0.009451	9.355×10^{-5}	**1.99**

We solve the field equations using described Finite Element method and compare the obtained results with the analytical solution for the square plate made of polyurethane foam derived in the Chapter 3.

The initial distribution of the pressure, as in the Chapter 4, is assumed sinusoidal:

$$p\left(x_1, x_2\right) = \sin\left(\frac{\pi x_1}{a}\right) \sin\left(\frac{\pi x_2}{a}\right) \tag{4.23}$$

The estimation of the error in $\mathbf{H}^1$ norms shows that the order of the error is optimal (linear) in $\mathbf{H}^1$-norm for the piecewise linear elements for the simply supported

Table 4–7: Relative Error of the Maximum Values of the Displacement and Microrotations

	Optimal η	u_1	u_2	u_3	φ_1	φ_2
Finite Element Solution	0.040760	-0.014891	-0.014891	0.307641	0.046767	-0.046767
Analytical Solution	0.040799	-0.014892	-0.014892	0.307674	0.046770	-0.046770
Relative Error (%)	**0.09**	**0.03**	**0.03**	**0.04**	**0.03**	**0.03**

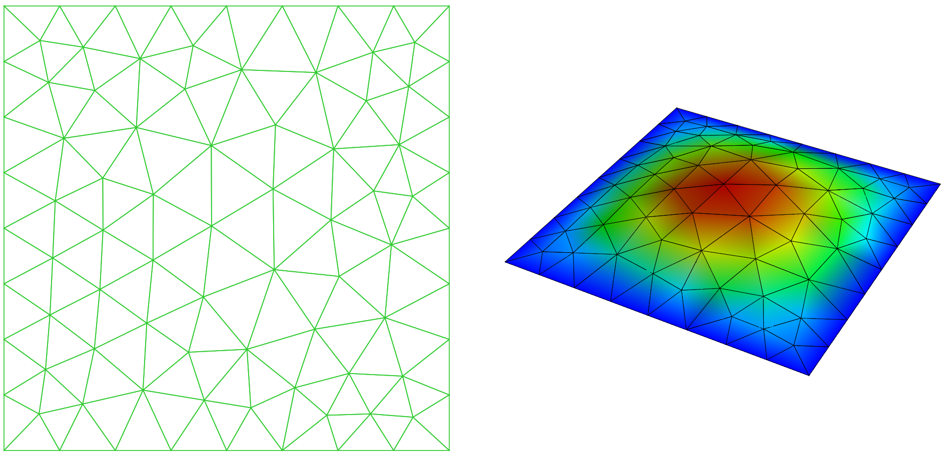

Figure 4–4: Hard simply supported square plate 2.0m×2.0m×0.1m made of polyurethane foam: the initial mesh and the isometric view of the resulting vertical deflection of the plate

plate. The results of the error estimation of the FEM approximation in $\mathbf{H}^1$ and L_2 norms performed for the elastic parameters corresponding to the polyurethane foam are given in the Tables 4–5 and 4–6 respectively.

The comparison of the maximum of the displacements u_i and microrotations φ_i calculated using Finite Element method with 320 thousand elements and the analytical solution for the micropolar plate theory is provided in the Table 4–7. The relative error of the approximation of the optimal value of the splitting parameter is 0.09%.

The Figure 4–4 represents the Finite Element modeling of the bending of the simply supported square plate made of polyurethane foam.

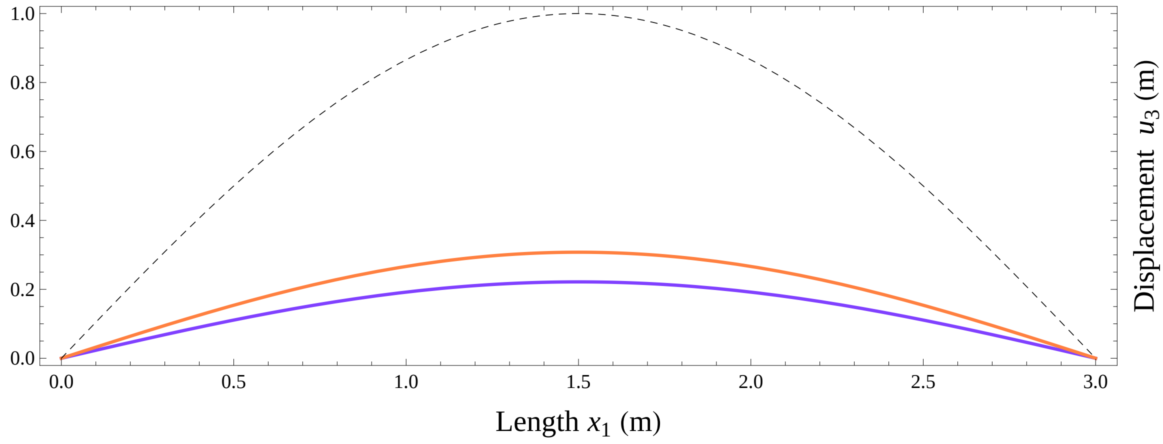

Figure 4–5: The cross section that contains the center of the micropolar square plate 3.0m×3.0m×0.1m made of polyurethane foam under the sinusoidal load: Cosserat clamped plate – solid blue line, Cosserat simply supported plate – solid orange line, initial sinusoidal load – dashed black line.

4.12 Finite Element Modeling of Clamped Cosserat Elastic Plates of Arbitrary Shape

The comparison of the distribution of the vertical deflection of the clamped and simply supported plates is given in the Figure 4–5.

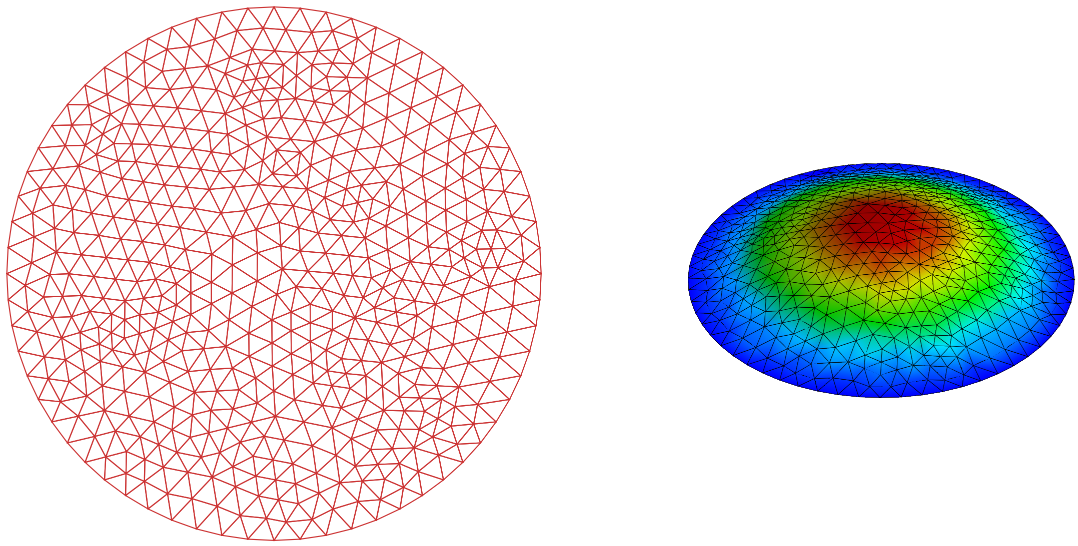

Figure 4–6: The circular Cosserat clamped plate of radius $R = 1.0m$ and thickness $h = 0.1m$ made of polyurethane foam under the uniform load: the initial mesh and the isometric view of the resulting vertical deflection of the plate.

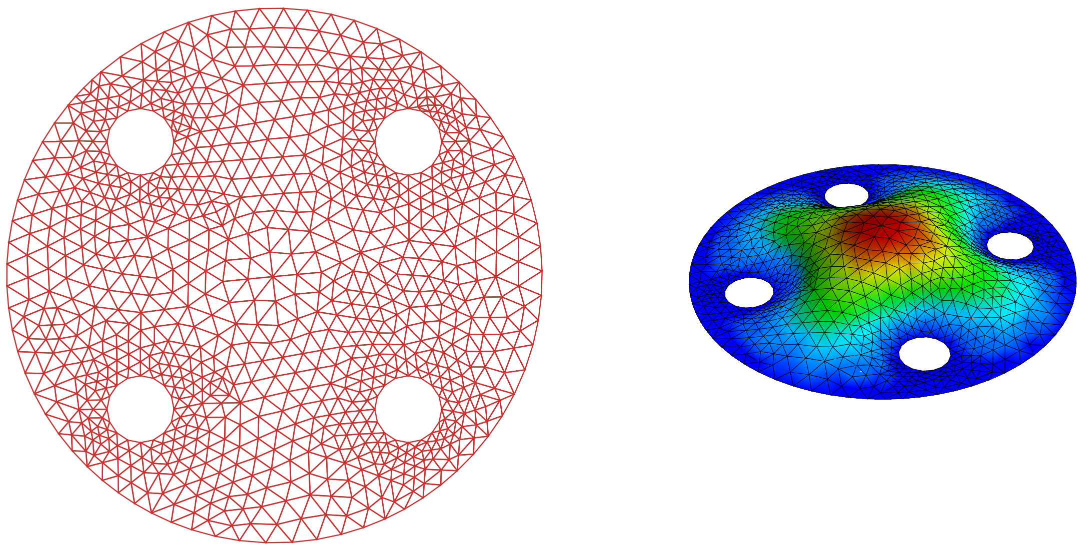

Figure 4–7: The circular Cosserat clamped plate of radius $R = 1.0m$ and thickness $h = 0.1m$ made of polyurethane foam with circular clamped holes under the uniform load: the initial mesh and the isometric view of the resulting vertical deflection of the plate.

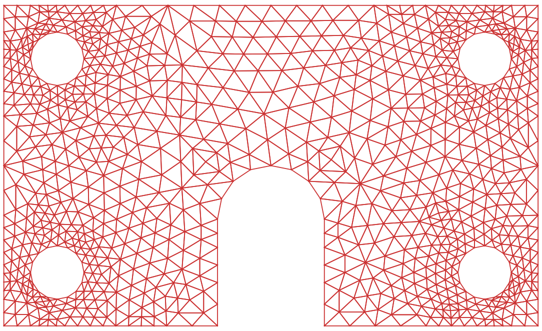
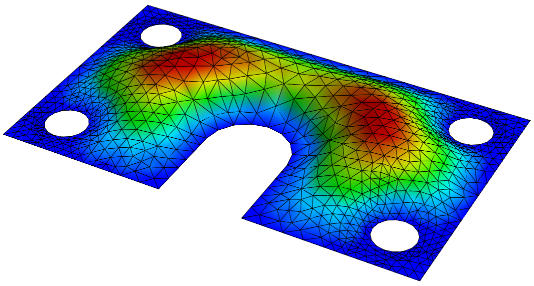

Figure 4–8: The clamped plate of size 10.0m×6.0m×0.1m made of polyurethane foam under the uniform load: the initial mesh and the isometric view of the resulting vertical deflection of the plate.

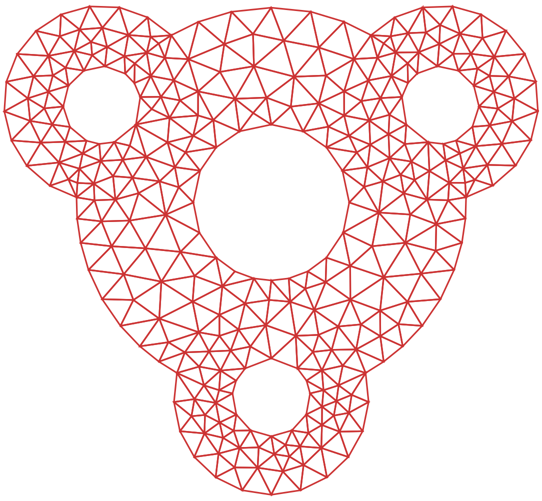
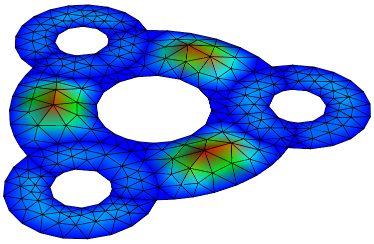

Figure 4–9: The clamped polyurethane gasket under the uniform load: the initial mesh and the isometric view of the resulting vertical deflection of the plate.

Chapter 5

Conclusion and Future Work

In this dissertation we presened the mathematical modeling of Cosserat elastic plates and their Finite Element computation. We developed the mathematical model for bending of Cosserat elastic plates, which assumes physically and mathematically motivated approximations over the plate thickness for stress, couple stress, displacement, and microrotation. The Generalized Hellinger-Prange-Reissner Principle allowed us to obtain the equilibrium equations, constitutive relations and optimal value for the minimization of the elastic energy with respect to the splitting parameter in the approximation of the σ_{33} stress component.

The comparison of the maximum vertical deflection for simply supported square plate with the analytical solution of the three-dimensional Cosserat elasticity confirmed the high order of approximation of the three-dimensional (exact) solution. The computations produced a relative error of the order 1% in comparison with the exact three-dimensional solution that is stable with respect to the standard range of the plate thickness. The results were shown to be compatible with the precision of the well-known Reissner model used for bending of simple elastic plates. Apart from the computational modeling and comparison, the experimental validation of the proposed mathematical model is needed.

We presented the Cosserat plate field equations as an elliptic system of nine differential equations in terms of the kinematic variables. We proposed the Finite Element Method for Cosserat elastic plates based on the efficient numerical algorithm for the calculation of the optimal value of the splitting parameter and the computation of the corresponding unique solution of the weak problem. We provided the numerical vaidation of the proposed FEM and showed that it converges to the analytical solution with optimal (quadratic) rate of convergence. The asymptotic order of the computational complexity of the proposed Finite Element algorithm was shown to be the same as of the classical Finite Element method. We provided the Finite Element modeling of the bending of clamped Cosserat elastic plates of arbitrary shapes under different loads.

The future work will include application of the developed micropolar plate theory to other engineering materials that were reported to be micropolar, numerical analysis of the plates under different loads with other boundary conditions (soft clamped, soft simply supported, free, etc), comparison of the existing plate models and the developed micropolar plate theory, dynamics model of thin micropolar elastic plates, the effect of material defects on the stress-strain characteristic of the plate and numerical analysis of the propagation of the dislocation and the interaction between the geometry and holes of the plate and the dislocation.

Reference List

[1] Altenbach H. and Eremeyev V. Thin-walled structures made of foams. *H. Cellular and Porous Materials: Modeling –Testing – Application, CISM Courses and Lecture Notes*, pages 167–242, 2010.

[2] Arencon D. and Ignacio J. Fracture toughness of polypropylene-based particulate composites. *Materials*, 2:2046–2094, 2009.

[3] Lebon M., Muller K., Bahain J., Frohlich, Falgueres C., Bertrand L., Sandt C., and Reiche I. Imaging fossil bone alterations at the microscale by SR-FTIR microspectroscopy. *Journal of Analytical Atomic Spectrometry*, 26:922–929, 2001.

[4] Narayanan N. and Ramamurthy K. Microstructural investigations on aerated concrete. *Cement and Concrete Research*, 30:457–464, 2000.

[5] Pabst W. Micropolar materials. *Ceramics*, 49:170–180, 2005.

[6] Kumar R. and Gupta R. Propagation of waves in transversely isotropic micropolar generalized thermoelastic half space. *International Communications in Heat and Mass Transfer*, 37:1452–1458, 2010.

[7] Neff P. and Jeong J. A new paradigm: the linear isotropic Cosserat model with conformally invariant curvature energy. *Zeitschrift fur Angewandte Mathematik und Mechanik*, 89:107–122, 2009.

[8] Kumar R. Wave propagation in micropolar viscoelastic generalized thermoelastic solid. *International Journal of Engineering Science*, 38, 2000.

[9] Merkel A., Tournat V., and Gusev V. Experimental evidence of rotational elastic waves in granular phononic crystals. *Phys. Rev. Lett*, 107, 2011.

[10] Surappa M. Aluminium matrix composites: Challenges and opportunities. *Sadhana*, 28:319–334, 2003.

[11] Kima H., Junga D., Jungb I., Cifuentesb J., Rheeb K., and Huib D. Enhancement of mechanical properties of aluminium/epoxy composites with silane functionalization of aluminium powder. *Composites: Part B*, 43, 2012.

[12] Gauthier R. Experimental investigations on micropolar media. *Mechanics of Micropolar media*, 1982.

[13] Gauthier R. and Jahsman W. A quest for micropolar elastic constants. *Journal of Applied Mechanics*, 42:369–374, 1975.

[14] Gerstle W., Sau N., and Aguilera E. *Micropolar Peridynamic Constitutive Model for Concrete*. 2007.

[15] Chang T., Lin H., Wen-Tse C., and Hsiao J. Engineering properties of lightweight aggregate concrete assessed by stress wave propagation methods. *Cement and Concrete Composites*, 28:57–68, 2006.

[16] Lakes R. Experimental microelasticity of two porous solids. *International Journal of Solid Structures*, 22(1):55–63, 1986.

[17] Purasinghe R., Tan S., and Rencis J. Micropolar elasticity model for the stress analysis of human bones. *Proceedings of the 11th Annual International Conference*, 1989.

[18] Thermal insulation materials made of rigid polyurethane foam (pur/pir). *BING Report*, 1, 2006.

[19] Morley M. *Building with Structural Insulated Panels*. Taunton Press, 2000.

[20] Ventsel E. and Krauthammer T. *Thin Plates and Shells*. Marcel Dekker, Inc., first edition, 2001.

[21] Monfared V. Effect of geometric factor and loading on strength of rectangular plate under bending. *Middle-East Journal of Scientific Research*, 11:1546–1549, 2012.

[22] Timoshenko S. and Woinowsky-Krieger S. *Theory of Plates and Shells*. McGraw-Hill, 1959.

[23] Botelho E. C., Silva R. A., Pardini L. C., and Rezende M. C. A review on the development and properties of continuous fiber/epoxy/aluminum hybrid composites for aircraft structures. *Materials Research*, 9:247–256, 2006.

[24] Khanna A. and Sharma A. Mechanical vibration of visco-elastic plate with thickness varation. *International Journal of Applied Mathematical Research*, 1:150–158, 2012.

[25] Castelain C., Mokrani A., Legentilhomme P., and Peerhossaini H. Residence time distribution in twisted pipe flows: helically coiled system and chaotic system. *Experiments in Fluids*, 22:359–368, 1997.

[26] Euler L. De motu vibratorio tympanorum. *Novi Commentari Acad Petropolit*, 10:243–260, 1766.

[27] Chladni E. *Entdeckungen ber die Theorie des Klanges*. 1787.

[28] Adrianov I. and Awrejcewicz J. Theory of plates and shells: New trends and applications. *International Journal of Nonlinear Sciences and Numerical Simulations*, 2004.

[29] Bernoulli J. Essai théorique sur les vibrations de plaques élastiques rectangularies et libres. *Nova Acta Acad Petropolit*, 5:197–219, 1789.

[30] Steinberg L. Mesoelastic deformation with strain singularities. *Mathematics and Mechanics of Solids*, 11(4):385–400, 2006.

[31] Reddy J. *Theory and analysis of elastic plates and shells*. CRC Press, Taylor and Francis, 2007.

[32] Love A. E. H. On the small free vibrations and deformations of elastic shells. *Philosophical trans. of the Royal Society (London)*, A(17):491–549, 1888.

[33] Love A. E. H. *A Treatise on the Mathematical Theory of Elasticity*. Cambridge University Press, 1892.

[34] Reissner E. On the theory of elastic plates. *Journal of Mathematics and Physics*, 23:184–191, 1944.

[35] Reissner E. The effect of transverse shear deformation on the bending of elastic plates. *Journal of Applied Mechanics*, 12:69–77, 1945.

[36] Steinberg L. Deformation of micropolar plates of moderate thickness. *International Journal Applied Mathematics and Mechanics*, 6(17):1–24, 2010.

[37] Steinberg L. and Kvasov R. Enhanced mathematical model for Cosserat plate bending. *Thin-Walled Structures*, 63:51–62, 2013.

[38] Donnell L. *Beams, Plates and Shells (Engineering societies monographs)*. McGraw-Hill Inc, 1976.

[39] Rossle A., Bischoff M., Wendland W., and Ramm E. On the mathematical foundation of the (1,1,2)-plate model. *International Journal of Solids and Structures*, 36:2143–2168, 1999.

[40] Eringen A. C. Theory of micropolar plates. *Journal of Applied Mathematics and Physics*, 18:12–31, 1967.

[41] Altenbach H. and Eremeyev V. On the linear theory of micropolar plates. *Journal of Applied Mathematics and Mechanics*, 2009.

[42] Sargsyan S. and Vardanyan S. Some problems of thermoelasticity of micropolar thin bars and plates. *IEEE*, 0-7803-9524-7/06(7):892–899, 2006.

[43] Sargsyan S. General theory of elastic micropolar thin shells. *AMIM*, 13(1):385–400, 2008.

[44] Reyes R. Comparison of elastic plate theories for micropolar materials. *Thesis*, 2010.

[45] Kvasov R. and Steinberg L. Numerical modeling of bending of Cosserat elastic plates. *Proceedings of the 5th Computing Alliance of Hispanic–Serving Institutions Annual Meeting*, pages 67–70, 2011.

[46] Kvasov R. and Steinberg L. Numerical modeling of bending of micropolar plates. *Thin-Walled Structures*, 2013.

[47] Ciarlet P. and Lions J. *Handbook of Numerical Analysis - Finite Element Methods (Part1)*, volume 2. Elsevier, 1991.

[48] Galerkin B. On electrical circuits for the approximate solution of the Laplace equation. *Engineering Bulletin*, 19:897–908, 1915.

[49] Hazewinkel M. *Encyclopaedia of Mathematics*. 1989.

[50] Courant R. Variational methods for the solution of problems of equilibrium and vibration. *Bull. Amer. Math. Soc.*, 49:1315–1332, 1943.

[51] Hrennikoff H. Solutions of problems in elasticity by the framework method. *Journal of Applied Mechanics*, pages 169–175, 1941.

[52] McHenry D. A lattice analogy for the solution of plane stress problems. *Journal of Civil Engineering*, 21:59–82, 1943.

[53] Turner M., Clough R., Martin H., and Topp L. Stiffness and deflection analysis of complex structures. *Journal of Aeronautical Science*, 23:805–824, 1956.

[54] Clough R. The finite element method in plane stress analysis. *Proceedings of 2nd ASCE Conference on Electronic Computation*, 1960.

[55] Huebner K., Dewhirst D., Smith D., and Byrom T. *The Finite Element Method for Engineers*. 2001.

[56] Strang W. and Fix G. *An Analysis of The Finite Element Method*. 1973.

[57] Babuška I. and Aziz A. Survey lectures on the mathematical foundation of the finite element method. *The Mathematical Foundation of the Finite Element Method with Applications to Partial Differential Equations*, pages 5–359, 1972.

[58] Oden J. and Reddy J. *An Introduction to the Mathematical Theory of Finite Elements*. Wiley, New York, 1976.

[59] Nowacki W. *Teoria Sprezystosci*. Panswowe Wydawnictwo Naukowe, 1970.

[60] Neff P. Relations of constants for isotropic linear Cosserat elasticity. *Zeitschrift fur Angewandte Mathematik und Mechanik*, 2008.

[61] Gurtin M. *The Linear Theory of Elasticity.* 1972.

[62] Shimakura N. *Partial Differential Operators of Elliptic Type.* 1992.

[63] Evans L. *Partial Differential Equations.* 2010.

[64] Nagle R., Saff E., and Snider A. *Fundamentals of Differential Equations and Boundary Value Problems.* 5th edition, 2008.

[65] Arnold D. and Falk R. Edge effects in the Reissiner-Mindlin plate theory. *Analytic and Computational Models of Shells*, 1989.

[66] Haggblad B. and Bathe K. Specifications of boundary conditions for Reissner-Mindlin plate bending finite elements. *International Journal for Numerical Methods in Engineering*, 30:981–1011, 1990.

[67] Solin P. Partial differential equations and the finite element method. 2005.

[68] Johnson C. *Numerical Solution of Partial Differential Equations by Finite Element Method.* Cambridge University Press, 1987.

[69] Conway J.B. *A Course in Functional Analysis.* 1985.

[70] Hughes T., Stein E., and R. de Borst. *Encyclopedia of Computational Mechanics*, volume 2. Cambridge University Press, 2004.

[71] Hughes T. *The Finite Element Method: Linear Static and Dynamic Finite Element Analysis.* Prentice-Hall, 1987.

[72] Costabel M., Dauge M., and Nicaise S. *Corner Singularities and Analytic Regularity for Linear Elliptic Systems. Part I: Smooth domains.* 2010.

[73] Costabel M., Dauge M., and Nicaise S. *Analytic Regularity for Linear Elliptic Systems in Polygons and Polyhedra*, volume 22. 2012.

[74] Agranovich M. Potential type operators and transmission problems for strongly elliptic systems in lipschitz domains. *Functional Analysis and Its Applications*, pages 165–183, 2012.

[75] Grubb G. Remainder estimates for eigenvalues and kernels of pseudo-differential elliptic systems. *Mathematica Scandinavica*, 43:275–307, 1978.

[76] Lax P. and Milgram A. Parabolic equations. *Contributions to the theory of partial differential equations. Annals of Mathematics Studies*, 33:167–190, 1954.

[77] Céa J. Approximation variationnelle des problèmes aux limites. *Ann. Inst. Fourier*, pages 345–444, 1964.

[78] Ainsworth M. and Oden T. *A Posteriori Error Estimation in Finite Element Analysis*. Wiley, 2000.

[79] Duran R. *Galerkin Approximations and Finite Element Methods*. 2010.

[80] Bacuta C., Nistor V., and Zikatanov L. Improving the rate of convergence of high-order finite elements on polyhedra. *Numerical Functional Analysis and Optimization*, 26:613–639, 2005.

[81] Lyness J.N. and Cools R. *A Survey of Numerical Cubature over Triangles*. 1994.